

jc685
01/27/00
PTO

LAW OFFICES
MILLEN, WHITE, ZELANO & BRANIGAN, P.C.
ARLINGTON COURTHOUSE PLAZA I
SUITE 1400
2200 CLARENDON BOULEVARD
ARLINGTON, VIRGINIA 22201

TELEPHONE: (703) 243-6333
CABLE: USALAW
INT'L TELEX: 64191
TELECOPIER: (703) 243-6410

Atty's Docket No. SGT-39

Applicant(s) : Joseph S. HAYDEN *et al.*

For : OPTICAL WAVEGUIDES ON GLASS SUBSTRATES AND LASERS
FORMED THEREFROM

The Honorable Commissioner
of Patents and Trademarks
Washington, D.C. 20231

jc678 U.S. PTO
09/492178
01/27/00

SUBMISSION OF APPLICATION UNDER 37 C.F.R. §1.53(f)

Sir:

Herewith is the above-identified application for Letters Patent including:

Applicant(s) Name(s) : Joseph S. HAYDEN - Clarks Summit, PA
David L. VEASEY - Boulder, CO
Norman A. SANFORD - Boulder, CO
David S. FUNK - Boulder, CO

Assignee (by unrecorded assignment) :

Pages of Application: Specification - 40
Claims - 2
Abstract - 1
Appendix - 69
Sheets of Drawings - 2

NO DECLARATION IS ATTACHED.

☐ Preliminary Amendment

☐ Information Disclosure Statement


☒ The benefit under 35 U.S.C. §119 is claimed of the filing date of:

60/117,477 filed January 27, 1999 and 60/162,458 filed October 29, 1999.

☐ A certified copy of the priority document(s) is attached.

Respectfully submitted,

MILLEN, WHITE, ZELANO & BRANIGAN, P.C.

By: 
John A. Sopp (Reg. No. 33,103)
Representative Capacity

Filed: January 27, 2000

OPTICAL WAVEGUIDES ON GLASS SUBSTRATES AND LASERS FORMED THEREFROM

Statements as to Rights to Inventions Made Under Federally Sponsored Research and Development

5 Certain aspects of these inventions were developed with support from NIST
(National Institute for Standards and Technology). The U.S. Government may have
rights in certain of these inventions.

Field of the Invention

10 This invention relates to the field of optics and lasers, and more specifically to
a method and apparatus of integrating one or more optical waveguides on a glass
substrate and of forming lasers therein.

Background of the Invention

15 The telecommunications industry commonly uses optical fibers to transmit large
amounts of data in a short time. One common light source for optical-fiber
communications systems is a laser formed using erbium-doped glass. One such system
uses erbium-doped glass fibers to form a laser that emits at a wavelength of about 1.536
micrometer and is pumped by an infra-red source operating at a wavelength of about
0.98 micrometer. One method usable for forming waveguides in a glass substrate is
described in U.S. Patent 5,080,503 issued Jan. 14, 1992 to Najafi et al., which is
20 hereby incorporated by reference. A phosphate glass useful for lasers is described in
U.S. Patent 5,334,559 issued Aug. 2, 1994 to Hayden, which is hereby incorporated
by reference. An integrated optic laser is described in U.S. Patent 5,491,708 issued
Feb. 13, 1996 to Malone et al., which is hereby incorporated by reference.

25 There is a need in the art for an integrated optical system, including one or more
high-powered lasers along with routing and other components, that can be

inexpensively mass-produced. The system should be highly reproducible, accurate, and stable.

Summary of the Invention

The invention provides, among its embodiments, a system and method for forming an optical system including a high-powered laser on a glass substrate, and a resulting glass-substrate-based optical system and method for operating the optical system. The invention is further directed to methods for forming optical waveguides on glass substrates, including: forming substrates with multiple waveguides and including wherein at least two of the multiple waveguides have differing wavelengths.

Further embodiments of the invention provide a laser component that includes a glass substrate doped with a laser species and having one or more, preferably multiple, waveguides defined by channels within the substrate. (As used herein, a "channel within the substrate" is meant to broadly include any channel formed on or in the substrate, whether or not covered by another structure or layer of substrate.) Each substrate waveguide (or "channel") is defined within the substrate as a region of increased index of refraction relative to the substrate. The glass substrate is doped with a laser species which can be optically pumped (preferably a rare-earth element such as Er, Yb, Nd, Ho, Tm, Sm, Tb, Dy or Pr or a combination of such elements such as Er and Yb) to form a laser medium which is capable of lasing at a plurality of frequencies. Mirrors or distributed Bragg reflection gratings may be located along the length of a waveguide for providing feedback to create a laser-resonator cavity. One or more of the mirrors or reflection gratings is made partially reflective for providing laser output.

The laser component may constitute a monolithic array of individual waveguides in which the waveguides of the array form laser resonator cavities with differing resonance characteristics (e.g., resonating at differing wavelengths). The component may thus be used as part of a laser system that outputs laser light at a plurality of selected wavelengths. In certain embodiments of the invention, the resonance characteristics of a waveguide cavity are varied by adjusting the width of the channel formed in the substrate which thereby changes the effective refractive index of the waveguide. The effective refractive index can be changed by modifying the diffusion

conditions under which the waveguides are formed as described below. Changing the effective refractive index thus changes the effective length of the waveguide cavity which determines the wavelengths of the longitudinal modes supported by the cavity. In another embodiment, the resonance characteristics of the waveguide cavities are individually selected by varying the pitch of the reflection gratings used to define the cavities which, along with the effective refractive index for the propagated optical mode, determines the wavelengths of light reflected by the gratings. In still other embodiments, the location of the gratings on the waveguides is varied in order to select a laser-resonator cavity length that supports the desired wavelength of light.

In a preferred embodiment, the waveguide or multiple waveguides, optionally as part of a laser element, are constructed from a glass substrate which is a phosphate alkali glass doped with a rare-earth element such as Er or Yb/Er. In the case of Yb/Er doped glass, it is preferred for maximal lasing efficiency that the Yb/Er ratio is from approximately 1:1 to 8:1, particularly 3:1 to 8:1. This has been discovered as a result of investigation as to the optimal erbium and ytterbium rare earth ion concentrations in rare earth doped laser glasses, in particular as erbium and ytterbium 1.54 μm laser sources and amplifiers employed in the fields of telecommunication and data transmission. Prior to this investigation, erbium/ytterbium doped glasses for such applications were typically characterized by low erbium concentration (generally much less than 1 wt% Er_2O_3 content) with a corresponding high ytterbium content (typically at a ion ratio of greater than 10 ytterbium ions for each erbium ion input to the glass); such glasses are disclosed in, for example, U.S. Patent No. 5,334,559 and U.S. Patent No. 5,491,708. Such high levels of Yb were initially expected to yield high output powers and high slope efficiency based on prior experience with silicate and phosphate glass formulations, see for example U.S. Patent No. 4,962,067. The prior art taught that low erbium doping levels (at most 0.15 mole% Er_2O_3) were required to avoid self quenching effects, and that the ytterbium content be set as high as possible (basically input Yb_2O_3 to near the solubility limit in the glass, at least 6 mole% Yb_2O_3) in order to optimize the amount of pumping light absorbed within the laser glass.

However, according to this invention, it has been discovered that glasses with a Yb/Er rare earth content of from about 1:1 to 8:1 (particularly the glass called NIST-

1T or IOG-1, a sodium-aluminum-phosphate glass having a content in melt of 1.15 wt% Er_2O_3 and 4.73 wt% Yb_2O_3) demonstrated a higher output power (up to 180 mW compared to a prior high of only 16 mW) and higher slope efficiency (of at least 28% compared to a prior high of only 27%).

5 The inventors first expected that the poor performance of the prior art glasses was attributed to, at least in part, residual hydroxyl groups left in the glass. Rare earth ions excited in the glass are known to exchange energy with hydroxyl vibrational overtones in the glass, effectively robbing the excited state ions of the stored energy otherwise used to produce amplified laser emission. To investigate this possibility a series of sodium-aluminum-phosphate glasses containing 0.5wt% Er_2O_3 and 8.94wt% Yb_2O_3 with different hydroxyl content were prepared. The residual hydroxyl content in these glasses is proportional to the measured infrared absorption at 3.0um and is detailed in Table 1.

Table 1 – Hydroxyl Content Investigation in Sodium-Aluminum-Phosphate Glass

15	Melt ID	Absorption at 3.0um [cm^{-1}]
	NIST-1L	0.72
	NIST-1H	1.77
	NIST-1J	6.02

20 The results of this work indicated that although residual hydroxyl content certainly was detrimental to laser performance, it could not alone account for the poor performance of devices fabricated in these three glasses. In fact, melt NIST-1H and NIST-1L were characterized by an absorption at 3.0um below 2.0cm^{-1} , a level expected to be low enough not to significantly influence laser performance. In particular, the absorption level in melt NIST-1L was less than 1.0cm^{-1} , a threshold value below which the prior art has shown is not an issue in evaluating laser performance of a given laser glass, see Cook, L.M. et al, Proc SPIE Vol. 505, pp 102-111 (1984).

25 As a result, it was determined that the selected doping levels of Er and Yb themselves must be far from optimal. In particular, it was realized that there are performance tradeoffs related to the Yb-doping concentration, the Er-doping concentration, and the Yb/Er-doping ratio within the glass. For example, as indicated

earlier, it had been generally thought that the more Yb doping will always result in better laser performance. The inventors instead selected an alternate approach to optimizing the amount of Er and the Yb/Er ratio. The approach involves evaluating the relative performance tradeoffs between Yb-Er cross-relaxation efficiency and the total number of inverted Er ions in the laser cavity.

Spectroscopic evaluations of the NIST-1 glass were performed to determine the cross relaxation coefficient of the Yb-Er energy transfer mechanism. The cross relaxation efficiency, η , of ytterbium to erbium ion in the glass was estimated by the inventors to be given by,

$$\eta = 1 - \tau_{\text{Yb-Er}} / \tau_{\text{Yb}}$$

where $\tau_{\text{Yb-Er}}$ is the measured lifetime of the $\text{Yb}^{3+} \text{ } ^2\text{F}_{5/2}$ level in a codoped sample with Er (measured at 1.79×10^{-3} seconds) and τ_{Yb} is the measured lifetime of $\text{Yb}^{3+} \text{ } ^2\text{F}_{5/2}$ level in a sample with no erbium (measured at 1.37×10^{-3} seconds). The value of η was thus calculated to be 0.87. Additional description of this modeling method, but applied to silicate glasses having greatly inferior laser properties, is provided in the SPIE article provided as Paper E in the attached Appendix which is incorporated by reference.

The doping selection modeling method provided the following conclusions: as more Yb is incorporated into a glass with a constant Er concentration, the average distance between Er ions and Yb ions decreases, thus causing a rise in the cross relaxation efficiency of Yb-Er energy transfer. The disadvantage of this is that more of the pump power is absorbed in a shorter distance. The result is that less Er ions will be inverted in a certain length, thus there will be less gain available as well as additional reabsorption loss in the 3-level Er ion laser system. Laser performance will suffer. The penalty will be higher thresholds and lower slope efficiencies. To obtain the best possible performance, both the Yb-Er cross relaxation and the total number of inverted ions as a function of pump power must be optimized simultaneously. For a particular device, based on the absorption characteristics of ytterbium at the excitation (pump) wavelength (the absorption cross section at the optimal pump wavelength of 980nm is $14.5 \times 10^{-21} \text{ cm}^2$) and the intended device length (2.2cm) the modeling pointed to a glass doped with 1.15 wt% Er_2O_3 and 4.73 wt% Yb_2O_3 with an Er concentration

of 1×10^{20} ions/cm³. Although Er concentrations up to 6×10^{20} ions/cm³ can be used, the total doping concentration is constrained only by the solubility for rare earths within the glass host, the levels as high as 10×10^{20} rare earth ions per cm³ are known, see U.S. Pat. 5,077,240 and 5,039,631. These unusual doping levels were selected despite the conventional wisdom that taught that such an erbium doping content was twice the maximum and that the selected ytterbium content was 1/4th to 1/5th the prior art levels for a high performance laser device. Based on the results achieved with the discovered optimal doping levels, lasers based thereon can provide more power than currently available from high end diode lasers for telecommunication and data transmission applications. Conventional diode lasers typically have output powers of 2 to 20 mW. The lasers of this invention have output power that is limited only by the available pump power, up to values that can exceed 20 mW, e.g., 25-180 mW. Such power levels allow the use of glass waveguide lasers in metropolitan area networks without the need for expensive optical amplifiers in the network. The advantages are shown particularly for lasers having a length of 15 mm or less.

In preferred embodiments, the doping level, i.e., concentration, of Er ions is from > 0 up to 5 or 6×10^{20} ions/cm³ and the Er/Yb ratio is about 4:1. Although ratio's of about 1, 1.5, 2, 2.5, 3, 3.5, 4.5, 5, 5.5, 6, 6.5, 7, 7.5 or 8 to 1 can be useful.

In another preferred embodiment, improved ion exchange methods are used to create channels defining the waveguides in the glass substrate. Generally, a surface of the glass substrate is exposed to an ion-exchange solvent through a mask layer having one or more line apertures corresponding to the channel or channels (for multiple waveguide embodiments).

Processing steps include the generation of waveguides within the glass substrate using K⁺-Na⁺ ion exchange through channel apertures fabricated by standard microlithographic techniques. For example, a KNO₃ solvent can be used applied through an aluminum mask layer to perform the K⁺-Na⁺ ion exchange. The exchange of K⁺ for Na⁺ ions in the substrate produces a channel in the exposed portion of higher refractive index than the remainder of the substrate, thus, defining a waveguide. Additionally, nitrate melts of any mixture of the following nitrate salts: lithium nitrate, sodium nitrate, potassium nitrate, rubidium nitrate, cesium nitrate,

copper nitrate, silver nitrate and thallium nitrate, for example, can be used for the ion-exchange to provide the waveguide.

However, the inventors have discovered that the glass is etched significantly when exchange is done in an aluminum crucible in the open atmosphere of box oven. Therefore, according to the invention, it was discovered that performing the ion-exchange in a borosilicate, e.g., pyrex, crucible, as opposed to an aluminum crucible, greatly reduced the amount of surface attack and etching of the phosphate glasses caused by the KNO_3 ion-exchange melt. Further, improved control of the water content of the melt by baking the KNO_3 at a temperature of 120°C or more, preferably about 120°C , for a period of 24-48 hours in an inert argon atmosphere was achieved. Additionally, providing a SiO_2 buffer layer coating by sputtering or CVD deposition will reduce surface scattering losses.

The ion-exchange process results in a slightly buried waveguide with the highest index in the waveguide occurring slightly below the surface. This provides the additional advantage of reducing scattering loss. This advantage can be even further enhanced to provide a channel with a shape and size optimized for laser operation by conducting a field assisted ion-exchange process using an electric field, particularly an electric field varied as a function of time where the electric field is applied using a liquid sodium nitrate electrode or a solid silver electrode. The temperature can also be varied as a function of time for further tailoring of the index profile within the waveguide.

According to this embodiment, lasers prepared from ion-exchanged waveguides can achieve a high power of over 20 mW, particularly 25 to 180 mW and a high slope efficiency of 28% or higher (previous state-of-the-art in phosphate glass was 16 mW power and 27% slope efficiency by D. Barbier, et al., at Conference on Optical amplifiers and applications, 1995). Further, a high coupling efficiency of pump light from the optical fiber is enabled by the low index change caused by potassium-sodium ion exchange. High coupling efficiency of signal light to the optical fiber is also achieved due to the low index change caused by potassium-sodium ion exchange.

Glasses used as substrates for the above ion-exchange methods include sodium-aluminum-phosphate formulations such as the composition described above, additional

glasses are disclosed in, for example, U.S. Patent No. 5,334,559 and U.S. Patent No. 5,491,708. Particular applicability is found with glass formulations identified above in the category of rare earth doped sodium-aluminum-phosphate compositions, in particular having the Er/Yb ratio described above. Rare earth ions of choice include erbium and ytterbium, resulting in compatibility with currently commercially available, inexpensive, semiconductor pump lasers and emission within the telecommunications wavelength region about 1.5 μm , particularly 1.54 μm , ytterbium alone to result in laser sources at 1.0 μm , for use in standardized clock apparatus, and neodymium to result in preparing laser sources for small, localized optical networks at 1.06 μm and optical sensors and for gas detection. However, further examples of useful devices for the described ion-exchange process include glasses doped with other rare earth ions, for example, Pr lasers, Ho lasers, Tm lasers, as well as Dy, Sm, Eu and Tb lasers. Representative wavelengths are listed below in Table 4, see, also, Emmett, et al., *Physics of Laser Fusion*, Vol. IV, "The future development of high-power solid state laser systems", Lawrence Livermore National Laboratory, UCRL-53344, November 1982.

Table 4 - Approximate wavelength ranges of several lanthanide dopants

Er	1520 - 1610 nm
Yb	985 - 1250 nm
Pr	1300 - 1400 nm
Ho	2000 - 2200 nm
Tm	1600 - 2100 nm
Nd	860-900 nm, 1020-1100 nm, 1320-1390 nm

According to this embodiment of the invention preparation of small waveguide laser sources that produce high output power and that exhibit low pumping threshold levels and high slope efficiency for generation of laser emission compared to the prior art can be achieved, for example.

A further preferred embodiment of carrying out ion exchange, in the manner described above or otherwise, the inventors have discovered that carrying out the process in the absence of ambient atmosphere is advantageous due to the lessening of

surface etching due to reactions of the glass surface with water vapor in the ambient air. According to this embodiment of the invention, processing conditions that allow successful fabrication of waveguide structures in phosphate glass substrates by ion exchange technology without the substrate exhibiting signs of chemical attack that influence waveguide integrity or quality are described.

This embodiment of the invention relates to waveguide lasers that are capable of high power operation and that exhibit low pumping threshold levels and high slope efficiency. These waveguides are prepared in rare earth doped phosphate laser glasses using ion exchange technology. Two basic technologies are commonly employed. In the first, ions of one type are exchanged for ions of another type within selected regions of a glass surface. The ions are selected such that the refractive index within the desired waveguide is higher than in the surrounding substrate glass. Here, the ion source is from a molten bath, often described as a salt batch, into which the glass is submerged.

Common salt baths contain alkali salts such as potassium nitrate, sodium nitrate, and/or other salts such as silver nitrate. In addition to a requirement of higher index within the waveguide, a second criteria in salt bath identity selection is to select ions that are highly mobile within the glass structure and offer melting points consistent with acceptable diffusion rates and melting points of the employed salts.

In a second technique, the ions to be placed into the glass are first applied as a solid to one or more glass surfaces. Electrodes are then placed onto the glass surfaces (in some cases the ion source can also act as an electrode, for example in the case of silver ion exchange) and an electric field through the glass then assists in driving the ion exchange process.

Additionally, both types of ion-exchange techniques can be conducted to provide the desired waveguides.

Glasses used as substrates for the lasers of this invention are of a sodium-aluminum-phosphate formulation such as the compositions listed in, for example, U.S. Patent No. 5,334,559. A simple example of waveguide fabrication to produce a waveguide laser in phosphate glass is disclosed in U.S. Patent No. 5,491,708.

Phosphate glasses are typically characterized by inferior chemical durability, and are particularly susceptible to attack by acidic solutions and by direct water attack. This can be demonstrated by a review of chemical resistance tests on common commercial phosphate glasses, see for example the Schott Optical Glass Catalog. Water, although not strongly acidic in nature, attacks the phosphorous sites within the glass structure leading to the formation of a phosphoric acid film on glass surfaces which are then responsible for acid attack of the remaining glass.

Phosphate glasses also have inferior resistance to alkali. Examples of this phenomena are demonstrated in the Laser Glass Brochure from Schott. All of the phosphate laser glasses in the brochure have inferior alkali resistance when compared to the silicate laser glasses listed in the same brochure. Any OH^- existing in a salt bath can combine with the alkali ions present, such as K^+ and/or Na^+ , and form an alkaline solution that will attack the surface of a phosphate glass submerged in the salt bath for ion exchange.

Schott Glass Technologies (SGT) and the National Institute of Standards and Technology (NIST) have engaged in a collaborative research effort to develop advanced guided wave laser sources through the fabrication of small compact laser waveguides in rare earth doped phosphate laser glasses. These waveguides were prepared within the glasses by ion exchange technologies, including replacement of sodium ions within the substrate glass by either potassium ions or silver ions from the surrounding environment. The ion exchange locations were first defined by preparation of a mask that defined the waveguide regions, typically narrow stripes on the glass surface of width less than $50\text{ }\mu\text{m}$.

Although the phosphate glasses developed for this work are designed to exhibit good chemical durability and have been characterized to offer superior chemical durability than conventional state-of-the-art phosphate optical glasses, the need for further improvement was identified. Particularly, it had been observed that resultant waveguides were of poor optical quality. In particular, glass surfaces were observed to be stained with a white appearance to the eye. In addition, sections of the waveguides were found to exhibit at various times the following defects: a) narrowing of the waveguide width at unpredictable locations, b) widening of the waveguide at

unpredictable locations (independent of other defects), and c) depressed regions relative to the surrounding, unexchanged, glass substrate.

Although not intending to be bound by this theory, it was believed that a dominant mechanism for chemical attack of the phosphate glasses during ion exchange was by residual hydroxyl ions within the salt bath or trapped within the glass/electrode interface during field assisted ion exchange. The mechanism was as follows: OH groups from the surrounding environment enter the glass, breaking the basic phosphorous/oxygen back bone responsible for the glass structure, i.e.:



In moderate cases of attack, glass durability is further degraded by the loss of backbone structure. In severe cases of attack, phosphorous could even be expected to leave the glass and migrate to the surface, presenting the white appearance observed in many of the defects within prepared waveguides.

The dominant source of water in molten salt bath ion exchange processes was thought to be residual hydroxyl within the starting salts since these chemicals are inherently hygroscopic. Ways to deal with control of this water were considered: addition of agents to the salt bath to "tie up", including powdered aluminum, silicic acid, anhydrous aluminum oxide, diatomaceous earth, free P_2O_5 , halogen containing chemicals that would react with OH to form volatile halide gases, etc.; and, bubbling of a dry gas through the salt bath to achieve direct water removal (dehydration).

A second source of water is the ambient air within the ion exchange furnace. Here, effective corrective actions discussed were: purging the oven environment (preferably prior to, but also during salt bath insertion) while at elevated temperatures with a dry gas and isolation of the salt bath from the environment (since the refractory within most furnaces acts as a sponge for atmospheric water during periods of inactivity that is later released upon application of high temperature to the furnace).

A third source of OH groups can be actual adsorbed water on the surface of the glass part to be treated. Phosphate glasses are known to adsorb water onto their

surfaces from the atmosphere. Diffusion coefficients for water into phosphate glasses have been evaluated at several orders of magnitude higher than silicate glasses for the same measurement temperature. Such surface absorbed water can provide hydroxyl that can further re-react with glass surfaces during later processing, for example during field assisted ion exchange.

A number of measures were studied to understand, and control or eliminate the waveguide defects:

1) The current aluminum ion exchange crucible would be modified to allow possible bubbling of dry, and possible reactive, gases through the melt prior to insertion of glass substrates. The role of reactive gases was stressed during the meeting. Normal "dry" gases might quickly reach chemical equilibrium with the moisture in the salt bath, preventing the gas bubble to further dry the melt. A reactive gas within the melt (in particular, the use of chlorine) would react with water diffusing from the melt into the bubble, effectively maintaining the chemical gradient between the melt and bubble and allowing additional drying action to take place.

2) The ion exchange oven would be equipped with gas purge lines to pressurize the oven for purposes of moisture removal. Care would be taken to purge the oven before insertion of the salt bath since the oven refractory were considered as a major moisture source when heated.

3) Alternative crucible materials would be considered. In particular, Schott had reason to believe from trials to ion exchange phosphate glasses for purposes of chemical tempering that fused silica crucibles might offer improved performance in terms of chemical attack of treated glasses.

4) The addition of drying or other agents that could "tie up" hydroxyl groups in the melt was also discussed but no clear implementation plan was apparent at the close of the review meeting.

5) A fixture would be designed to allow placement and or removal of a preheated glass plate into a preheated and presumably dry salt bath without opening the oven to the surrounding ambient air within the ion exchange laboratory. This step would provide an opportunity to keep the glass/salt bath

system isolated from room air during the entire course of the ion exchange process.

6) Since molten salt baths are expected to accumulate hydroxyl, or other contamination with time from the surrounding environment and treated glass plates, salt baths would be changed more frequently, in particular upon first visual evidence of a defect problem.

The corrective steps described above make possible the preparation of waveguide laser sources without the occurrence of waveguide defects linked to chemical attack of the phosphate glass substrate. This should enable the easier commercialization of these waveguide sources. Without this invention, reproducible performance levels in devices fabricated in a large scale manufacturing environment would be expected to exhibit erratic performance and/or low yield with associated high manufacturing costs due to unpredictable chemical attack from residual hydroxyl groups with associated defect creation that impacted device performance.

Additional embodiments of this invention are directed to optical devices having multiple waveguides on a substrate. The processes described above, while also applicable to preparing singular waveguides and lasers based thereon, are additionally applicable in preparing substrates having multiple waveguides and lasers based thereon.

A substrate containing multiple waveguides can be provided by photolithographic techniques and ion-exchange methods discussed above. Both involve applying a mask over the substrate to define the channels which will constitute the waveguide. By applying a mask with multiple channels over the substrate, a substrate with multiple waveguides therein can be formed. Additionally, multiple waveguides having differing refractive indices, and thus capable of providing lasing at differing wavelengths when incorporated in a laser device, can be formed by applying a mask which defines channels of differing width. The resulting waveguides formed by photolithography or ion-exchange techniques will have differing widths and thus differing refractive indices and can, thus, be used in a laser device to provide a laser capable of operation at differing wavelengths depending upon which waveguide is pumped. In other words, the waveguides form laser-resonator cavities with distinct

resonance characteristics to provide a distinct lasing action at a selected wavelength when pumped. These waveguides can also be modified in any of the manners discussed above and below to vary their properties. The substrates used to provide the multiple waveguide devices are preferably based on the glasses discussed above.

5 Another embodiment of the invention is directed to modifying or tuning the wavelengths of a waveguide or waveguides in a substrate. This can be done by heating of the substrate which will alter the wavelengths of the waveguides therein. Where the substrate containing waveguide(s) is part of a laser device, it was expected that the heating thereof would increase the wavelength of the laser due to expansion of the diffraction grating periodicity. What the inventors have discovered, however, is that
10 for substrates containing solid state waveguides provided as channels in the substrate, as discussed above, heating has a fine tuning effect on altering the wavelength of the waveguide. Thus, for example, while semiconductor DFB lasers are increased in wavelength upon heating, the increase of wavelength upon heating of laser devices with waveguides according to this invention is significantly lower as a function of the
15 temperature, e.g., the increase of wavelength as a function of temperature is roughly 15 times lower than that for semiconductor DFB lasers. The inventors have discovered that while heating expands the glass increasing the wavelength, the extent of increase is offset by the temperature effecting a decrease of the refractive index with temperature of the glass forming the waveguide(s). The theory behind this and experiments
20 supporting it are described in the Journal of Non-Crystalline solids (JNCS) article attached as Paper E in the Appendix, particularly at page 14 and in Figure 14. According to the invention, therefore, the temperature control requirements for maintaining a stable wavelength are relaxed with the waveguides according to the invention, i.e., a variance in the temperature will not have as significant effect on the
25 tuning, allowing finer tuning thereof.

In another aspect of the invention it may be of advantage to fabricate active waveguide devices, either having one or multiple waveguides, that employ regions of active (for example, rare earth doped) and passive (for example lanthanum doped) glass
30 sections. This is preferably done by preparing the active and passive sections separately and bonding them together. Examples of the sections to be bonded together include the

single or multiple waveguide devices discussed above. There are a number of techniques possible to complete the bonding operation, including the use of UV or thermally curable epoxy adhesives available on the open market. There are other techniques that do not require adhesive materials, including a process wherein the parts to be bound are joined by a high temperature fusion process.

According to the invention, such bonded parts can be formed in the following manner. Glass blocks to be joined are first cut to a size suitable to yield one or more finished devices. The surfaces to be joined are then ground and polished. A high quality polish is not a requirement but is an advantage. However, simple grinding with 600 grit emery paper is adequate. Next, the samples are thoroughly cleaned using techniques well known in the optical industry. The surfaces to be joined are then placed in direct contact, forming a multiple laminate structure. A fusion of the glass pieces is then conducted by heating the entire assembly to a temperature above, generally about 100°C above, the glass transformation point, T_g , for a period of time to effect fusion thereof, preferably between 0.5 and 2 hours. The fused parts are then cooled, for example, to about 30°C above T_g , held there to allow thermal uniformity, for example for 2-4 hours, followed by a slow cooling ramp drop, e.g., of 30°C to 50°C, to room temperature. The joined fused parts can then be cut, ground, and polished as needed. The waveguide can be provided in the fused blocks before the fusion takes place, in which case they must be aligned to be in communication, or the waveguide can be provided in the fused block after fusion thereof.

For a glass such as NIST-1T discussed above, the glass transformation point, T_g , as measured by dilatometry is 474°C. Consequently, a good fusion temperature is 575°C to 590°C, with controlled cooling onset point of about 500°C. Note that the softening point of the NIST-1T glass is in the range of 560°C to 565°C. It is thus equivalent to say that the fusion is performed at a temperature above the softening point of the glass.

One disadvantage of the fusion process is that the joined parts need to be closely matched in thermal expansion and in T_g , e.g., in the range of $\pm 30^\circ\text{C}$ for T_g and in the range of ± 1 to $\pm 10 \times 10^{-7}/\text{K}$ in thermal expansion. Higher mismatches in thermal expansion lead to high levels of residual stress at the glass/glass boundary points due to unequal thermal contraction during the cooling of the joined assembly to room

temperature. This criteria is readily satisfied by substituting lanthanum for the active rare earth ions in the NIST-1T glass to prepare the passive material. In this way, the changes in these properties are minimized without altering the sodium-aluminum-phosphate base glass composition. If necessary, the base composition can also be modified to bring the

5 Tg and thermal expansion values closer, but this can be done without seriously altering the ion exchange properties so that waveguide fabrication in both the passive and active portions of the prepared assembly can be conducted with minimal adjustment to accommodate different diffusion properties that could alter ion exchange behavior.

Waveguides prepared in accordance with any of the above descriptions, having

10 multiple or single waveguides of the same or differing wavelengths, are useful in preparing lasers by providing the waveguide with a grating pattern. Examples of methods for producing lasers from waveguides of the type discussed above are provided in the Papers A, B and C provided in the attached Appendix, which are incorporated herein by reference. These references also discuss methods generally applicable to

15 production of waveguides and those teachings are additionally incorporated by reference herein. In general, lasers are fabricated from the waveguides by providing a reflecting element at both ends of the waveguide. The reflecting elements can be those known in the art. Included as embodiments are waveguides having optically polished ends provided with mirrors on both ends. An additional preferred

20 embodiment, is providing the waveguide with a diffraction grating on one end of the waveguide. In a preferred embodiment, the grating is provided by etching onto the glass substrate containing the waveguide(s). One preferred type of grating is a DBR grating as known in the art. Such gratings are advantageous because they provide a narrow reflection line and thus provide a laser with a narrower wavelength.

25 One embodiment provides making the photoresist grating by evaporation of a chromium coating with the specimen inclined 60 degrees to the normal of the evaporation source beam. This results in a hard metal coating on the tops of the photoresist bars that constitute the grating and thus allows a more selective sputter etch of the grating and the use of higher DC bias voltages for the etching process.

30 One embodiment provides a DBR grating exposure in standard photoresist using an optical phase mask. Additionally, providing a SiO₂ buffer layer coating by

sputtering or CVD deposition will reduce surface scattering losses. While it is difficult to get standard photoresist to properly adhere to phosphate glasses, application of sputter deposited SiO₂ on the surface of the phosphate glass, e.g., 1-2 nm, will greatly improve adhesion of the photoresist during processing.

5 One embodiment provides for actively monitoring the diffraction efficiency of the photoresist grating mask during photoresist developing. This optimizes the contrast of the photoresist grating and thereby provides for enhanced etch selectivity.

 One embodiment provides etching of the grating by Ar-ion sputtering in a standard Reactive-Ion-Etching system. No CFC (chlorinated fluoro-carbon) emissions, as with reactive-ion-etching of silica glass, are observed.

10 One embodiment provides many gratings that are exposed in photoresist fabricated on each single glass chip on a wafer in a single exposure using a silica plate that has multiple pitch phase masks printed on it.

 One embodiment provides a nearly sinusoidal grating without excess loss due to improved isotropic plasma etching using only Argon gas at low pressure.

15 One embodiment provides an isotropic etching in an argon ion plasma leaving a smooth surface resulting in lower grating scattering losses.

 One embodiment provides each grating with accurate line width control due to phase mask exposure of photoresist and control of differential linewidth using phase masks with more than one period on a single substrate.

20 One embodiment provides a laser wavelength that is selected by printing a single pitch grating over an array of optical waveguides with each waveguide in the array having a different refractive index.

 One embodiment provides a laser wavelength that is selected by fabricating a single pitch grating on an array of identical optical waveguides where each waveguide crosses the grating at varying angles.

25 One embodiment provides a mode field shape and size that is optimized for laser operation using a field assisted ion-exchange process where the electric field is varied as a function of time.

In one embodiment, the invention can provide a monolithic single-frequency waveguide laser in a spectroscopically superior phosphate glass, for example, with an initial laser linewidth was 500 kHz.

5 The present invention provides predictable emission wavelength if effective index of the waveguide is known.

The present invention provides high power, e.g., up to 80 mW (previous state-of-the art for an Er-doped DBR laser was ~ 2 mw by Technical University of Denmark Microelectronic Centret. Technology was sputter deposited silica doped with Er).

10 The present invention demonstrates a Yb/Er-doped phosphate glass laser using a DBR surface relief grating. The previous best device like this utilized an external fiber grating and produced power of 2.2 mW at 70 mW coupled pump power by A. Yenyay, et al., Lehigh University & Lucent, April 29, 1997 in IEEE Photonics Technology Letters. This Yenyay demonstration did not operate as a single frequency laser.

15 The present invention provides high slope efficiency of 26 percent (previous state-of-the-art for similar devices was about 11 percent by Yenyay, et al., Lehigh University & Lucent).

The following provides some specific embodiments of features discussed above, however, the invention is in no way limited thereto.

20 The present invention provides a process for forming waveguides onto (or into) the surface of a glass substrate. In one embodiment, photo-lithographic techniques define waveguides by changing the index of refraction of waveguide channels formed into the surface of the substrate. In one such embodiment, a glass wafer, approximately 10 cm by 10 cm by 1 mm is cut from a slab of IOG-1 laser glass
25 available from Schott Glass Technologies, Inc., of Duryea, PA, USA. The surfaces of interest, including a "top" major surface (where "top" refers to an orientation and not necessarily to the placing of the device as used in operation) are polished to optical smoothness. The glass wafer will have a plurality of segments according to one embodiment of the present invention.

In one embodiment, the top surface of the wafer will be processed to form a large number (e.g., in one embodiment, one hundred devices) of individual segments (each forming an optical system) which will be diced apart and individually packaged. For example, in one embodiment, each segment is a portion of the wafer diced to about 1.5 cm by 0.5 cm.

Another embodiment is directed to segment having forty laser waveguides organized in eight sets. The segments may be processed, for example, according to one of the methods described in Paper A, Paper B, and/or Paper C of the Appendix, to form a plurality of sets (e.g., in one embodiment, each set has five waveguides; and in another embodiment, each set is used such that one waveguide is used, and the other four provide redundancy in case one or more do not function properly). In this embodiment, each set is overlaid with a diffraction Bragg reflector (DBR) which forms one mirror of a laser, and each DBR is fabricated to a different spacing designed to resonate at a different output wavelength. In one embodiment, only eight of the forty waveguides are used for eight respective lasers; the others are provided for redundancy. Thus, the DBR for one set is designed such that all five waveguides of that set will lase at the same wavelength, and any one of these waveguides can be used as the laser for the desired wavelength of that set. However, each of the DBRs are designed for a different output wavelength. Thus the segment is designed to provide eight lasing waveguides each outputting light at one of eight predetermined wavelengths that are tuned by the eight DBRs. In one embodiment, an input mirror (e.g., a multi-layer dielectric mirror) is deposited on an end face of segment opposite the DBRs. In other embodiments, an external mirror is placed against that face to provide the feedback function desired for lasing and the pump-light-launching function. The input mirror is designed to transmit as much light as possible at the pump wavelength (in one embodiment, 0.98 micrometers), while reflecting as much light as possible at the output wavelength (in one embodiment, a selected wavelength near 1.54 micrometers as tuned by the corresponding to the DBR). In one embodiment, the segment is used in a communications system that uses dense wavelength-division multiplexing (DWDM), wherein, for example, forty different wavelengths are each modulated to carry a different channel of information, and then all forty channels are passed on a single optic

fiber. In one such embodiment, each channel's wavelength differs from the next channel's wavelength by 0.8 nanometers. Thus, for example, a segment could be designed to output laser light at wavelengths of 1.5360, 1.5368, 1.5376, 1.5384, 1.5400, 1.5408 and 1.5416 micrometers. Other segments of a system could be designed to lase at eight other channel wavelengths. Thus, a forty-channel system only needs five such different part numbers (i.e., unique part designs), rather than forty different part numbers in conventional approaches.

In another embodiment a segment is used as part of a multi-wavelength laser source. In this embodiment, a pump light source (for example, a semiconductor laser diode lasing at about 0.98 micrometers; this source can even be very "noisy," emitting a range of frequencies from perhaps as low as 0.96 and as high as 1.00 micrometers, and still provide a suitable source for laser emitting at e.g., 1.5360 micrometers) is coupled through a suitable launch-end mirror by butting against the end of a selected waveguide of a set of waveguides. In one such embodiment, eight pump laser diodes are used. At the other end of the segment, eight optic fibers are held by an alignment block, such that each respective fiber is optically coupled to the emitting end of the top or first waveguide of the eight respective sets. If any one of the first waveguides is non-functional, the alignment block can be moved down to couple to the next waveguide of the eight sets.

In another embodiment, a segment is used as part of another multi-wavelength laser source with the output fibers connected to the middle waveguide of each set of waveguides. A different pumping mechanism can be used wherein each pump is coupled through a lens (which can be a conventional convex-type lens or a diffraction or holographic lens) that helps concentrate the light from the pumps into the waveguides.

In another embodiment, a segment is used as part of a single-wavelength laser source. This embodiment provides a single output wavelength selected from the eight available. This embodiment also provides an optical fiber for coupling light from a pump laser diode into the desired waveguide. It is to be understood that any of the above pump-coupling methods and apparatus could be used in the other discussed embodiments.

5 In another embodiment, a segment having a laser comprising a waveguide, DBR mirror and optional input mirror is provided. The single laser has an external launch mirror. Other embodiments include redundant waveguides all operating at a single wavelength, other waveguides each having a DBR tuned to a unique wavelength, or both, all integrated on a single segment.

10 In another embodiment, a packaged device that includes a segment according to one of the other embodiments of the present invention is provided. The device includes a hermetic package, and is pumped, in this embodiment, by a fiber, and coupled to an output fiber. While this embodiment includes a laser as described above, it is otherwise a passive device. Such a device takes a pump light input, which can be noisy as described above, and outputs a "clean" laser output light at a different frequency, wherein the output is stable and has a very narrow wavelength spectrum.

15 In another embodiment an integrated device that includes a segment according to one of the other embodiments of the present invention is provided. The device includes active components such as a pump laser diode, a photodetector (e.g., a light-sensing diode), a thermistor and electrical connections between and to these components. Some embodiments also include a temperature maintaining device (such as a resistor or thermo-electric device to heat and/or cool device) in order to maintain a constant temperature. Some embodiments also include an output modulator to
20 encode information on the output light. Some such embodiments also include an output combiner to combine the modulated light into a single fiber.

In another embodiment, a laser using direct (butt) coupling of pump laser diode to a segment as described in other embodiments is described.

25 In another embodiment, a top laser using lensed coupling of a pump laser diode to a segment according to one of the embodiments of the present invention is provided.

Lasers incorporating waveguides according to the invention have potentially narrower line widths than current state-of-the-art semiconductor lasers primarily because of the long upper state lifetime of the Er laser manifold in phosphate glass. The Schallow-Townes relationship gives an ultimate limit for solid state lasers of less
30 than 1 Hz compared to approximately 10-100 kHz for diode lasers. The lasers of this

invention have been demonstrated to have line widths of less than or equal to 500 kHz, much better than the typical 1 MHz laser line widths for standard WDM lasers sources used today.

5 The relative intensity noise (RIN) of solid state waveguide lasers is a distinct advantage over semiconductor lasers for analog fiber telecommunications. This is especially true as analog modulation frequencies increase to multi-GHz transmission rates as is expected to become common place in the near future. The only excess contribution above the shot noise photon statistics is the relaxation oscillation peak which occurs around 500 kHz. Beyond 500 kHz, the RIN drops rapidly in waveguide
10 lasers. This, combined with high glass saturation power, means very low noise lasers can be achieved. In contrast, semiconductor lasers typically have relaxation oscillations between 3 and 10 GHz, which is a potentially important frequency range for optical analog communications.

15 There are advantages of putting the DBR grating within a passive section of glass attached to the active glass containing the laser waveguide. This is because when the pump light reaches the DBR grating, it is not reflected but is instead coupled out of the waveguide at an acute angle, thus the pump light intensity gets depleted very rapidly as it traverses in the DBR grating. If the DBR grating were prepared in erbium doped glass, the resultant population of excited erbium ions within the active glass inside the
20 DBR grating leads to an increase in the spontaneous emission noise. And also introduces a loss within the laser cavity which reduces the efficiency.

Another embodiment of this invention is the fabrication of a single-frequency 1.32-1.4 um laser in Nd-doped phosphate glass fused to La-doped glass, as shown in Figure 2. In this invention, a waveguide is fabricated in the Nd-La fused substrate
25 using the ion exchange process described above. A DBR grating is written in the La section of the substrate. It is necessary to write the DBR grating in the passive section of the substrate since Nd acts as a three level laser system near 1.3 um. Such a design minimizes loss and noise as described above and thus increases the efficiency of the laser. The period of the grating is fabricated to be such that it reflects a single
30 wavelength in the range of 1.32--1.4 um thus produces a single frequency laser in this range. Many water absorption peaks occur in this region of the optical spectrum,

therefore such a laser could be used as a high power laser source for the detection of low level water concentration in high purity gases.

5 Finally, the glass waveguide lasers discussed here will not suffer at all from wavelength drift as in semiconductor lasers. As a semiconductor laser ages, the high optical intensity in the laser cavity causes a change in the index of refraction of the semiconductor material, and consequently a change in the optical characteristics of the laser cavity that results in the wavelength of the laser drifting over time. At some point, the change in the material is so severe that a longitudinal mode hop occurs that causes a large wavelength shift since longitudinal modes in semiconductor lasers have large frequency spacing. When such a event occurs in a WDM network, the effect is usually catastrophic and may bring down the whole network for a short time while the problem source is isolated. This effect is not well studied in phosphate glasses but our intuition is that the effect will not be large. Since the longitudinal modes are also very close (within WDM channel tolerances) mode hopping will not be as severe an effect if aging does in the phosphate glass.

15 Thus, the devices described here are capable of replacing current semiconductor based laser sources for application in telecommunications and data transmission applications within the 1.5 um telecommunications band. Output powers exceed that required (20 mW) when pumped with inexpensive 980 nm class pump lasers available on the market today.

20 The devices described can also provide small, compact laser sources for localized optical networks operating at either 1.5 um or near 1.0 um through the use of erbium and neodymium rare earths respectively. In particular, the inventors foresee the need for inexpensive, compact, efficient sources at 1.0 um for use in localized networks within individual aircraft, automobiles, seacraft, etc. Here, the short distance for optical transmission allows the use of conventional optical fiber (that is optimized at 1.3 um and 1.5 um but suffers from dispersion issues at 1.0 um) without accumulated distortion from dispersion effects, in combination with the additional advantage of employing less costly, and easier to operate and maintain than detectors at 1.3 um or 1.5 um, detectors that are sensitive at 1.0 um.

A wide variety of rare earth species and combinations of species can be supported in the glass formulations of this invention. Combined with the laser structures of this invention, a number of laser wavelengths can be made available as coherent light sources for diagnostic and spectroscopic analysis completed with optical techniques.

The entire disclosure of all applications, patents and publications, cited above and below, as well as of U.S. provisional application no. 60/117,477 filed January 27, 1999, and U.S. provisional application no. 60/162,458 filed October 29, 1999, from which this application claims priority are hereby incorporated by reference in their entirety.

Examples

In the foregoing and in the following examples, all temperatures are set forth uncorrected in degrees Celsius; and, unless otherwise indicated, all parts and percentages are by weight.

Example 1: Er/Yb ratio

An Er:Yb-codoped glass having 1.15 wt% Er_2O_3 and 4.73 wt% Yb_2O_3 and a high phosphorous content named NIST-1T, shown in Table 2, was prepared as follows. Chemical compounds were weighed in the proper amounts to produced the desired composition and melted within a fused silica crucible at temperatures in excess of 1200°C to produce vitrified material of limited optical quality, referred to as cullet. To obtain glass of high optical quality for use in laser fabrication, this cullet was then remelted within a platinum crucible at temperatures of 1200°C to 1300°C. Once this melting was complete, the glass melt was stirred and refined at temperatures up to 1400°C for three hours prior to casting the molten glass into a steel mold. The cast glass was annealed at 530°C for two hours before being cooled to room temperature at a cooling rate of 30°C/hr.

Table 2 – NIST-1T Example Composition

	Oxide	Mole%
5	P ₂ O ₅	60
	Al ₂ O ₃	13
	Na ₂ O	24
	La ₂ O ₃	1.1
	Er ₂ O ₃	0.4
	Yb ₂ O ₃	1.5

10 The glass casting produced was first cut to yield characterization samples with the following property results:

Table 3 – NIST-1T Property Characterization Results

	Property	Expected Result	Measured Result
15	Nd	1.523 ± 0.003	1.52100
	Vd	67.53 ± 0.05	67.50
	density, ρ [gm/cm ³]	2.74 ± 0.03	2.74
	Absorption at 3.0um [cm ⁻¹]	< 2.0	1.20

20 Based on these measured properties, in comparison to the expected results known from prior melts of this glass composition, the proper chemical identity of the prepared glass was assured. It is common practice in the glass industry to have high confidence that the composition is that intended when the index, nd, Abbe number, vd, and density, ρ, agree with expected values within the tolerance ranges indicated in Table 3. The measured optical properties and the measured density value combined with the recorded input weights of rare earth species into the glass allowed the calculation of the following additional properties:

25 Table 4 – NIST-1T Calculated Property Results

Property	Desired Result	Calculated Result
Yb ³⁺ content [10 ²⁰ ions/cm ³]	4.0 ± 5%	3.97
Er ³⁺ content [10 ²⁰ ions/cm ³]	1.0 ± 5%	0.99
Refractive Index at 1.54um	no particular value	1.511

5 The rare earth contents values were verified in this manner. Thirty-eight glass plates were then prepared from the remaining glass from the produced casting. Each plate measured 50mm x 50mm x 2mm in thickness and was polished on the 50mm x 50mm faces with a high quality polish normally applied to Schott's commercial filter glass product line.

Waveguide lasers were fabricated in the NIST-1T phosphate glasses. Waveguides were formed by K^+-Na^+ exchange through channel apertures ranging in width from 3 to 8 μm . The apertures were etched in a 200 nm thick Al mask layer. Standard metal deposition and microlithography techniques were employed to form the waveguide mask. The exchange was performed in a shallow aluminum crucible containing molten KNO_3 at 375 °C for 4 hours in a box furnace.

15 The ion exchanged specimens were blocked with a similar glass using glycothalate wax and were diced using an automatic wafer dicing saw that employed a resonoid blade. The specimens were cut to a dimension of approximately 2.2 cm x 1 cm. The waveguides were parallel to the 2.2 cm long dimension. The waveguide end facets were polished roughly using Al_2O_3 powder grits of 25 μm size and 9 μm size on flat glass lapping blocks. After the rough polish, the final polish was done using a mixture of cerium oxide and water which was dispensed onto soft lapping material on an automatic polishing machine. After polishing was completed, the samples were deblocked in acetone by the process of ultrasound.

20 Several measurements were performed to determine the properties of the ion exchanged waveguides. The refractive index as a function of position within the sample was analyzed using the method of refractive near-field scanning. The dimensions of transverse modes of the waveguides were measured by coupling light into one end of the waveguide and imaging the light emerging from the other end onto a calibrated infrared camera.

25 To test the Yb/Er-codoped lasers, we typically pumped the waveguides using a tunable $Ti:Al_2O_3$ laser. Figure 1 shows a schematic of the laser measurement setup. Placing broadband dielectric mirrors on the polished waveguide end faces formed the laser cavities. The mirrors were held in place by small spring clips with index matching oil between the end facet and the mirror. The pump laser light was launched

30

through one of the mirrors with a 4X microscope objective. The laser output and unabsorbed pump light were collimated with a 16X microscope objective and separated using filters. The mirror through which the pump light was launched had a reflectance of >99.9 % and 15 % at 1540 and 960 nm, respectively. The output coupler had a reflectance of 80 % at 1540 nm and 15 % at 960 nm. Neither the waveguide length nor the cavity output couplings were optimized. Additional information for this example can be found in the JNCS article provided as Paper D in the attached Appendix.

The unique set of rare earth content in melt NIST-1T was employed to demonstrate higher output power (up to 180mW compared to a prior high of only 16 mW) and higher slope efficiency (of at least 28% compared to a prior high of 27%) than observed in the prior art, see Barbier, D., et al, Integrated Optics and Optical Fibre Communications, 11th International Conference on, and 23rd European Conference on Optical Communications (Conf. Publ. No.: 448) on Pages: 41 - 44, Vol. 4.

Example 2: Ion-Exchange

Waveguide lasers were fabricated in Yb/Er-codoped and Yb-doped IOG-1 (equivalent to NIST-1T and NIST-1X) phosphate glasses, discussed in Example 1. The Yb/Er glass was doped with 1.15 wt % Er_2O_3 (1.0×10^{20} ions/cm³) and 4.73 wt % Yb_2O_3 (4.0×10^{20} ions/cm³). For the Yb-doped laser, the glass was doped with 4.73 wt % Yb_2O_3 (4.0×10^{20} ions/cm³). Waveguides were formed by K^+ - Na^+ exchange through channel apertures ranging in width from 3 to 8 μm . The apertures were etched in a 200 nm thick Al mask layer. Standard metal deposition and microlithography techniques were employed to form the waveguide mask. The exchange was performed in a shallow aluminum crucible containing molten KNO_3 at 375 °C for 4 h in a box furnace. The initial ion exchanges took no steps to avoid the interaction of water vapor or oxygen with the ion exchange solvent. Subsequent experiments revealed that this process was not reliable in terms of repeatability and waveguide laser yield. The ion exchanged specimens were blocked with a similar glass using glycothalate wax and were diced using an automatic wafer dicing saw that employed a resonoid blade. The specimen was cut to a dimension of approximately 2.2 cm x 1cm. The waveguides

were parallel to the 2.2 cm long dimension. The waveguide end facets were polished roughly using Al_2O_3 powder grits of 25 μm size and 9 μm size on flat glass lapping blocks. After the rough polish, the final polish was done using a mixture of cerium oxide and water which was dispensed onto soft lapping material on an automatic polishing machine. After polishing was completed, the samples were deblocked in acetone by the process of ultrasound.

Several measurements were performed to determine the properties of the ion exchanged waveguides. The refractive index as a function of position within the sample was analyzed using the method of refractive near-field scanning. The dimensions of transverse modes of the waveguides were measured by coupling light into one end of the waveguide and imaging the light emerging from the other end onto a calibrated infrared camera.

To test the Yb/Er-codoped Fabry-Perot lasers (lasers with no etched gratings), we typically pumped the waveguides using a tunable $\text{Ti}:\text{Al}_2\text{O}_3$ laser. Figure 1 shows a schematic of the laser measurement setup. Placing broadband dielectric mirrors on the polished waveguide end faces formed the laser cavities. The mirrors were held in place by small spring clips with index matching oil between the end facet and the mirror. The pump laser light was launched through one of the mirrors with a 4X microscope objective. The laser output and unabsorbed pump light were collimated with a 16X microscope objective and separated using filters. The mirror through which the pump light was launched had a reflectance of $>99.9\%$ and 15% at 1540 and 960 nm, respectively. The output coupler had a reflectance of 80% at 1540 nm and 15% at 960 nm. Neither the waveguide length nor the cavity output couplings were optimized.

A Yb-doped waveguide laser was tested using a setup similar to the one shown in Fig 1. The Yb^{3+} device was 10 mm in length. The pump-input mirror had a reflectance of 50% at 950 nm and 98% at 1030 nm. Two output couplers with transmittances of 7% and 21% at 1020 nm were investigated. These output couplers had reflectances of 32% and 34% at 950 nm, respectively.

Example 3: Crucible ion-exchange Protected from Ambient Environment

Using a sealed Al crucible that was designed by David Funk for the purpose of electric-field assisted ion exchange using liquid nitrate contacts on both sides of the wafer, indications of defect-free glass after ion exchange were observed. The was
5 corroded around the edges where the polished Al to glass seal leaked, but was defect and corrosion free in the interior where little air was leaked into the chamber. Subsequent experiments led to sealing a crucible with a graphite gasket material that was air tight. This led to a repeatable demonstration of defect free/corrosion free ion exchange in NIST-1 (IOG-1) phosphate glasses.

10 While the process has not completely eliminated corrosion of the glass in the region of the waveguides, the remaining corrosion is mitigated and uniform and also rinses away in the etching material used to etch the Al mask from the samples.

Example 4:

An array of monolithic, single-frequency distributed-Bragg-reflector (DBR)
15 waveguide lasers has been successfully demonstrated operating near 1536 nm wavelengths. The lasers were fabricated by forming waveguides in Yb/Er co-doped phosphate glass by ion exchange. The slope efficiency for each laser as a function of launched pump power is 26% and the thresholds occur at 50 mW of launched pump power. An output power of 80 mW was achieved with 350 mW of coupled pump
20 power. Each laser exhibits stable operation on a single longitudinal mode and all have linewidths less than 500 kHz. A comb of waveguides with varying effective indices allows the selection of wave length using a single-period grating.

The description is the first reported monolithic, single-frequency DBR, waveguides lasers in $\text{Yb}^{3+}/\text{Er}^{2+}$ -co-doped phosphate glass. Over the past several years,
25 the growth in the demand for telecommunications bandwidth generated by new telecommunications services, cable television (CATV), and data communication has drive the rapid development of wavelength division multiplexing (WDM) where information is simultaneously transmitted on several different wavelengths in the same optical fiber channel. The development of WDM systems has placed demands on laser

sources that are difficult to meet using existing technologies such as semiconductor distributed feedback (DFB) lasers. Issues of concern for such systems include wavelength selectivity, wavelength stability over laser lifetime, tunability, process yield, power limitations, and costs.

5 Integrated, single-frequency, solid-state lasers using the Er^{3+} ion offer a very promising and competitive alternative to DFB lasers for use in future WDM communications systems and for CATV. Several demonstrations of the waveguide and fiber laser technology have been discussed in the literature. One primary advantage of solid-state waveguide lasers is that they offer the possibility for arrays of lasers
10 operating on many wavelengths on a single glass chip. Rare-earth-doped waveguide lasers can also provide kilohertz linewidths with high radiance, low noise, and easy coupling to optical fibers.

Single-transverse-mode waveguides at 1535 nm wavelength were fabricated in a commercially available phosphate alkali glass that was co-doped with 0.99×10^{20}
15 ions/ cm^3 and 3.97×10^{20} Yb^{3+} ions/ cm^3 .^{7,8} Phosphate glass is a very good host material for ytterbium and erbium ions since the sensitization efficiency is nearly unity and large doping concentrations are possible before the onset of concentration quenching. The guides were formed by ion exchange of K^+ for Na^+ using line apertures 3 to 8 μm wide etched in a 200 nm thick aluminum mask layer. The exchange time was 4 hours in an
20 aluminum crucible containing molten KNO_3 at 375°C. Inspection of the samples using refractive near-field scanning after the ion exchange revealed that the regions of the glass surface corresponding to the location of the mask openings had become recessed by approximately 1 μm during the exchange process. The mechanism behind the etching of the glass during the exchange is currently under investigation, and it is
25 thought that it is caused by residual water in the hygroscopic nitrate melt. The surface quality of the glass in the recessed regions, as observed using a 1000x Nomarski contrast microscope, appears identical to the original surface of the glass and apparently does not cause significant scattering losses.

The waveguide end faces were polished perpendicular to the channels. The
30 length of the waveguides prior to the grating fabrication step was 2.2 cm. Measurements of the waveguide mode-field dimensions showed that a single transverse

mode was supported in each of the waveguides. For the guide formed with the $6.5\text{ }\mu\text{m}$ mask aperture, the $1/e$ full-widths of the mode-field intensity were $16\text{ }\mu\text{m}$ wide by $11\text{ }\mu\text{m}$ deep at $1.54\text{ }\mu\text{m}$ wavelength. It supported multiple transverse modes at the 977 nm pump wavelength. However, when the device was lasing, the pump energy was confined primarily within the lowest-order transverse mode, which had $1/e$ dimensions of $13\text{ }\mu\text{m}$ wide by $9.5\text{ }\mu\text{m}$ deep. All measurements of the intensity profile are within an estimated experimental error of $\pm 10\%$.

A DBR surface relief grating was fabricated holographically in a $0.5\text{ }\mu\text{m}$ thick layer of Shipley 1805 photoresist using a 90° corner that split a collimated laser beam into two beams. The corner was mounted on a rotation stage so that the angle of the two beams could be varied. One surface of the corner was a mirror, and the other surface was a vacuum chuck for holding the sample. Light from a 457.8 nm Ar-ion laser was spatially filtered by focusing through a $15\text{ }\mu\text{m}$ pinhole using a $20\times$ objective lens. The beam was collimated using a 76 mm diameter lens with a 350 mm focal length. The exposure angle was set to write a grating with a pitch of $\Lambda = 507.8\text{ nm}$. For a waveguide with estimated effective index of 1.515 ± 0.003 , this pitch should provide laser operation at $\lambda = 1538.6\text{ nm} \pm 3\text{ nm}$. The exposure time for the photoresist was 18 s with 3.85 nW incident in each arm of the 0.44 cm^2 exposed region (0.8 cm long \times 0.55 cm wide). The grating was developed in undiluted Shipley CD-30⁸ developer. During the development, the diffraction of light from a 632.8 nm HeNe laser was monitored. When the first-order diffracted power reached a peak, the grating was removed, rinsed, and dried.

Before the DBR grating was formed by transferring the photoresist pattern into the glass by Ar-ion sputtering, 40 nm of Cr was deposited on the surface with the specimen inclined 60° to the electron-beam evaporation source. Mounting the specimen in this way causes Cr to accumulate only on the tops of the grating lines and not in the grooves, thus providing a durable etch mask. The grating was etched in the glass for 20 minutes using a reactive ion etching system with a 6.67 Pa (50 mTorr) Ar-ion plasma. The low-pressure plasma created a large self-bias voltage of 1700 V when running at 365 W of coupled power with frequency 13.5 MHz . The electrode spacing was 3.2 cm . After etching, the sample was cleaned ultrasonically in photoresist

stripper at 85°C. Fig. 1 of Paper D in the Appendix is an illustration of the completed DBR laser array.

The waveguide laser cavities were formed by placing a thin, highly reflecting (R=99.9% at 1540 nm, R=15% at 997 nm) dielectric mirror on the pump input facet. The mirror was held in place by a spring clip, and index-matching fluid was used between the mirror and the waveguide facet. The DBR grating was used as the laser output coupler. We tested the laser by coupling light from a Ti-Al₂O₃ laser turned to a wavelength of 977 nm using a 4x objective lens with a numerical aperture of 0.1. The launching efficiency was estimated to be between 65 and 71 percent. To determine the launching efficiency we measured the Fresnel reflectance of the input mirror, the loss of the launching objective, and the excess coupling loss. Fig. 10 of Paper D in the Appendix shows the laser output power as a function of launched pump power and the spectrum of the laser. The waveguide diffusion aperture for this waveguide was 8 μm. The slope efficiency as a function of launched pump power is calculated to be 26 percent when we take the coupling factor to be 71 percent.

We estimated the reflectance of the grating using the simplified laser formula derived from the theory of Rigrod:

$$\frac{P_1}{P_2} = \frac{1 - R_1}{1 - R_2} \frac{R_2}{R_1}$$

where P_1 is the output power at the grating end and P_2 is the output power at the end opposite the grating. R_1 is the grating reflectance and R_2 is the reflectance of the attached mirror. We used two mirrors with reflectances of 80 and 90 percent for R_2 . For both cases, we calculated the grating reflectances, R_1 , to be 65 percent.

To investigate the longitudinal mode structure of the laser we coupled the laser output into an optical fiber scanning Fabry-Perot interferometer with a free spectral range of 124 GHz. Fig. 11 of Paper D in the Appendix shows that the laser operated on a single longitudinal mode when the coupled pump power did not exceed 300 mW. The laser was robustly single frequency with TE polarization, and no mode hopping was observed. The inset in Fig. 11 shows that a second longitudinal mode appeared

when coupled pump power exceeded 300 mW. In this pump regime, the laser was unstable and exhibited mode hopping, single-frequency operation, and dual-frequency operations. By measuring the frequency spacing between the longitudinal modes we determined that the physical length of the laser cavity was 1.4 cm.

5 We measured the linewidth of the laser using a conventional self-heterodyne configuration with a 75 MHz frequency shift. The path length difference between the two arms was 10 km corresponding to linewidth resolution limit of 30 kHz for a gaussian line shape. Optical isolations were used in both arms to prevent optical linewidth narrowing due to feedback; however, the output end of the laser was not
10 beveled. Fig. 12 of Paper D in the Appendix shows the self-heterodyne spectrum. The laser linewidth we obtained from this measurement was 500 kHz.

Finally, we measured the laser wavelengths of other waveguides on the chip using an automatic spectrum analyzer with a resolution of 0.1 nm. Seven of the eleven waveguides on the chip exhibited laser oscillation. The waveguides formed through the
15 smaller apertures did not achieve threshold because the smaller mode volumes caused a reduction of the gain such that the 45 percent transmittance loss of grating could not be overcome. Fig. A5 in Paper A of the Appendix shows the change in wavelength trend as we scanned the waveguides. The wavelength increases as the diffusion aperture width increases, which is consistent with increasing effective index as the
20 aperture width increases.

This example has demonstrated an array of high power, robustly single-frequency, integrated, DBR waveguide lasers operating near 1536 nm wavelength. The slope efficiencies of the lasers are 26 percent based on launched pump power, and the threshold is less than 50 mW when pumped at a wavelength of 977 nm. The linewidths
25 of the lasers were measured to be 500 kHz, and the outputs were linearly polarized in a TE mode. We are currently investigating the temperature stability of the lasers and the relative intensity noise (RIN). We expect that with diode laser pumping, the RIN will be similar to other results presented for single-frequency fiber lasers and will fall below - 150 db/Hz above 10 MHz. We anticipate that the output power and efficiency
30 will increase and the threshold power will decrease when the grating reflectance is increased. This is possible with only minor adjustments to the grating fabrication

process. Further improvements will also be realized by directly coating the high reflector onto the waveguide end facets. We have shown that lasers with several output wavelengths can be integrated on a single glass substrate. This example shows that stable, multi-wavelength, WDM sources with wavelengths falling on the International Telecommunications Union (ITU) grid can be realized by writing several gratings of varying period in Yb/Er-co-doped glass waveguides formed by ion exchange.

Example 5:

Compact solid-state lasers based on the $1.5\ \mu\text{m}$ Er^{3+} transition hold promise as sources for optical fiber communication systems. Yb^{2+} is commonly used as a sensitizer in Er^{3+} lasers because it has a much larger absorption cross section near 980 nm than Er^{3+} , and it efficiently transfers its excited state energy to the upper level of the Er^{3+} laser. The $\text{Er}^{3+}/\text{Yb}^{3+}$ glass waveguide laser, in particular, has several advantages over lasers in Er^{3+} -doped or $\text{Er}^{3+}/\text{Yb}^{3+}$ -co-doped glass fiber and bulk crystalline or glass hosts. Ion-exchanged waveguides can be fabricated in glasses with large ytterbium concentrations (-5-15%) which allows the devices to be substantially shorter than fiber lasers. This results in lower polarization and output power noise, caused by thermal and mechanical stress-induced birefringence, and a smaller device volume. Short ($\sim 1\text{-}2\ \text{cm}$) laser cavities are also of interest because of the potential for realizing high-pulse-repetition rate (GHz), passively mode-locked lasers. Unlike bulk devices, waveguide lasers can be designed to operate in a single transverse mode independent of the operating power or pump laser transverse mode profile, and to not require the alignment of bulk mirrors. In addition, the mode field sizes in waveguides can be designed to closely match those of optical fiber for efficient coupling with fiber optic systems. One disadvantage of $\text{Er}^{3+}/\text{Yb}^{3+}$ glass wavelength lasers, up to this point, has been the relatively low output powers (up to a few milliwatts) available from these devices. Increased output power will greatly expand the utility of these devices. This paper describes a cw $\text{Er}^{3+}/\text{Yb}^{3+}$ -co-doped phosphate glass waveguide laser which has produced 168 mW of output power at around 1540 nm for 611 mW of launched pump power at 979 nm.

Waveguides were fabricated in a commercially available phosphate glass. The glass was co-doped with 1.15 wt % Er_2O_3 (0.99×10^{20} ions/cm³) and 4.73 wt % Yb_2O_3 (3.97×10^{20} ions/cm³). Waveguides were formed by K^+ - Na^+ exchange through a 200 nm thick Al mask layer with channel apertures ranging from 3 to 8 μm in width. The exchange occurred in a KNO_3 melt at 375°C for 4 hours in an Al crucible. The laser results reported here are for a 6.5 μm wide mask aperture. Inspection of the samples after the ion exchange process revealed that the regions of the glass surface corresponding to the location of the mask openings had become recessed by one or two microns during the exchange process. The widths of the etched channels were close to the widths of the mask apertures and uniform in width and depth.

In another embodiment, the refractive index as a function of position within the exchanged sample was analyzed using a refractive near-field scanning method. Fig. B1 in Paper B of the Appendix shows the index depth profile at the center of the waveguide formed with the 6.5 μm mask aperture for a wavelength of 633 nm. This method allows the relative position and absolute index values to be determined with an accuracy of 0.7 μm and 0.001, respectively.

In another embodiment, the transverse modes of the waveguides were characterized by coupling light at the wavelength of interest into one end of the waveguides and imaging the light emerging from the other end onto a calibrated infrared camera. The uncertainty of the mode dimensions determined using this method are ~10%. The device supported a single transverse mode at 1.54 μm having dimensions of 14.5 μm wide by 7.5 μm deep (measured at the 1/e points). The waveguide supported multiple transverse modes at 980 nm. However, when the device was lasing, the pump energy was confined primarily within the lower order transverse mode which had dimensions of 6.4 μm wide by 3.6 μm deep.

In another embodiment, the device was pumped with a Ti^{3+} sapphire laser. The waveguide laser cavities were formed by placing thin dielectric mirrors on the polished waveguide end faces. The mirrors were held in place by small spring clips, and index matching oil was used between the mirror and waveguide end faces to reduce losses. The pump laser was launched through one of the mirrors with a 4X microscope objective. The laser output and unabsorbed pump were collimated with a 16X

microscope objective and separated using filters. The laser cavity was 20 mm in length. The mirror through which the pump was launched had reflectivities of >99.9% and 15% at 1536 and 980 nm, respectively. The output coupler had a reflectivity of 80% at 1536 nm and transmitted 85% of the incident pump power.

5 Neither the waveguide length nor the cavity output coupling has been optimized. The launching efficiency was estimated to be $\leq 71\%$, including losses due to the transmission of the input mirror and launching objective. The laser output power characteristics for two different pump wavelengths are illustrated in Fig. B2 of Paper B in the Appendix. When pumped at 979 nm, the launched pump power threshold was 10 51 mW. A maximum output power of 168 mW was obtained for 611 mW of launched 979 nm pump power. A lower threshold could be obtained by turning the pump laser off of the Yb^{3+} absorption peak. For a pump wavelength of 960 nm, the threshold was 23 mW. The slope efficiency for both pump wavelengths was $\sim 28\%$.

Using the broad-band cavity described above, the $\text{Er}^{3+}/\text{Yb}^{3+}$ laser usually 15 operated at several wavelengths simultaneously. A typical laser spectrum showing simultaneous operation at 1536.0, 1540.7 and 1544.8 nm is depicted in Fig. B3 of Paper B in the Appendix. The wavelength(s) of operation could be shifted by passing some of the collimated 1.5 μm laser output through a prism and reflecting it back through the prism and into the waveguide using a dielectric mirror. This formed a 20 weakly-coupled, external cavity. By rotating the prism, it was possible to produce wavelengths ranging from 1536 to 1595 nm.

A common feature of many three-level rare-earth lasers is sustained relaxation oscillations which can be caused by small fluctuations in the pump laser power. Fluctuations in output power at frequencies ranging from ~ 0.5 to 1.5 MHz were 25 observed in this laser. The amplitude of the fluctuations decreased with pump power. Figure in B4 Paper B of the Appendix shows the output power as a function of time for pump power levels just above threshold and 9.4 times threshold. At the low pump power, the output power fluctuations of $\sim 30\%$ (peak to peak) of the average power were observed. At the high pump power, the fluctuations decreased to $\sim 5\%$ (peak to 30 peak) of the average power. The Ti^{3+} :sapphire pump laser exhibited output power

fluctuations of ~2-3%. Using a diode laser as the pump source should result in much quieter operation of the Er^{3+} laser.

Output powers exceeding 160 mW at 1.5 μm are now available from glass waveguide lasers fabricated using a simple thermal ion exchange process.

5 Improvements in the waveguide fabrication process to optimize the waveguide geometry (such as incorporating a field assisted ion exchange and fabricated buried waveguides), as well as adjustments in the cavity length and coupling, should improve the performance of these devices.

Example 6:

10 Waveguide lasers and amplifiers in glasses codoped with Er^{3+} and Yb^{3+} are promising candidates for compact multifunctional devices operating near 1.5 μm . The large gain bandwidth resulting from the inhomogeneously broadened glass host makes these devices ideal for narrow-line sources useful in wavelength division multiplexing applications. In addition, due to the short cavity lengths, these waveguide lasers offer

15 the possibility of high repetition rate (GHz) mode-locked lasers using semiconductor saturable absorbers. Such lasers would be ideal as sources for soliton communications systems. Other applications requiring an eye-safe wavelength, such as remote sensing and range finding could benefit from compact, high power cw or Q-switched waveguide laser sources based on these materials. Additionally, optical amplifiers offering gain

20 in the range 1530 to 1550 nm may be realized.

It is known that the Er^{3+} concentration must be kept relatively low (~1 wt %) in these devices in order to reduce the deleterious effects of cooperative upconversion. However, the concentration of sensitizing Yb^{3+} is not limited due to any ion-ion interaction, and is expected to have a significant effect on device performance. Various

25 authors have investigated this problem theoretically. This example reports experimental results for waveguide lasers fabricated by $\text{K}^+\text{-Na}^+$ ion exchange in silicate glasses with $\text{Yb}^{3+}:\text{Er}^{3+}$ ratios of 3:1, 5:1, and 8:1. In addition, we show how it is possible to increase the signal mode volume and optimize the pump-signal overlap through judicious choice of host material and ion exchange processing parameters. The

result is an $\text{Er}^{3+}/\text{Yb}^{3+}$ waveguide laser producing as much as 19.6 mW at 1.54 μm with 398 mW of launched pump power at 974.5 nm.

The devices were fabricated in a commercially available laser glass. The glass is a phosphorus-free, mixed-alkali, zinc-silicate glass. Nominally, all three glasses were doped with 1 wt% Er_2O_3 ($0.85 \times 10^{20} \text{ cm}^{-3}$) and the glasses designated NIST10A, NIST10C, and NIST10E contain $\text{Er}^{3+}:\text{Yb}^{3+}$ ratios of 3:1 ($2.47 \times 10^{20} \text{ Yb}^{3+} \text{ ions cm}^{-3}$), 5:1 ($4.16 \times 10^{20} \text{ cm}^{-3}$), and 8:1 ($6.83 \times 10^{20} \text{ cm}^{-3}$), respectively. The results reported were obtained by ion exchange through 3 μm apertures in 150 nm thick Al mask layers. The ion exchange was carried out in a melt of 100% KNO_3 for 14 hours at 400°C.

The optical modes of the waveguides at the signal wavelength were evaluated by coupling at 1.5 μm LED into a waveguide while the output was imaged onto an infrared camera. The waveguides supported a single transverse mode of dimensions $20.5 \pm 2.1 \mu\text{m}$ wide by $11.5 \pm 1.2 \mu\text{m}$ deep (measured at the 1/e points) at the signal wavelength. Since the host glass is a mixed alkali glass which contains potassium, the introduction of additional potassium by the ion exchange process leads to a very small index change. As a result, the optical mode is not tightly confined. Although the waveguides supported multiple transverse modes at the pump wavelength, an examination of the pump mode while the device was lasing showed that only the lowest-order mode was excited. The result is excellent overlap between the pump and signal modes. The pump mode measured $15.2 \pm 1.5 \mu\text{m}$ wide by $7.0 \pm 0.7 \mu\text{m}$ deep.

Waveguide losses were estimated at 860 nm, away from the broad Yb^{3+} absorption peak. Cutback measurements performed on samples prepared identically to the laser sample indicated an average waveguide loss of $0.25 \pm 0.11 \text{ dB/cm}$ for NIST10A, $0.32 \pm 0.08 \text{ dB/cm}$ for NIST10C, and $0.66 \pm 0.12 \text{ dB/cm}$ for NIST10E. The coupling efficiency for the pump light was determined by measuring the pump throughput at 860 nm and correcting for losses from the input and output optics, as well as waveguide loss using the above reported loss Figures. Coupling efficiencies typically fell between 50% and 70%. The coupling efficiency was assumed to be identical at 860 nm and 975 nm.

For laser characterization, dielectric mirrors were attached to the polished end facets of the waveguide laser sample with index matching fluid and held in place by a

small clip. The input mirror had a reflectance at 1536 nm of 99.9% and a transmittance at the pump wavelength of >90%. Various output couplers with reflectances ranging from 60 to 98% were used. All output couplers were also transmissive at the pump wavelength. The waveguide devices were pumped by a
5 Ti:sapphire laser operating at 974.5 nm, which is the peak of the Yb^{3+} absorption spectrum in this glass host. Pump light was coupled into the waveguide with a 4X (0.10 NA) microscope objective, and the output signal light was collected by a 20X objective. For signal power measurements, the output from the waveguide was focused onto an InGaAs power meter.

10 The laser performance was investigated as a function of device length as well as output coupler reflectance. Figure C1 in Paper C of the Appendix shows a plot of laser signal power vs. launched pump power for two different output couplers, for a 1.68 cm long device fabricated in the glass with 5 Yb^{3+} per Er^{3+} ion. The slope efficiencies and laser thresholds were determined by fitting a line to the laser data. The
15 lowest threshold was achieved when using a 98% reflector as output coupler. This device lased with a launched pump power threshold of approximately 59 mW. The slope efficiency of this device was 2.0% with respect to launched pump power. The highest slope efficiency was realized with a 70% reflector used as an output coupler. In this case, a slope efficiency of 6.5% was achieved with a launched pump power
20 threshold of 86 mW. For a launched pump power of 398 mW, this laser produced 19.6 mW of output power.

A plot of slope efficiency vs. output coupler reflectance for each host glass appears in Figure C2 of Paper C of the attached Appendix. Data for device lengths in each glass which were experimentally determined to give the highest slope efficiency
25 are plotted. Highest slope efficiency performance in each host is also compared in Table 1.

Table 1: Performance data for highest slope efficiency devices fabricated in IOG10 silicate glass with different Yb³⁺:Er³⁺ dopant ratios.

Yb ³⁺ :Er ³⁺	Device length	Output coupler reflectance (%)	Slope efficiency	Launched pump threshold	Output with 400 MW pump (mW)
	(cm)	(%)		(m/W)	
3:1	1.80	80	5.2	52	17.9
5:1	1.68	70	6.5	86	20.4
8:1	1.42	70	5.0	238	8:1

The experiment results indicate that the optical dopant ratio is close to 5 Yb³⁺ for each Er³⁺. Increasing the dopant ratio from 3:1 to 5:1 leads to an improvement in slop efficiency. Further increasing the dopant ratio to 8:1 does not improve the efficiency of the device, but does lead to a substantial penalty in pump power requirements. Recent efforts have been directed toward expanding the above results using a rigorous scalar model. In addition, alteration of the potassium content of the host glass is being investigated as a way to adjust the model value and decrease pump threshold requirements.

We Claim:

1. An optical device comprising a glass substrate doped with a laser species and having two or more waveguides defined by channels in the substrate having a distinct refractive index from the substrate wherein at least two of the waveguides are defined by channels having differing widths such that they have distinct effective refractive indices from each other.

2. An optical device of claim 1, wherein the substrate is comprised of an alkali phosphate glass doped with Er and Yb.

3. An optical device of claim 2, wherein the waveguides are comprised of an alkali phosphate glass doped with Er and Yb, which has been treated so that the refractive index is higher than that of the substrate.

4. An optical device of claim 3, wherein the optical device is prepared by applying a mask to the substrate glass having apertures of a width and length corresponding to the waveguides to be formed in the substrate and conducting ion-exchange by contact with an ion-exchange solvent to form the waveguides through the apertures.

5. An optical device of claim 3, wherein the optical device is prepared by applying a mask to the substrate glass having apertures of a width and length corresponding to the waveguides to be formed in the substrate and conducting photolithography to form the waveguides through the apertures.

6. An optical device of claim 1, which further comprises a reflecting element in association with the waveguide to provide a laser effect when pumped.

7. The optical device of claim 6, wherein the reflecting element is a diffraction grating provided on the substrate.

8. A method for preparing an optical device having at least one active doped region substrate, at least one passive doped region substrate and at least one waveguide defined therein which comprises bringing a separate active doped substrate and a separate passive doped substrate in contact with each other and heating at a temperature above the softening temperature of the substrates to fuse them together, the waveguide being provided either before or after fusing the substrates.

9. An optical device having at least one active doped region substrate, at least one passive doped region substrate and at least one waveguide defined therein which is prepared by the process of claim 8.

10. An optical device of claim 9, wherein at least one region of the substrate is comprised of an alkali phosphate glass doped with Er and Yb.

11. An optical device of claim 9, which is a laser comprising the fused active doped region and passive doped region substrate and at least one waveguide defined therein.

12. A method for modifying the wavelength of one or more waveguides contained as channels of differing refractive index material in a laser species-containing substrate which comprises heating the substrate.

13. The method of claim 12, wherein the method results in expansion the waveguide(s) to increase the wavelength which is offset by a reduction in the refractive index of the waveguide.

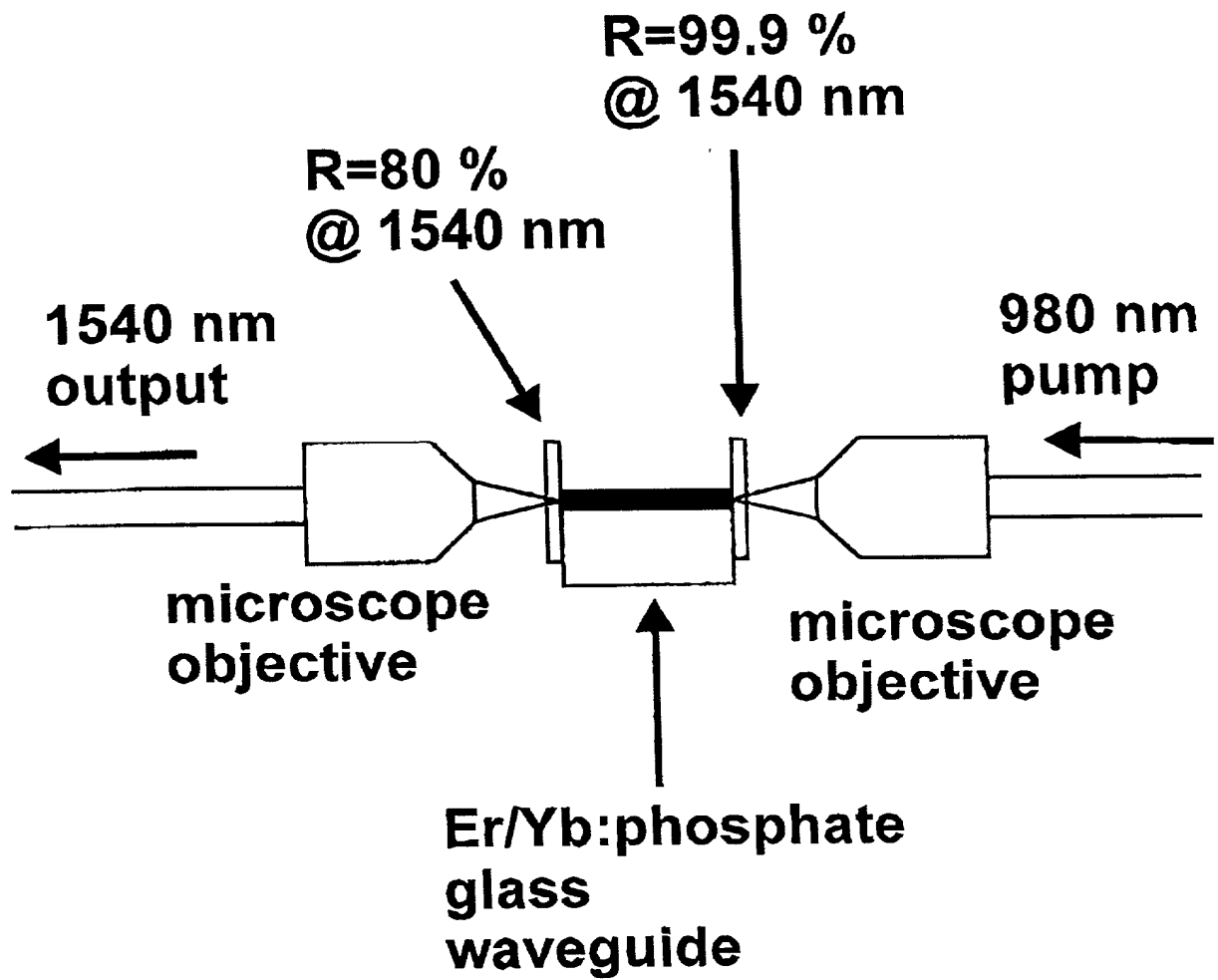
14. The method of claim 12, wherein the modifying of the wavelength upon heating occurs at a rate which is about 15 times less than that observed for DFB lasers.

15. The method of claim 12, wherein the substrate is comprised of an alkali phosphate glass doped with Er and Yb.

ABSTRACT

The invention is directed to optical devices comprising a solid-state structured glass substrate having at least one waveguide incorporated therein, particularly waveguides and lasers incorporating such structure. The invention is also directed to methods for modifying such devices and their properties. The waveguides and lasers of the invention provide advantageous high power and increased slope efficiency and find use, for example, in telecommunications applications.

Figure 1 – Test Apparatus for Waveguide Lasers



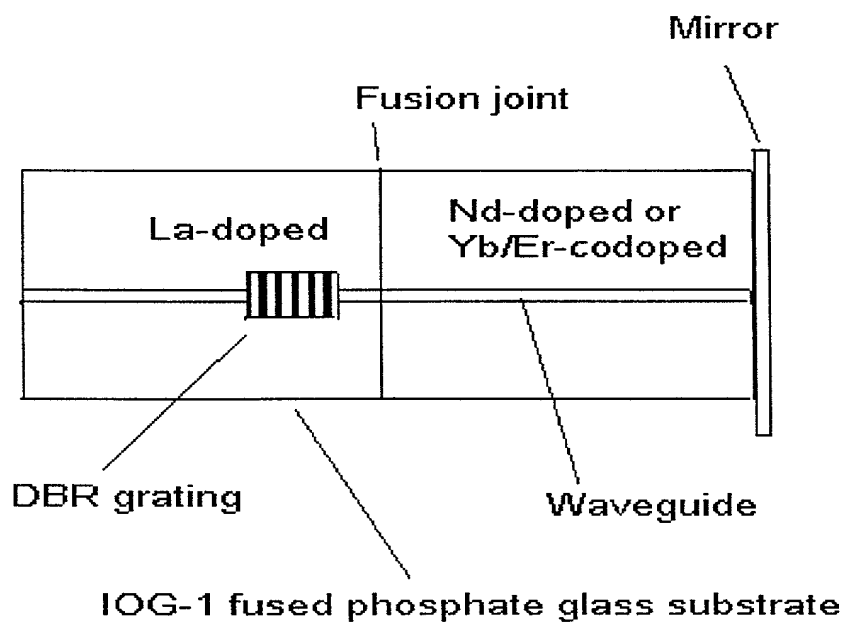


Fig. 2

APPENDIX - PAPERS A - E

100-443887-1000

Paper A.

Arrays of Distributed-Bragg-Reflector Waveguide Lasers at 1536 nm in Yb/Er-co-doped Phosphate Glass*

David L. Veasey, David S. Funk, Norman A. Sanford
Optoelectronics Division, National Institute of Standards and Technology,
325 Broadway, MC 815.04
Boulder CO 80503-3328, USA
Phone: (303) 497-5952
E-mail: veasey@boulder.nist.gov dfunk@boulder.nist.gov
sanford@boulder.nist.gov

Joseph S. Hayden
Schott Glass Technologies, Inc.
400 York Ave., Duryea, PA 18642, USA
Phone: (717) 457-7485 ext 351
E-mail: jhayden@sp230L.attmail.com

We have successfully demonstrated an array of monolithic, single-frequency distributed-Bragg-reflector (DBR) waveguide lasers operating near 1536 nm wavelengths. The lasers were fabricated by forming waveguides in Yb/Er-co-doped phosphate glass by ion exchange. The slope efficiency for each laser as a function of launched pump power is 26 % and the thresholds occur at 50 mW of launched pump power. An output power of 80 mW was achieved with 350 mW of coupled pump power. Each laser exhibits stable operation on a single longitudinal mode and all have linewidths less than 500 kHz. A comb of waveguides with varying effective indices allows the selection of wavelength using a single-period grating.

* Contribution of the U.S. Government. Not subject to copyright

We describe in this letter the first reported monolithic, single-frequency distributed-Bragg-reflector (DBR), waveguide lasers in $\text{Yb}^{3+}/\text{Er}^{3+}$ -co-doped phosphate glass. Over the past several years, the growth in the demand for bandwidth generated by new telecommunication services, cable television (CATV), and data communication has driven the rapid development of wavelength division multiplexing (WDM) where information is simultaneously transmitted on several different wavelengths in the same optical fiber channel. The development of WDM systems has placed demands on laser sources that are difficult to meet using existing technologies such as semiconductor distributed feedback (DFB) lasers. Issues of concern for such systems include wavelength selectivity, wavelength stability over laser lifetime, tunability, process yield, power limitations, and costs.

Integrated, single-frequency, solid-state lasers using the Er^{3+} ion offer a very promising and competitive alternative to DFB lasers for use in future WDM communications systems and for CATV. Several demonstrations of the waveguide and fiber laser technology have been discussed in the literature.¹⁻⁵ One primary advantage of solid-state waveguide lasers is that they offer the possibility for arrays of lasers operating on many wavelengths on a single glass chip. Rare-earth-doped waveguide lasers can also provide kilohertz linewidths with high radiance, low noise, and easy coupling to optical fibers.^{3,4,6}

Single-transverse-mode waveguides at 1535 nm wavelength were fabricated in a commercially available phosphate alkali glass that was co-doped with $0.99 \times 10^{20} \text{ Er}^{3+}$ ions/cm³ and $3.97 \times 10^{20} \text{ Yb}^{3+}$ ions/cm³.^{7,8} Phosphate glass is a very good host material for ytterbium and erbium ions since the sensitization efficiency is nearly unity and large

(A 2)

16

doping concentrations are possible before the onset of concentration quenching.⁹ The guides were formed by ion exchange of K^+ for Na^+ using line apertures 3 to 8 μm wide etched in a 200 nm thick aluminum mask layer. The exchange time was 4 hours in an aluminum crucible containing molten KNO_3 at 375 °C. Inspection of the samples using refractive near-field scanning after the ion exchange revealed that the regions of the glass surface corresponding to the location of the mask openings had become recessed by approximately 1 μm during the exchange process.¹⁰ The mechanism behind the etching of the glass during the exchange is currently under investigation, and we think it is caused by residual water in the hygroscopic nitrate melt.⁹ The surface quality of the glass in the recessed regions, as observed using a 1000x nomarski contrast microscope, appears identical to the original surface of the glass and apparently does not cause significant scattering losses.

The waveguide end faces were polished perpendicular to the channels. The length of the waveguides prior to the grating fabrication step was 2.2 cm. Measurements of the waveguide mode-field dimensions showed that a single transverse mode was supported in each of the waveguides. For the guide formed with the 6.5 μm mask aperture, the 1/e full-widths of the mode-field intensity were 16 μm wide by 11 μm deep at 1.54 μm wavelength. It supported multiple transverse modes at the 977 nm pump wavelength. However, when the device was lasing, the pump energy was confined primarily within the lowest order transverse mode, which had 1/e dimensions of 13 μm wide by 9.5 μm deep. All measurements of the intensity profile are within an estimated experimental error of $\pm 10\%$.

(13)

17

A DBR surface relief grating was fabricated holographically in a 0.5 μm thick layer of Shipley 1805¹ photoresist using a 90° corner that split a collimated laser beam into two beams.¹¹ The corner was mounted on a rotation stage so that the angle of the two beams could be varied. One surface of the corner was a mirror, and the other surface was a vacuum chuck for holding the sample. Light from a 457.8 nm Ar-ion laser was spatially filtered by focusing through a 15 μm pinhole using a 20x objective lens.

The beam was collimated using a 76 mm diameter lens with a 350 mm focal length. The exposure angle was set to write a grating with a pitch of $\Lambda = 507.8$ nm. For a waveguide with estimated effective index of 1.515 ± 0.003 , this pitch should provide laser operation at $\lambda = 1538.6$ nm ± 3 nm. The exposure time for the photoresist was 18 s with 3.85 mW incident in each arm on the 0.44 cm² exposed region (0.8 cm long x 0.55 cm wide). The grating was developed in undiluted Shipley CD-30⁸ developer. During the development, the diffraction of light from a 632.8 nm HeNe laser was monitored.¹² When the first-order diffracted power reached a peak, the grating was removed, rinsed, and dried.

Before transferring the photoresist pattern into the glass by Ar-ion sputtering, we deposited 40 nm of Cr on the surface with the specimen inclined 60° to the electron-beam evaporation source. Mounting the specimen in this way causes Cr to accumulate only on the tops of the grating lines and not in the grooves, thus providing a durable etch mask. We etched the grating in the glass for 20 minutes using a reactive ion etching system with a 6.67 Pa (50 mTorr) Ar-ion plasma. The low-pressure plasma created a large self-bias voltage of 1700 V when running at 365 W of coupled power with frequency 13.5 MHz. The electrode spacing was 3.2 cm. After etching, the sample was cleaned ultrasonically in photoresist stripper at 85 °C. Figure 1 is an illustration of the completed DBR laser



array. An atomic force microscope micro-graph of a typical grating etched in this type of phosphate glass can be found in reference [11].

The waveguide laser cavities were formed by placing a thin, highly reflecting ($R=99.9\%$ at 1540 nm, $R=15\%$ at 977 nm) dielectric mirror on the pump input facet. The mirror was held in place by a spring clip, and index-matching fluid was used between the mirror and the waveguide facet. The DBR grating was used as the laser output coupler. We tested the laser by coupling light from a $\text{Ti:Al}_2\text{O}_3$ laser tuned to a wavelength of 977 nm using a 4x objective lens with a numerical aperture of 0.1. The launching efficiency was estimated to be between 65 and 71 percent. To determine the launching efficiency we measured the Fresnel reflectance of the input mirror, the loss of the launching objective, and the excess coupling loss. Figure 2 shows the laser output power as a function of launched pump power and the spectrum of the laser. The waveguide diffusion aperture for this waveguide was 8 μm . The slope efficiency as a function of launched pump power is calculated to be 26 percent when we take the coupling factor to be 71 percent.

We estimated the reflectance of the grating using the simplified laser formula derived from the theory of Rigrod:¹¹

$$\frac{P_1}{P_2} = \frac{1-R_1}{1-R_2} \sqrt{\frac{R_2}{R_1}} \quad (1),$$

where P_1 is the output power at the grating end and P_2 is the output power at the end opposite the grating. R_1 is the grating reflectance and R_2 is the reflectance of the attached mirror. We used two mirrors with reflectances of 80 and 90 percent for R_2 . For both cases we calculated the grating reflectance, R_1 , to be 65 percent.

(13)

19

To investigate the longitudinal mode structure of the laser we coupled the laser output into an optical fiber scanning Fabry Perot interferometer with a free spectral range of 124 GHz. Figure 3 shows that the laser operated on a single longitudinal mode when the coupled pump power did not exceed 300 mW. The laser was robustly single frequency with TE polarization, and no mode hopping was observed. The inset in Figure 3 shows that a second longitudinal mode appeared when the coupled pump power exceeded 300 mW. In this pump regime, the laser was unstable and exhibited mode-hopping, single-frequency operation, and dual-frequency operation. By measuring the frequency spacing between the longitudinal modes we determined that the physical length of the laser cavity was 1.4 cm.

We measured the linewidth of the laser using a conventional self-heterodyne configuration with a 75 MHz frequency shift.¹⁴ The path length difference between the two arms was 10 km corresponding to a linewidth resolution limit of 30 kHz for a gaussian line shape.¹⁵ Optical isolators were used in both arms to prevent optical linewidth narrowing due to feedback; however, the output end of the laser was not beveled. Figure 4 shows the self-heterodyne spectrum. The laser linewidth we obtained from this measurement was 500 kHz.

Finally, we measured the laser wavelengths of other waveguides on the chip using an automatic spectrum analyzer with a resolution of 0.1 nm. Seven of the eleven waveguides on the chip exhibited laser oscillation. The waveguides formed through the smaller apertures did not achieve threshold because the smaller mode volumes caused a reduction of the gain such that the 45 percent transmittance loss of grating could not be overcome. Figure 5 shows the change in wavelength trend as we scanned the

(A)

20

waveguides. The wavelength increases as the diffusion aperture width increases, which is consistent with increasing effective index as the aperture width increases.

In conclusion, we have demonstrated an array of high power, robustly single-frequency, integrated, DBR waveguide lasers operating near 1536 nm wavelength. The slope efficiencies of the lasers are 26 percent based on launched pump power, and the threshold is less than 50 mW when pumped at a wavelength of 977 nm. The linewidths of the lasers were measured to be 500 kHz, and the outputs were linearly polarized in a TE mode. We are currently investigating the temperature stability of the lasers and the relative intensity noise (RIN). We expect that with diode laser pumping, the RIN will be similar to other results presented for single-frequency fiber lasers and will fall below -150 dB/Hz above 10 MHz.^{3,4} We anticipate that the output power and efficiency will increase and the threshold power will decrease when the grating reflectance is increased. This is possible with only minor adjustments to the grating fabrication process. Further improvements will also be realized by directly coating the high reflector onto the waveguide end facets. We have shown that lasers with several output wavelengths can be integrated on a single glass substrate. This demonstration shows that stable, multi-wavelength, WDM sources with wavelengths falling on the International Telecommunications Union (ITU) grid can be realized by writing several gratings of varying period in Yb/Er-co-doped glass waveguides formed by ion exchange.

(A7)

21

References

- ¹T. Kitagawa, F. Bilodeau, B. Malo, S. Theriault, J. Albert, D.C. Johnson, K.O. Hill, K. Hattori, and Y. Hibino, *Electron. Lett.* **30**, 1311 (1994).
- ²A. Yenlay, J.-M.P. Delavaux, J. Toulouse, D. Barbier, T.A. Strasser, and J.R. Pedrazanni, *IEEE Photonics Technol. Lett.* **9**, 1099 (1997).
- ³J.T. Kringlebotn, J.-L. Archambault, L. Reekie, J.E. Townsend, G.G. Vienne, and D.N. Payne, *Electron. Lett.* **30**, 972 (1994).
- ⁴W.H. Loh, B.N. Samson, L. Dong, G.J. Cowle, and K. Hsu, *J. Lightwave Technol.* **16**, 114 (1998).
- ⁵G.J. Vossler, C.J. Brooks, and K.A. Winick, *Electron. Lett.* **31**, 1162 (1995).
- ⁶T.Y. Fan, R.L. Byer, *IEEE J. Quantum Electron.* **24**, 895 (1988).
- ⁷IOG-1 laser glass, Schott Glass Technologies, Inc., 400 York Avenue, Duryea, PA.
- ⁸Specific materials and process chemicals are reported only to make the process reproducible and are not endorsed by the U.S. Government. Other materials and chemicals may work as well or better.
- ⁹P. Fournier, P. Meshkini, M.A. Fardad, M.P. Andrews, and S.I. Najafi, *Electron. Lett.* **33**, 293 (1997).
- ¹⁰B. Grochli, B. Gisin, N. Gisin and H. Zbinden, *Opt. Engineering*, **34**, 2309 (1995), N. H. Fontaine and M. Young, "Refracted near-field scanning of fibers and waveguides," submitted to *J. Lightwave Technol.*
- ¹¹D.L. Veasey, K.J. Malone, J.A. Aust, N.A. Sanford, and A. Roshko, *Proc. 7th Eur. Conf. on Int. Opt.* p. 579, Delft, (1995), J.E. Roman and K.A. Winick, *Appl. Phys. Lett.* **61**, 2744 (1992).
- ¹²L. Li, M. Xu, G.I. Stegeman, C.T. Seaton, *SPIE Proc.* **835**, 72 (1987).
- ¹³W.W. Rigrod, *J. Appl. Phys.* **36**, 1487 (1965).
- ¹⁴D.H. McMahon, W.A. Dyes, *J. Lightwave Technol.* **6**, 1162 (1988).
- ¹⁵J.W. Goodman, *Statistical Optics*, Wiley & Sons, 1985, p. 168.

(A 8)

22

Figure 1 is a scatter plot showing the relationship between Diffusion Aperture Width (μm) on the x-axis and Laser Wavelength (nm) on the y-axis. The x-axis ranges from 5 to 8 μm , and the y-axis ranges from 1536.0 to 1536.4 nm. Five data points are plotted, showing a general upward trend. A dashed line represents a linear fit to the data.

Diffusion Aperture Width (μm)	Laser Wavelength (nm)
5.0	1536.01
5.5	1536.09
6.0	1536.05
7.0	1536.25
7.5	1536.23

FIG. A5

Paper B

170 mW cw at 1540 nm from an erbium/ytterbium co-doped glass waveguide laser

D. S. Funk, D. L. Veasey, P. M. Peters and N. A. Sanford
National Institute of Standards and Technology,
Optoelectronics Division, 814.04,
325 Broadway, Boulder, CO 80303
phone: (303)-497-3289 fax: (303)-497-3367
dfunk@boulder.nist.gov

J. S. Hayden
Schott Glass Technologies, Inc., R&D-Materials Group,
400 York Avenue, Duryea, PA 18642
phone: (717)-457-7485 fax: (717)-457-3438
jshayden@sg230L.attmail.com

Compact solid state lasers based on the 1.5 μm Er^{3+} transition hold promise as sources for optical fiber communication systems. Yb^{3+} is commonly used as a sensitizer to Er^{3+} lasers because it has a much larger absorption cross section near 980 nm than Er^{3+} , and it efficiently transfers its excited state energy to the upper level of the Er^{3+} laser. The $\text{Er}^{3+}/\text{Yb}^{3+}$ glass waveguide laser, in particular, has several advantages over lasers in Er^{3+} -doped or $\text{Er}^{3+}/\text{Yb}^{3+}$ -co-doped glass fiber and bulk crystalline or glass hosts. Ion-exchanged waveguides can be fabricated in glasses with large ytterbium concentrations (~5-15 %) which allows the devices to be substantially shorter than fiber lasers. This results in lower polarization and output power noise, caused by thermal and mechanical stress-induced birefringence, and a smaller device volume. Short (~1-2 cm) laser cavities are also of interest because of the potential for realizing high pulse repetition rates (GHz), passively mode-locked lasers. Unlike bulk devices, waveguide lasers can be designed to operate in a single transverse mode independent of the operating power or pump laser transverse mode profile, and do not require the alignment of bulk mirrors. In addition, the mode field sizes in waveguides can be designed to closely match those of optical fiber for efficient coupling with fiber optic systems. One disadvantage of $\text{Er}^{3+}/\text{Yb}^{3+}$ glass waveguide lasers, up to this point, has been the relatively low output powers (up to a few milliwatts¹⁻⁴) available from these devices. Increased output power will greatly expand the utility of these devices. This paper describes a cw $\text{Er}^{3+}/\text{Yb}^{3+}$ -codoped phosphate glass waveguide laser which has produced 168 mW of output power at around 1540 nm for 611 mW of launched pump power at 979 nm.

Waveguides were fabricated in a commercially available phosphate glass.⁵ The glass was co-doped with 1.15 wt % Er_2O_3 (0.99×10^{20} ions/cm³) and 4.73 wt % Yb_2O_3 (3.97×10^{20} ions/cm³). Waveguides were formed by K^+/Na^+ exchange through a 200 nm thick Al mask layer with channel apertures ranging from 3 to 8 μm in width. The exchange occurred in a KNO_3 melt at 375 °C for 4 hours in an Al crucible. The laser results reported here are for a 6.5 μm wide mask aperture. Inspection of the samples after the ion exchange process revealed that the regions of the glass surface corresponding to the location of the mask openings had become recessed by one to two microns during the exchange process. The widths of the etched channels were close to the widths of the mask apertures and uniform in width and depth. The mechanism behind the apparent etching of the glass during the exchange process is currently under investigation.

The refractive index as a function of position within the exchanged sample was analyzed using a refractive near-field scanning method.⁶ Figure 1 shows the index depth profile at the center of the waveguide formed with the 6.5 μm mask aperture for a wavelength of 633 nm. This method allows the relative position and absolute index values to be determined with an accuracy of 0.7 μm and 0.001, respectively.

The transverse modes of the waveguides were characterized by coupling light at the wavelength of interest into one end of the waveguide and imaging the light emerging from the other end onto a calibrated infrared camera. The uncertainty of the mode dimensions determined using this method are ~10 %. The device supported a single transverse mode at 1.54 μm having dimensions of 14.5 μm wide by 7.5 μm deep (measured at the 1/e points). The waveguide supported multiple transverse modes at 980 nm. However,

(5)

24

when the device was lasing, the pump energy was confined primarily within the lowest order transverse mode which had dimensions of $6.4 \mu\text{m}$ wide by $3.6 \mu\text{m}$ deep.

The device was pumped with a Ti^{3+} :sapphire laser. The waveguide laser cavities were formed by placing thin dielectric mirrors on the polished waveguide end faces. The mirrors were held in place by small spring clips, and index matching oil was used between the mirror and waveguide end face to reduce losses. The pump laser was launched through one of the mirrors with a 4X microscope objective. The laser output and unabsorbed pump were collimated with a 16X microscope objective and separated using filters. The laser cavity was 20 mm in length. The mirror through which the pump was launched had reflectivities of $>99.9\%$ and 13% at 1536 and 980 nm, respectively. The output coupler had a reflectivity of 80% at 1536 nm and transmitted 85% of the incident pump power. Neither the waveguide length nor the cavity output coupling has been optimized. The launching efficiency was estimated to be $\leq 71\%$, including losses due to the transmission of the input mirror and launching objective. The laser output power characteristics for two different pump wavelengths are illustrated in Figure 2. When pumped at 979 nm, the launched pump power threshold was 51 mW. A maximum output power of 163 mW was obtained for 611 mW of launched 979 nm pump power. A lower threshold could be obtained by tuning the pump laser off of the Yb^{3+} absorption peak. For a pump wavelength of 960 nm, the threshold was 23 mW. The slope efficiency for both pump wavelengths was $\sim 28\%$.

Using the broad band cavity described above, the $\text{Er}^{3+}/\text{Yb}^{3+}$ laser usually operated at several wavelengths simultaneously. A typical laser spectrum showing simultaneous operation at 1536.0, 1540.7, and 1544.8 nm is depicted in Figure 3. The wavelength(s) of operation could be shifted by passing some of the collimated $1.5 \mu\text{m}$ laser output through a prism and reflecting it back through the prism and into the waveguide using a dielectric mirror. This formed a weakly-coupled, external cavity. By rotating the prism, it was possible to produce wavelengths ranging from 1536 to 1595 nm.

A common feature of many three level rare earth lasers is sustained relaxation oscillations which can be caused by small fluctuations in the pump laser power. Fluctuations in output power at frequencies ranging from ~ 0.5 to 1.5 MHz were observed in this laser. The amplitude of the fluctuations decreased with pump power. Figure 4 shows the output power as a function of time for pump power levels just above threshold and 9.4 times threshold. At the low pump power, the output power fluctuations of $\sim 30\%$ (peak to peak) of the average power were observed. At the high pump power, the fluctuations decreased to $\sim 5\%$ (peak to peak) of the average power. The Ti^{3+} :sapphire pump laser exhibited output power fluctuations of $\sim 2-3\%$. Using a diode laser as the pump source should result in much quieter operation of the Er^{3+} laser.

Output powers exceeding 160 mW at $1.5 \mu\text{m}$ are now available from glass waveguide lasers fabricated using a simple thermal ion exchange process. Improvements in the waveguide fabrication process to optimize the waveguide geometry (such as incorporating a field assisted ion exchange and fabricating buried waveguides), as well as adjustments in the cavity length and output coupling, should improve the performance of these devices.

¹ J. E. Román, M. Hempstead, W. S. Brockleby, S. Noun, J. S. Wilkinson, P. Camy, C. Lermiaux and A. Béguin, "Ion-exchanged Er/Yb waveguide laser at $1.5 \mu\text{m}$ pumped by a laser diode," *Electron. Lett.*, vol. 31, p. 1345, 1995.

² G. L. Vossler, C. J. Brooks and K. A. Winick, "Planar Er:Yb glass ion exchange waveguide laser," *Electron. Lett.*, vol. 31, p. 1162, 1995.

³ D. Barbier, J. M. Delavaux, R. L. Hyde, J. M. Jouanno, A. Kervorkian and P. Gastaldo, "Tunability of Yb/Er integrated optical lasers in phosphate glass," *Amplifiers and their Applications, 1995 Tech. Dig. Ser.*, Davos: Switzerland, vol. 18, paper PD3.

⁴ J. Amin, D. L. Veasey, N. A. Sanford and J. S. Hayden, "Waveguide lasers by ion-exchange in Er-doped glass," in *Rare-Earth-Doped Devices, Proc. SPIE*, vol. 2996, p. 135, 1997.

⁵ IOG-1 laser glass, Schott Glass Technologies, Inc., 400 York Avenue, Duryea, PA. The IOG-1 tradename is used to allow the reader to reproduce the experiment and does not imply endorsement by the National Institute of Standards and Technology.

⁶ B. Groebli, B. Gisin, N. Gisin and H. Zbinden, "Measuring refractive index profiles of integrated LiNbO_3 waveguides," *Opt. Engineering*, vol. 34, p. 2309, 1995.

62

25

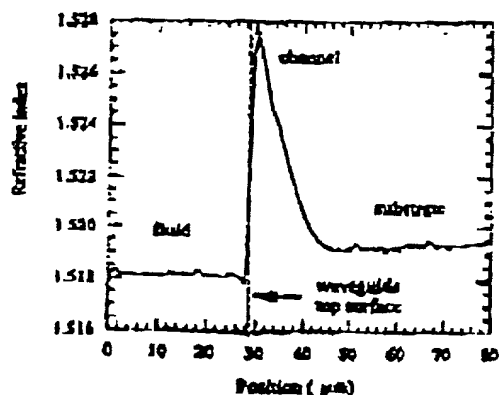


Fig B1. Refractive index profile at 633 nm of an $\text{Er}^{3+}/\text{Yb}^{3+}$ phosphosilicate glass waveguide, obtained using a refracted near-field scanning method.

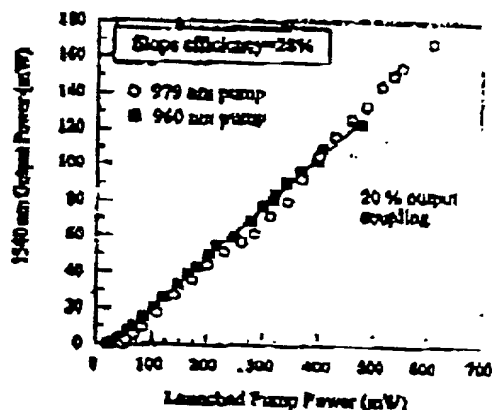


Fig B2. 1540 nm output power as a function of pump power for a 20 mm long $\text{Er}^{3+}/\text{Yb}^{3+}$ waveguide laser. Curves are shown for two different pump wavelengths.

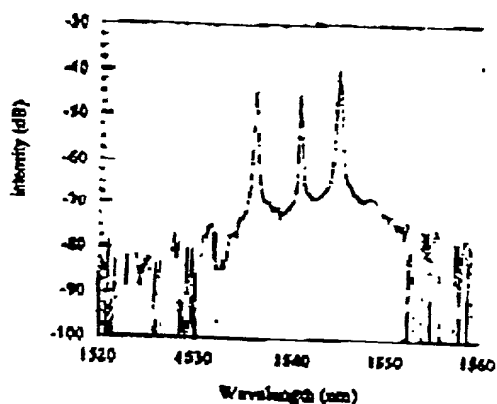


Fig B3. Laser output spectrum of an $\text{Er}^{3+}/\text{Yb}^{3+}$ waveguide laser spectrum for 106 mW of launched pump power.

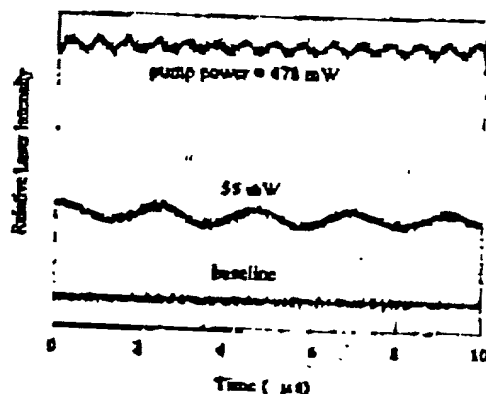


Fig B4. Output power fluctuations in time for pump powers just above threshold (55 mW) and 9.4 times threshold (478 mW).

Paper C

Ion-exchanged $\text{Er}^{3+}/\text{Yb}^{3+}$ glass waveguide lasers in silicate glasses¹

P. M. Peters, D. L. Veasey, D. S. Funk and N. A. Sanford
Optoelectronics Division, 815.04, National Institute of Standards and Technology, 325
Broadway, Boulder, CO 80303

S. N. Houde-Walter
The Institute of Optics, University of Rochester, Rochester, NY 14627

J. S. Hayden
R&D-Materials Group, Schott Glass Technologies, Inc., 400 York Avenue, Duryea, PA
18642

Waveguide lasers and amplifiers in glasses codoped with Er^{3+} and Yb^{3+} are promising candidates for compact multifunctional devices operating near 1.5 μm . The large gain bandwidth resulting from the inhomogeneously broadened glass host makes these devices ideal for narrow-line sources useful in wavelength division multiplexing applications. In addition, due to the short cavity lengths, these waveguide lasers offer the possibility of high repetition rate (GHz) mode-locked lasers using semiconductor saturable absorbers. Such lasers would be ideal as sources for soliton communications systems. Other applications requiring an eye-safe wavelength, such as remote sensing and range finding, could benefit from compact, high power cw or Q-switched waveguide laser sources based on these materials. Additionally, optical amplifiers offering gain in the range 1530 to 1550 nm may be realized.¹

It is known that the Er^{3+} concentration must be kept relatively low (~ 1 wt %) in these devices in order to reduce the deleterious effects of cooperative upconversion. However, the concentration of sensitizing Yb^{3+} is not limited due to any ion-ion interaction, and is expected to have a significant effect on device performance. Various authors have investigated this problem theoretically.^{2,3} In this paper we report experimental results for waveguide lasers fabricated by K^+/Na^+ ion exchange in silicate glasses with $\text{Yb}^{3+}:\text{Er}^{3+}$ ratios of 3:1, 5:1, and 8:1. In addition, we show how it is possible to increase the signal mode volume and optimize the pump-signal overlap through judicious choice of laser host material and ion exchange processing parameters. The result is an $\text{Er}^{3+}/\text{Yb}^{3+}$ waveguide laser producing as much as 19.6 mW at 1.54 μm with 398 mW of launched pump power at 974.5 nm.

The devices were fabricated in a commercially available laser glass.⁴ The glass is a phosphorus-free, mixed-alkali, zinc silicate glass. Nominally, all three glasses were doped with 1 wt% Er_2O_3 ($0.85 \times 10^{20} \text{ cm}^{-3}$) and the glasses designated NIST10A, NIST10C, and NIST10E contain $\text{Er}^{3+}:\text{Yb}^{3+}$ ratios of 3:1 ($2.47 \times 10^{20} \text{ Yb}^{3+} \text{ ions cm}^{-3}$), 5:1 ($4.16 \times 10^{20} \text{ cm}^{-3}$), and 8:1 ($6.83 \times 10^{20} \text{ cm}^{-3}$), respectively. The results reported were obtained by ion exchange through 3 μm apertures in 150 nm thick Al mask layers. The ion exchange was carried out in a melt of 100% KNO_3 for 14 hours at 400 °C.

¹ Contribution of the U.S. Government, not subject to copyright.

(C)

The optical modes of the waveguides at the signal wavelength were evaluated by coupling a 1.5 μm LED into a waveguide while the output was imaged onto an infrared camera. The waveguides supported a single transverse mode of dimensions 20.5 ± 2.1 μm wide by 11.5 ± 1.2 μm deep (measured at the $1/e$ points) at the signal wavelength. Since the host glass is a mixed alkali glass which contains potassium, the introduction of additional potassium by the ion exchange process leads to a very small index change. As a result the optical mode is not tightly confined. Although the waveguides supported multiple transverse modes at the pump wavelength, an examination of the pump mode while the device was lasing showed that only the lowest-order mode was excited. The result is excellent overlap between the pump and signal modes. The pump mode measured 15.2 ± 1.5 μm wide by 7.0 ± 0.7 μm deep.

Waveguide losses were estimated at 860 nm, away from the broad Yb^{3+} absorption peak. Cutback measurements performed on samples prepared identically to the laser sample indicated an average waveguide loss of 0.25 ± 0.11 dB/cm for NIST10A, 0.32 ± 0.08 dB/cm for NIST10C, and 0.66 ± 0.12 dB/cm for NIST10B. The coupling efficiency for the pump light was determined by measuring the pump throughput at 860 nm and correcting for losses from the input and output optics, as well as waveguide loss using the above reported loss figures. Coupling efficiencies typically fell between 50% and 70%. The coupling efficiency was assumed to be identical at 860 nm and 975 nm.

For laser characterization, dielectric mirrors were attached to the polished end facets of the waveguide laser sample with index matching fluid and held in place by a small clip. The input mirror had a reflectance at 1536 nm of 99.9% and a transmittance at the pump wavelength of >90%. Various output couplers with reflectances ranging from 60 to 98% were used. All output couplers were also transmissive at the pump wavelength. The waveguide devices were pumped by a Ti:sapphire laser operating at 974.5 nm, which is the peak of the Yb^{3+} absorption spectrum in this glass host. Pump light was coupled into the waveguide with a 4X (0.10 NA) microscope objective, and the output signal light was collected by a 20X objective. For signal power measurements, the output from the waveguide was focused onto an InGaAs power meter.

The laser performance was investigated as a function of device length as well as output coupler reflectance. Figure 1 shows a plot of laser signal power vs. launched pump power for two different output couplers, for a 1.68 cm long device fabricated in the glass with 5 Yb^{3+} per Er^{3+} ion. The slope efficiencies and laser thresholds were determined by fitting a line to the laser data. The lowest threshold was achieved when using a 98% reflector as output coupler. This device lased with a launched pump power threshold of approximately 59 mW. The slope efficiency of this device was 2.0% with respect to launched pump power. The highest slope efficiency was realized with a 70% reflector used as an output coupler. In this case, a slope efficiency of 6.5% was achieved with a launched pump power threshold of 86 mW. For a launched pump power of 398 mW, this laser produced 19.6 mW of output power.

A plot of slope efficiency vs. output coupler reflectance for each host glass appears in Figure 2. Data for device lengths in each glass which were experimentally

(C)

27

determined to give the highest slope efficiency are plotted. Highest slope efficiency performance in each host is also compared in Table 1.

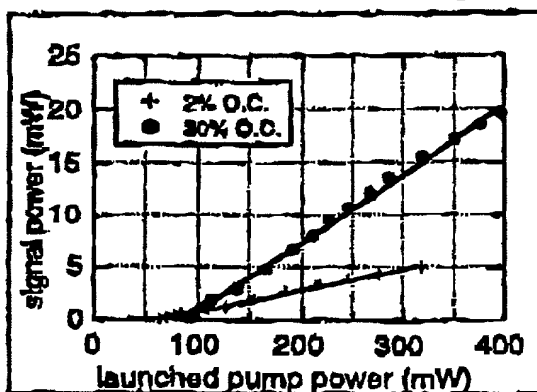


Fig. C1: Signal power vs. launched pump power for a 1.68 cm long device fabricated in the 5 Yb:1 Er silicate glass.

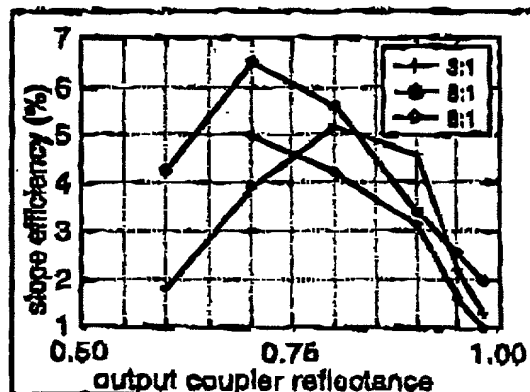


Fig. C2: Slope efficiency vs. output coupler reflectivity for lasers fabricated in silicate glasses with different Yb:Er ratios.

Table 1: Performance data for highest slope efficiency devices fabricated in IOG10 silicate glass with different Yb³⁺:Er³⁺ dopant ratios.

Yb ³⁺ :Er ³⁺	Device length (cm)	Output coupler Reflectance (%)	Slope efficiency (%)	Launched pump threshold (mW)	Output with 400 mW pump (mW)
3:1	1.80	80	5.2	52	17.9
5:1	1.68	70	6.5	86	20.4
8:1	1.42	70	5.0	238	8.1

The experimental results indicate that the optimal dopant ratio is close to 5 Yb³⁺ for each Er³⁺. Increasing the dopant ratio from 3:1 to 5:1 leads to an improvement in slope efficiency. Further increasing the dopant ratio to 8:1 does not improve the efficiency of the device, but does lead to a substantial penalty in pump power requirements. Recent efforts have been directed toward expanding the above results using a rigorous scalar model developed at NIST.⁵ In addition, alteration of the potassium content of the host glass is being investigated as a way to adjust the modal volume and decrease pump threshold requirements.

¹ D. Barbier, M. Rattay, F. Saint André, G. Clauss, M. Trouillon, A. Kevorkian, J. -M. P. Delavaux and B. Murphy, *IEEE Photon. Technol. Lett.* 9, 315 (1997).

² F. Di Pasquale and M. Federighi, *IEEE J. Quantum Electron.* 30 2127 (1994).

³ J. Nilsson, P. Scheer and B. Jaskorzynska, *IEEE Photon. Technol. Lett.* 6 383 (1994).

⁴ IOG-10 laser glass, Schott Glass Technologies, Inc., 400 York Avenue, Duryea, PA. The IOG-10 trademark is used to allow the reader to reproduce the experiment and does not imply endorsement by the National Institute of Standards and Technology.

⁵ D. L. Veasey, J. M. Gary and J. Amin, *Proc. SPIE* 2996 109 (1997).

Express Mail, mailing label number: EL 042 915 874

Date of Deposit: 27 Jan 1999
I hereby certify that the paper or fee is being deposited with the United States Patent and Trademark Office, via "Express Mail Post Office to Addressee" service on the date indicated above and is addressed to the United States Patent and Trademark Office, Washington, D.C. 20540.

Charles J. Lemire
Charles J. Lemire

Paper D

DRAFT DRAFT DRAFT**Yb/Er-codoped and Yb-doped Waveguide Lasers in Phosphate Glass***

David L. Veasey, David S. Funk, Philip M. Peters, Norman A. Sanford,
Gregory E. Obarski, Norman Fontaine, Matt Young, Adelle P. Peskin^a, Wei-chih
Liu^b, S.N. Houde-Walter^c, Joseph S. Hayden^d

*National Institute of Standards & Technology
Optoelectronics Division, 325 Broadway, MC 815.04
Boulder, CO 80303-3328
E-mail: veasey@boulder.nist.gov*

*^aNational Institute of Standards & Technology
High Performance Systems and Services Division, 325 Broadway, MC 890.02
Boulder, CO 80303-3328
E-mail: peskin@boulder.nist.gov*

*^bRochester Theory Center
University of Rochester, Rochester, NY 14627
E-mail: weliu@pas.rochester.edu*

*^cThe Institute of Optics
University of Rochester, Rochester, NY 14627
E-mail: shw@optics.rochester.edu*

*^dSchott Glass Technologies, Inc.
400 York Ave., Duryea, PA 18642, USA
E-mail: jhayden@sg2301.attmail.com*

Abstract

We present experimental and theoretical results of our recent work on the development of waveguide lasers using rare-earth-doped phosphate glasses. An improvement has been achieved over previously reported waveguide laser results using the process of ion exchange in a commercially available Yb/Er-co-doped phosphate glass composition. We have demonstrated slope efficiencies near 30 percent with output powers approaching 200 mW for 1540 nm Fabry-Perot waveguide lasers. These lasers are continuously tunable over approximately 70 nm. In addition, Yb-doped Fabry-Perot waveguide lasers have been fabricated and tested. These lasers

* Contribution of the U.S. Government. Not subject to copyright

operate near 1020 nm wavelength with slope efficiency of 67 %. We have also realized arrays of single-frequency distributed-Bragg-reflector waveguide lasers operating near 1.5 μm by etching a grating in ion-exchanged waveguides. Each laser in the array operates at a different wavelength. The slope efficiencies as a function of launched pump power are 26 % and the thresholds occur at approximately 50 mW of launched pump power.

Temperature tuning of the wavelengths is also demonstrated.

1. Introduction

Waveguides in rare-earth-doped materials for lasers and amplifiers have been fabricated using a number of different methods. These include thermal and field-assisted ion exchange in bulk-doped silicate and phosphate glasses^[1-8] and film deposition of several rare-earth-doped dielectric films that are formed into optical channel waveguides. Film deposition or formation methods include rf sputtering,^[9-10] plasma-enhanced chemical vapor deposition,^[11] flame hydrolysis,^[12] ion implantation,^[13] laser ablation,^[14] and sol-gel deposition^[15]. In this paper we restrict our discussion to waveguide lasers that are formed by ion-exchange in Yb/Er-codoped and Yb-doped phosphate glasses. We report on the development of the glass used to fabricate waveguide lasers and present recent measurement results for waveguide lasers. These measurements include slope efficiency and threshold, wavelength tuning, relative intensity noise and linewidth for single frequency distributed Bragg reflector (DBR) waveguide lasers. We conclude this paper with a brief discussion of a method to optimize the performance of waveguide lasers using a combination of experimental results and theoretical predictions.

DRAFT DRAFT DRAFT**2. Experimental Procedures****2.1 Development of Phosphate Glass**

Perhaps the most critical step in the development of a robust waveguide laser technology is the design and realization of a suitable laser glass that supports ion exchange. The laser properties that must be engineered in the glass include the absorption and emission cross sections of the laser transition and the absorption and emission cross sections of the optical pump energy level. The spontaneous emission lifetimes must also be optimized for the laser and pump transition with the laser transition lifetime relatively long and the lifetime of the pump level as short as possible. Laser operation is also improved by reducing or eliminating the effects of cooperative upconversion. In codoped glasses, such as Yb/Er-codoped glass, the energy transfer efficiency from the sensitizing ion must be maximized. Yb codoping with Er in phosphate glasses can provide near unity sensitizing efficiencies.^[16]

In addition to optimizing the rare-earth ion spectroscopic properties, the glass must have properties that allow the fabrication of channel waveguides. The most common way to form waveguides in bulk glasses is the process of ion exchange, where alkali ions in the glass are exchanged for ions with larger polarizability, thus causing an increase in the refractive index near the glass surface. Such a process requires that the starting glass contain alkali-oxide components such as Na_2O or K_2O . At the same time, the chemical treatments employed in conventional waveguide fabrication by lithographic technology demand that the host glasses offer chemical durability so that substrate surfaces are not degraded during the processing of devices.

A final requirement for waveguide laser glasses is that the rare-earth doping concentration be as large as possible to reduce cavity lengths and mode-volumes. It is

DRAFT DRAFT DRAFT

important that the doping concentration of the active rare earth ions be variable in a manner such that it can be altered without significantly altering the base glass matrix. Without this feature, each doping level can possibly represent a unique processing challenge as processing conditions may need to be adjusted to accommodate changes in base glass properties.

Based on the requirements set out above, we developed a glass that had both good laser and spectroscopic properties and good properties for ion exchange. The resulting glass composition, (with the commercial designation IOG-1^[17]), is given in mole percent oxide in Table 1. Al_2O_3 is added chiefly to increase durability since phosphate containing glasses with P_2O_5 content higher than 50 mole percent are normally react with molten salt baths and the other processing chemicals used in waveguide preparation (i.e. to remove ion diffusion barriers). The incorporation of a high total lanthanide content (denoted as R_2O_3 in Table 1) also contributes to enhanced chemical durability and allows for variation in active ion concentration with minimal impact on glass properties. The alkali oxide of choice is Na_2O since the sodium ion is known to be very mobile in glass and because sodium ion also exchanges well with potassium or silver for waveguide preparation.

All glasses were melted using high purity raw materials. Transition metal content in the glasses was estimated at 20 ppm Fe and less than 1 ppm for all other common transition metals. Lanthanum, erbium, and ytterbium rare earth compounds were selected to minimize the introduction of other lanthanide elements (less than 1000 ppm total). Melting and refining temperatures were typically 1250 to 1350 °C, with refining periods of 2 to 3 hours. Produced glass was cast into molds and annealed at 530 °C for 2 hours and cooled to room temperature at 30 °C/hr. Cast blocks were then used to prepare

DRAFT DRAFT DRAFT

characterization samples for refractive index, density and residual hydroxyl content at 3.0 μm and 3.333 μm . The measurements of index and density allowed calculation of estimated index values at lasing wavelengths and number density allowed calculation of estimated index values at lasing wavelengths and number density of rare earth input content using standard techniques.^[18] Absorption at these wavelengths was monitored and held to levels of less than 1.0 cm^{-1} and 1.8 cm^{-1} , respectively.

2.2 Spectroscopic Measurements

Yb/Er-codoped and Yb-doped IOG-1 glass samples with were prepared for measurement of spectral absorption. Both glasses were doped with Yb concentration of $4 \times 10^{20} \text{ cm}^{-3}$ and the codoped sample contained $1 \times 10^{20} \text{ cm}^{-3}$ Er ions. The dimensions of the characterization samples were 9-mm thick, 21-mm tall and 10 mm wide. The absorption spectra were measured using an automatic spectrophotometer. The emission cross section spectrum for the erbium ions was calculated using the theory of McCumber^[19] as applied by Miniscalco and Quimby^[20] using the measured spectral absorption. The Yb emission cross section was obtained from measured spontaneous emission spectra and scaled to give the measured radiative decay rate. To measure the emission spectra, the samples were pumped at a wavelength of 974 nm and the spectra were recorded using a 0.3-m triple grating spectrometer.

The lifetime of the $^4I_{13/2}$ Er laser manifold in the codoped glass was measured in the limit of vanishing excitation power by chopping a 974 nm pump laser beam at 50 Hz using an acoustooptic modulator. The fluorescence decay near 1550 nm wavelength was observed to determine the 1/e lifetime. The lifetime of the $^2F_{5/2}$ Yb level was measured similarly by observing fluorescence decay near 974 nm.

2.3 Waveguide Laser Fabrication Process

Waveguide lasers were fabricated in Yb/Er-codoped and Yb-doped IOG-1 phosphate glasses. The Yb/Er glass was doped with 1.15 wt % Er_2O_3 (1.0×10^{20} ions/cm³) and 4.73 wt % Yb_2O_3 (4.0×10^{20} ions/cm³). For the Yb-doped laser, the glass was doped with 4.73 wt % Yb_2O_3 (4.0×10^{20} ions/cm³). Waveguides were formed by K^+ - Na^+ exchange through channel apertures ranging in width from 3 to 8 μm . The apertures were etched in a 200 nm thick Al mask layer. The exchange was performed in a crucible containing molten KNO_3 at 375 °C for 4 h. The Yb/Er laser results reported below are for a waveguide formed using a 6.5 μm mask aperture and the Yb laser results are for a 3 μm mask aperture.

A distributed Bragg reflector (DBR) surface relief grating was fabricated on a comb of eleven waveguides using a separate codoped specimen in a 0.5 μm thick layer of photoresist. A 90° corner split a collimated laser beam into two beams for a holographic exposure.^[21] The exposure angle was set to write a grating with a period of $\Lambda = 507.8$ nm. For a waveguide with estimated effective index of 1.515 ± 0.003 , this period was calculated to provide laser operation at $\lambda = 1538.6 \text{ nm} \pm 3 \text{ nm}$. During the development of the photoresist, the diffraction of light from a 632.8 nm HeNe laser was monitored.^[22] When the first-order-diffracted power reached a maximum, the grating was removed, rinsed, and dried.

Before transferring the photoresist pattern into the glass by Ar-ion sputtering, we deposited 40 nm of Cr on the surface with the specimen inclined 60° to the electron-beam evaporation source. Mounting the specimen in this way causes Cr to accumulate only on the tops of the grating lines and not in the grooves, thus providing a durable etch mask.

DRAFT DRAFT DRAFT

We etched the grating in the glass for 20 minutes using a reactive ion etching system with 6.67 Pa (50-mTorr) Ar-ion plasma. The low-pressure plasma created a large self-bias voltage of 1700 V when running at 365 W of coupled power with frequency 13.5 MHz. The electrode spacing was 3.2 cm. After being etched, the sample was cleaned ultrasonically in photoresist stripper at 85 °C. Figure 1 shows a schematic of a completed DBR laser array.

2.4 Waveguide and Laser Measurements

Several measurements were performed to determine the properties of the ion exchanged waveguides. The refractive index as a function of position within the sample was analyzed using the method of refractive near-field scanning.^[23] The dimensions of transverse modes of the waveguides were measured by coupling light into one end of the waveguide and imaging the light emerging from the other end onto a calibrated infrared camera.

To test the Yb/Er-codoped Fabry-Pérot lasers (lasers with no etched gratings), we typically pumped the waveguides using a tunable Ti: Al₂O₃ laser. Figure 2 shows a schematic of the laser measurement setup. Placing broadband dielectric mirrors on the polished waveguide end faces formed the laser cavities. The mirrors were held in place by small spring clips with index matching oil between the end facet and the mirror. The pump laser light was launched through one of the mirrors with a 4X microscope objective. The laser output and unabsorbed pump light were collimated with a 16X microscope objective and separated using filters. The mirror through which the pump light was launched had a reflectance of >99.9 % and 15 % at 1.54 and 0.96 μm , respectively. The

DRAFT DRAFT DRAFT

output coupler had a reflectance of 80 % at 1.54 μm and 15 % at 0.96 μm . Neither the waveguide length nor the cavity output couplings were optimized.

The Yb-doped waveguide laser was tested using a setup similar to the one shown in Fig 2. The Yb³⁺ device was 10 mm in length. The pump-input mirror had a reflectance of 50 % at 950 nm and 98 % at 1030 nm. Two output couplers with transmittances of 7 % and 21 % at 1020 nm were investigated. These output couplers had reflectances of 32 % and 34 % at 950 nm, respectively.

The configuration shown in Fig 2 was also used to evaluate the slope efficiency and threshold of a Yb/Er-codoped DBR laser. The DBR grating was used as the output coupler instead of the end mounted mirror. To investigate the longitudinal mode structure of the laser we coupled the laser output into an optical fiber scanning Fabry-Perot interferometer with a free spectral range of 124 GHz.

We measured the linewidth of the DBR laser using a conventional self-heterodyne configuration with a 75 MHz frequency shift.^[24] The path length difference between the two arms in the self-heterodyne system was 10 km, corresponding to a linewidth resolution limit of 30 kHz for a Gaussian line shape.^[25] Optical isolators were used in both arms to prevent optical linewidth narrowing due to feedback; however, the output end of the laser was not beveled.

Several other laser parameters were measured for the DBR laser. We measured the laser wavelengths of other waveguides on the chip using an automatic spectrum analyzer with a resolution of 0.1 nm to determine the variation in wavelength as a function of diffusion aperture width. The excess relative intensity noise (RIN) of the DBR laser formed with an 8 μm diffusion aperture between 0.1 and 1.1 GHz was measured using a

DRAFT DRAFT DRAFT

shot noise calibrated RIN measurement system that employs a rf spectrum analyzer. A grating-stabilized, 974-nm pigtailed laser diode served as the pump source. Light from the pump was coupled to a waveguide laser using aspheric lenses. The output power of the DBR laser was set to 2 mW for the measurement. The wavelength of the DBR laser was temperature tuned by varying the temperature of the laser chip from 30 °C to 80 °C using a resistive heater in contact with the waveguide mount.

3. Experimental Results**3.1 Spectroscopic Results and Lifetimes**

Figure 3a shows the spectral dependence of absorption and emission cross sections of the erbium ions in Yb/Er-codoped IOG-1. The peak emission cross section of the Er^{3+} using this method was found to be $6.6 \times 10^{-21} \text{ cm}^2$ at 1542 nm. The measured upper state lifetime of the $^4\text{I}_{13/2}$ Er manifold was measured to be 8.1 ms in the limit of vanishing excitation power. Figure 3b shows the spectral dependence of the absorption and emission cross sections for IOG-1 glass doped with a Yb concentration of $4 \times 10^{20} \text{ cm}^{-3}$. The peak emission cross section of the $^2\text{F}_{5/2}$ laser manifold is $1.27 \times 10^{-20} \text{ cm}^2$ and occurs at a wavelength of 974 nm. The radiative lifetime of the $^2\text{F}_{5/2}$ level was measured to be 1.4 ms. The peak absorption cross section was at 974 nm and was $1.28 \times 10^{-20} \text{ cm}^2$. Uncertainties in these reported cross sections are $\leq 20 \%$. A discussion of the Yb-Er cross relaxation efficiency will follow in the discussion section.

3.2 Waveguide Measurement Results

Visual inspection of the waveguide samples after the ion exchange revealed that regions of the glass surface corresponding to the location of the mask openings had become recessed by approximately 1 μm during the exchange process. The widths of the

DRAFT DRAFT DRAFT

recessed channels were close to the widths of the mask apertures and uniform in width and depth. The surface quality of the glass in the recessed regions, observed using a 1000x Nomarski contrast microscope, appears identical to the original surface of the glass and apparently does not cause significant scattering losses. The waveguide end faces were polished perpendicular to the channels. The final sample length was 22 mm.

Figure 4 shows the refractive index depth profile obtained from the refracted ray measurement method at the center of the waveguide formed with the 6.5 μm mask aperture. The data was taken using a wavelength of 635 nm. The spatial resolution is $\sim 1 \mu\text{m}$, and the uncertainty of the absolute index value is ~ 0.001 . The index profile indicates a maximum index change of 0.008 that is typical of potassium-sodium ion exchange.

The waveguide supported a single transverse mode having dimensions of 16 μm wide by 11 μm deep (measured at the 1/e points of intensity profile) at 1540 nm. It supported multiple transverse modes at 980 nm. However, when the devices were lasing, the pump energy was confined primarily within the lowest order transverse mode, which had dimensions of 13 μm wide by 9.5 μm deep. The uncertainty of the mode dimensions determined using this method are $\sim 10\%$.

3.3 Yb/Er Fabry-Perot Waveguide Laser Measurement Results

The laser output power as a function of coupled pump power for the 22 mm device pumped at 960 nm, is shown in Figure 5. We estimated the coupling efficiency of the incident pump power to be between 65 and 71 %, including losses due to the transmittance of the input mirror and launching objective. The coupled pump power shown on the x-axis in Figure 5 was calculated based on a 71 % coupling efficiency. The uncertainty of the power measurements are estimated to be 5 %. The threshold pump power was 23

DRAFT DRAFT DRAFT

mW, and the slope efficiency was 28 %. One end of the waveguide was accidentally chipped during our experiments and necessitated the repolishing of the end face. The output powers as a function of coupled pump powers of the resulting 20-mm long waveguide laser, when pumped at 979 nm, are also shown in Fig. 5. The launched pump power threshold was 51 mW, and a maximum output power of 170 mW was obtained for 610 mW of launched pump power. At these power levels, there was no change in the slope efficiency as a function of pump power, suggesting that the Yb ions are not saturating as they do in Yb/Er-codoped silica fiber lasers. [26]

The Yb/Er-laser usually operated at several wavelengths simultaneously. A typical laser spectrum showing simultaneous operation at 1.536, 1.541, and 1.545 μm is depicted in Figure 6. The laser spectrum could be shifted in wavelength by passing some of the collimated 1.5 μm laser output through a prism and reflecting it back through the prism and into the waveguide using a dielectric mirror. This operation formed a weakly coupled, external cavity. The cavity is shown in Fig. 7a. Rotating the output coupler mirror produced wavelengths ranging from 1536 to 1595 nm.

Tuning of the laser was also accomplished using the extended cavity configuration shown in Figure 7b. We used a first order grating with a reflectance of 0.6 for the laser output coupler. We rotated the grating and could tune the laser from 1525 nm to 1564 nm when the coupled pump power was 280 mW at a wavelength of 980 nm. The laser output power as a function of wavelength is illustrated in Fig. 8a. Three representative spectra of the laser are shown in Fig. 8b.

3.4 Yb-doped waveguide laser measurement results

DRAFT DRAFT DRAFT

The laser output power as a function of launched pump power is shown in Figure 9. The launching efficiency of the pump for these measurements was 45 %. For the 7 % output coupler, the threshold when pumped at 949 nm was 18 mW of coupled pump power. For the 21 % output coupler, the threshold pump power was 25 mW, and up to 120 mW of output power was obtained. The slope efficiency was 67 % when based on coupled pump power.

Like the Yb/Er laser, the Yb laser typically operated at several wavelengths simultaneously. At lower pump powers, the longer wavelength transitions dominate due to ground state re-absorption losses, which are larger at shorter wavelengths. As the pumping intensity in the waveguide increases, the Yb-ion ground state population and hence the ground state re-absorption loss is reduced, and the shorter wavelength transitions, which lie closer to the peak of the Yb^{3+} emission cross section, are favored.

The Yb-doped waveguide laser was tuned by reflecting some of the collimated laser output power back into the waveguide using the first-order reflection from a diffraction grating having 1200 grooves/mm. The cavity was similar to Fig. 7b. Rotating the grating tuned the laser continuously from 986 nm to 1050 nm.

3.4 Single-frequency Yb/Er-codoped DBR lasers

Figure 10 shows the DBR laser output power as a function of launched pump power and the spectrum of the laser. The waveguide diffusion aperture for this waveguide was 8 μm . The slope efficiency as a function of launched pump power is calculated to be 26 % when we take the pump coupling factor to be 71 %.

We estimated the reflectance of the grating using the simplified laser formula derived from the theory of Rigrod:^[27]

DRAFT DRAFT DRAFT

$$\frac{P_1}{P_2} = \frac{1 - R_1}{1 - R_2} \sqrt{\frac{R_2}{R_1}} \quad (2),$$

where P_1 is the output power at the grating end and P_2 is the output power at the end opposite the grating. R_1 is the grating reflectance and R_2 is the reflectance of the attached mirror. We used two mirrors with reflectances of 80 and 90 percent for R_2 . For both cases we calculated the grating reflectance R_1 to be 65 percent.

Figure 11 shows that the laser operated on a single longitudinal mode when the coupled pump power did not exceed 300 mW. The laser was robustly single frequency with TE polarization, and no mode hopping was observed. The inset in Figure 11 shows that a second longitudinal mode appeared when the coupled pump power exceeded 300 mW. In this pump regime, the laser was unstable and exhibited mode hopping, single-frequency operation, and dual-frequency operation. By measuring the frequency spacing between the longitudinal modes we determined that the effective physical length of the laser cavity was 1.4 cm.

Figure 12 shows the self-heterodyne spectrum. The laser linewidth we obtained from this measurement was 500 kHz. Seven of the eleven waveguides on the chip exhibited laser oscillation. The waveguides formed through the smaller apertures did not achieve threshold because the smaller mode volumes caused a reduction of the gain such that the 35 % transmittance loss of the grating could not be overcome. Table 3 shows the laser operating wavelengths as we scanned the comb of waveguides that had diffusion aperture widths ranging from 5 to 8 μm . In general, the wavelength increases as the diffusion aperture width increases, which is consistent with increasing effective index as the

DRAFT DRAFT DRAFT

aperture width increases. A visible defect was apparent on waveguide No. 4 that caused a deviation from the trend.

The results of the RIN measurements are shown in Figure 13. Figure 13a shows that the RIN dropped to less than -150 dB/Hz for frequencies above ~0.5 GHz. The data have not been smoothed. We estimate the uncertainty in the RIN to be 2 dB/Hz. By measuring the relative amplitude noise (with respect to the noise floor) between 100 kHz and 10 MHz, we found that the relaxation oscillation peak was located near 350 kHz as shown in Fig. 13b. These noise measurements are consistent with those of Er-doped fiber lasers, and we expect lower RIN when the laser is operated further above threshold.^[26]

The wavelength as a function of temperature is shown in Fig. 14. The tuning range for the test laser varied linearly from 1536 nm to 1536.8 nm for a change in wavelength $\Delta\lambda$, of 0.8 nm. This tuning range matches well with the predicted tunability of the laser of 0.6 nm over 50 °C. The prediction is based on the thermal expansion coefficient of the glass and the change in refractive index as a function of the change in temperature, and is approximated by the following equations:

$$\Delta\lambda \cong 2\Lambda \frac{\Delta n}{\Delta T} \Delta T + 2n\Lambda \left(\frac{1}{\Lambda} \frac{\Delta\Lambda}{\Delta T} \right) \Delta T; \quad \frac{\Delta n}{\Delta T} = -3.2 \times 10^{-6} / ^\circ \text{C}; \quad \frac{1}{\Lambda} \frac{\Delta\Lambda}{\Delta T} = 1 \times 10^{-5} / ^\circ \text{C} \quad (3)$$

where Λ is the grating period and n is the refractive index of the glass. The wavelength stability as a function of temperature is roughly 15 times smaller than that of typical semiconductor DFB lasers.^[28] Thus the temperature control requirements for maintaining a stable wavelength are relaxed.

4. Discussion

It is important to note that the lengths of 22 mm and 20 mm are not optimum lengths for these Yb/Er-codoped waveguide lasers. Using a waveguide laser simulation tool, we predicted the laser output characteristics as a function of length and waveguide mode-field size. The simulation is based on a phenomenological model which incorporates the Yb/Er laser rate equations on a three dimensional grid, the forward and backward propagating laser signals, and the forward propagating pump signal.^[29] The propagating intensity profiles were approximated by elliptical functions that approximated the measured transverse laser mode dimensions and the fundamental pump mode dimension. The glass and laser parameters we used in the model are listed in Table 2. The Yb-Er cross relaxation coefficient (C_{cr}) and the cooperative upconversion coefficient (C_{up}) were the fitting parameters. Reasonable approximations of other laser and waveguide parameters based on actual measurements and analyses were used for other quantities. Figure 5 shows the actual laser data compared to results of the laser simulation. We used $C_{cr} = 3.5 \times 10^{-16} \text{ cm}^3/\text{s}$ and $C_{up} = 2.5 \times 10^{-18} \text{ cm}^3/\text{s}$ to obtain the best fit. Using C_{cr} and the approximate equation for cross relaxation quantum efficiency,

$$\eta = \frac{C_{cr} N_{Er} \tau_{21}^{Yb}}{1 + C_{cr} N_{Er} \tau_{21}^{Yb} (1 + \tau_{32}^{Er} N_{Yb} / \tau_{21}^{Yb} N_{Er})} \quad (1)$$

from reference 6, we calculated the cross relaxation quantum efficiency to be 97 %, a typical efficiency for phosphate glasses.¹⁷ In this equation, we assumed that the lifetime, τ_{32} , is approximately 2.8 μs .

DRAFT DRAFT DRAFT

Simulations using different waveguide laser lengths ranging from 1 to 2 cm were performed. Figure 15 shows how the output power varies as a function of cavity length for several output coupling reflectances ranging from 80 to 95 %, and constant laser pump power of 500 mW. Figure 16 shows the output power as a function of mode width, mode depth and output mirror reflectivity for optimized waveguide lasers. The best solutions are color-coded in red; these ranged from 175 to 185 mW continuous wave output, assuming a nominal cavity length of 1 cm and launched 974-nm pump power of 500 mW. The optimum solution has an output mirror reflectance of 82.9%, a laser mode field with dimensions 6 μm by 12 μm , and a continuous-wave output power of 184 mW at 1.54 μm . The optimization used an adaptive simulated annealing algorithm^[30], driven by a waveguide solver^[31] and the laser rate equation model^[29]. Details of the optimization method will be presented in a later paper.

5. Conclusions

In summary, we have presented an introduction to the development of phosphate-based laser glass for the fabrication of waveguide lasers. Recent results obtained for Yb/Er-codoped waveguide lasers formed by ion exchange in IOG-1 base glass show a dramatic improvement over previously demonstrated waveguide lasers. The lasers presented in this paper have produced output powers in the 1500 nm telecommunication window approaching 200 mW without saturation. Slope efficiencies of 28 % have been achieved. Wavelength tuning has been performed over 70 nm using external cavities. Simulations of Yb/Er-doped waveguide lasers indicated that further improvement of laser performance is possible by optimizing output coupling, cavity length, and doping concentrations. Low-noise DBR lasers that operate on a single longitudinal mode at 1536

DRAFT DRAFT DRAFT

nm have been fabricated and tested. The fabrication process can be applied to the manufacture of monolithic laser arrays with wavelengths conforming to the ITU grid for wavelength-division-multiplexed telecommunications. In addition to these results, we have demonstrated Yb-doped waveguide lasers in phosphate glass operating over a wavelength range of 986 to 1050 nm. These demonstrations of efficient integrated optical lasers clearly show that waveguide lasers are a promising new technology that can be used in many applications that have previously been the domain of semiconductor laser sources.

Acknowledgement

The authors acknowledge the National Science Foundation (PHY-94-15583) and the U.S. Army Research Office (DAAH04-95-1-0300) for support of the University of Rochester effort.

DRAFT DRAFT DRAFT

Table 1: IOG-1 Base
Glass Composition
(mole %)

P_2O_5	60
Na_2O	24
Al_2O_3	13
R_2O_3	3
$R = \Sigma \text{ Rare Earths}$	

Table 1. Vcsey

DRAFT DRAFT DRAFT

Table 2. Parameters used to model the Yb/Er codoped waveguide laser

Length of Waveguide Laser Cavity	$L = 2 \text{ cm}$
Signal Field diameters (elliptical $1/e$ full width)	$W_{sx} = 16 \text{ } \mu\text{m}, W_{sy} = 11 \text{ } \mu\text{m}$
Pump Field diameters (elliptical, $1/e$ full width)	$W_{px} = 13 \text{ } \mu\text{m}, W_{py} = 9.5 \text{ } \mu\text{m}$
Signal Effective Index	$n_s = 1.515$
Pump Effective Index	$n_p = 1.515$
Spontaneous Emission Lifetime of ${}^4I_{13/2}$	$\tau_{21} = 8.1 \text{ ms} = 1/A_{21}$
Stimulated Emission Cross Section @ 1540 nm (${}^4I_{13/2} \rightarrow {}^4I_{15/2}$)	$\sigma_{21} = 4.62 \times 10^{-21} \text{ cm}^2$
Absorption Cross Section @ 1540 nm (${}^4I_{15/2} \rightarrow {}^4I_{13/2}$)	$\sigma_{12} = 4.13 \times 10^{-21} \text{ cm}^2$
Er Pump Absorption Cross Section @ 977 nm (${}^4I_{15/2} \rightarrow {}^4I_{11/2}$)	$\sigma_{13} = 1.9 \times 10^{-21} \text{ cm}^2$
Yb Absorption Cross Section @ 977 nm (${}^2F_{7/2} \rightarrow {}^2F_{5/2}$)	$\sigma_{56} = 1.04 \times 10^{-20} \text{ cm}^2$
Yb Emission Cross Section @ 977 nm (${}^2F_{5/2} \rightarrow {}^2F_{7/2}$)	$\sigma_{65} = 1.19 \times 10^{-20} \text{ cm}^2$
Yb-Er Cross Coupling Coefficient C_{cr}	Fitting parameter, see text
Upconversion Coefficient C_{up}	Fitting parameter, see text
Signal Wavelength	$\lambda_s = 1540 \text{ nm}$
Pump Wavelength	$\lambda_p = 977 \text{ nm}$
Er Ion Density	$N_{er} = 1 \times 10^{20} \text{ cm}^{-3}$
Yb Ion Density	$N_{yb} = 4 \times 10^{20} \text{ cm}^{-3}$
High Reflector Reflectance	$R_1 = 0.9995$
Output Coupler Reflectance	$R_2 = 0.80$
Nonradiative Lifetime of Level ${}^4I_{11/2}$	$\tau_{32} = 2.8 \text{ } \mu\text{s} = 1/A_{32}$
Excess Waveguide Scattering Loss	$\alpha_{is} = 0.1 \text{ dB/cm}$ $\alpha_{ip} = 0.2 \text{ dB/cm}$

Table 2. Veasay

DRAFT DRAFT DRAFT

Table 3. List of waveguides, mask aperture widths, and corresponding DBR laser output wavelengths

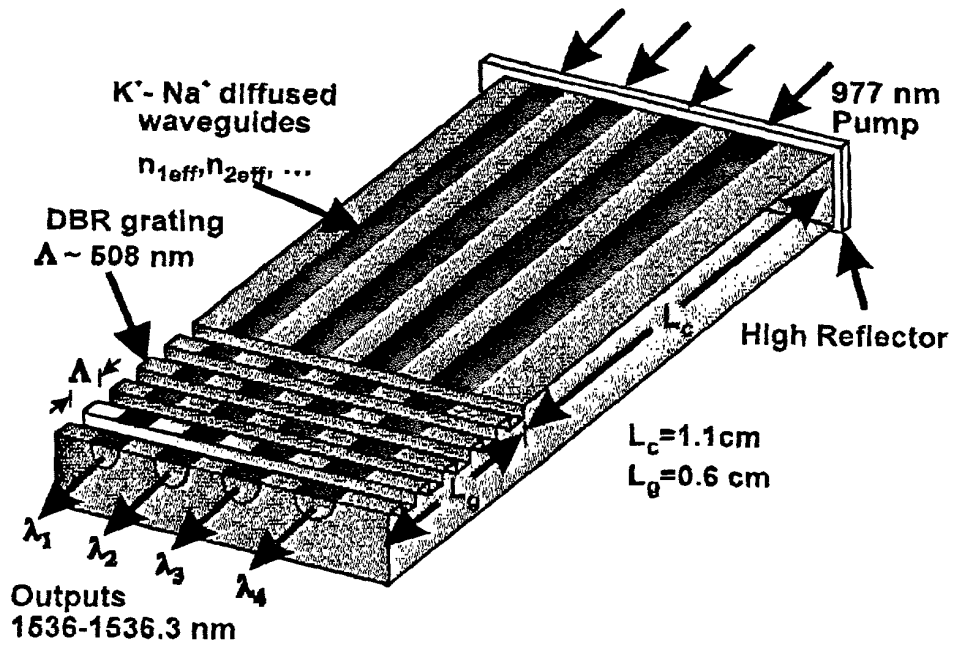
Waveguide	Aperture width (μm)	Wavelength (nm)
1	8.0	1536.02
2	7.5	1536.09
3	7.0	1536.05
4*	6.5	1535.15
5	6.0	1536.26
6	5.5	1536.24
7	5.0	1536.32

* observed defect in sample

Table 3. Veasey

DRAFT DRAFT DRAFT

Figure 1. Veasey



DRAFT DRAFT DRAFT

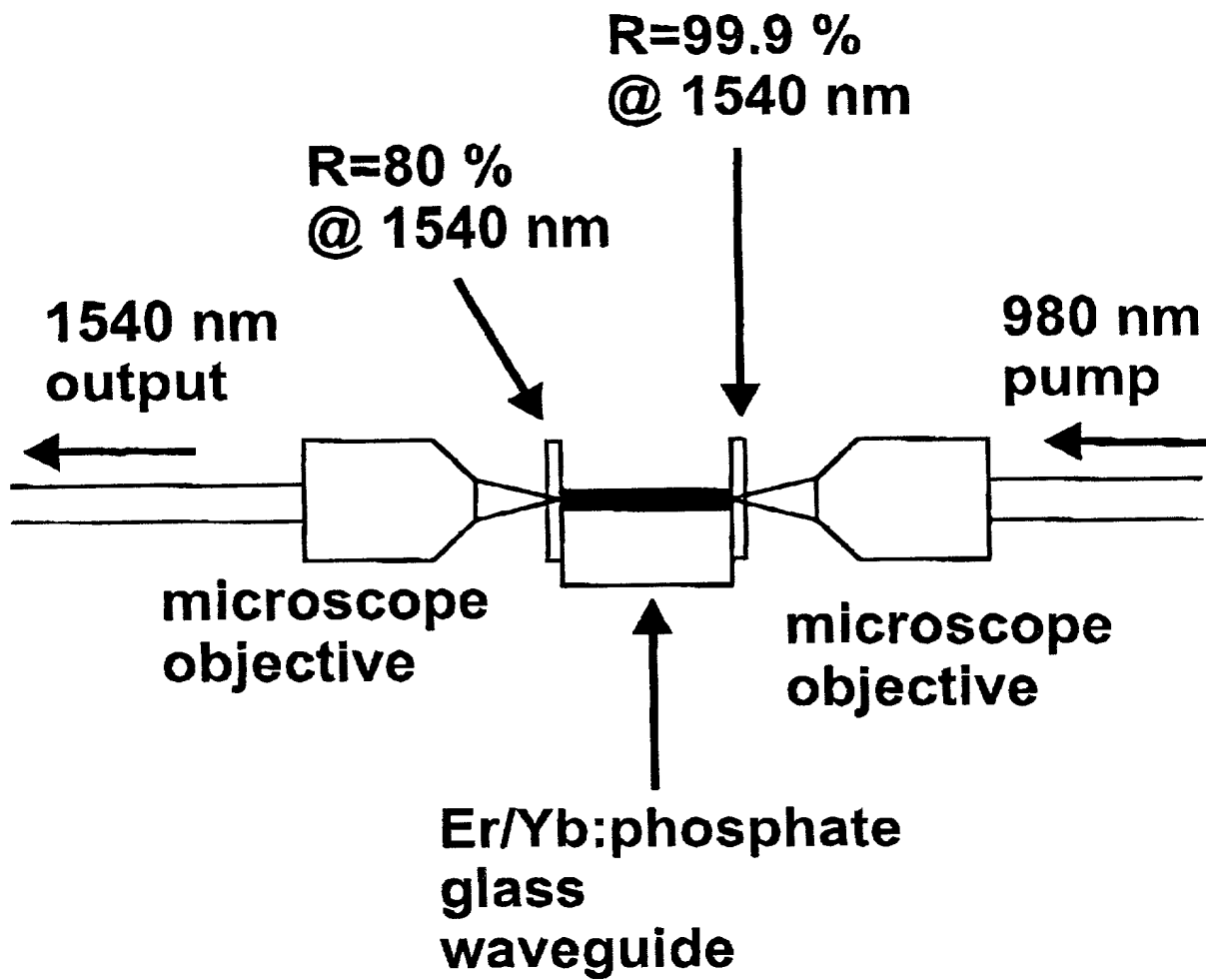


Figure 2. Veasey

DRAFT DRAFT DRAFT

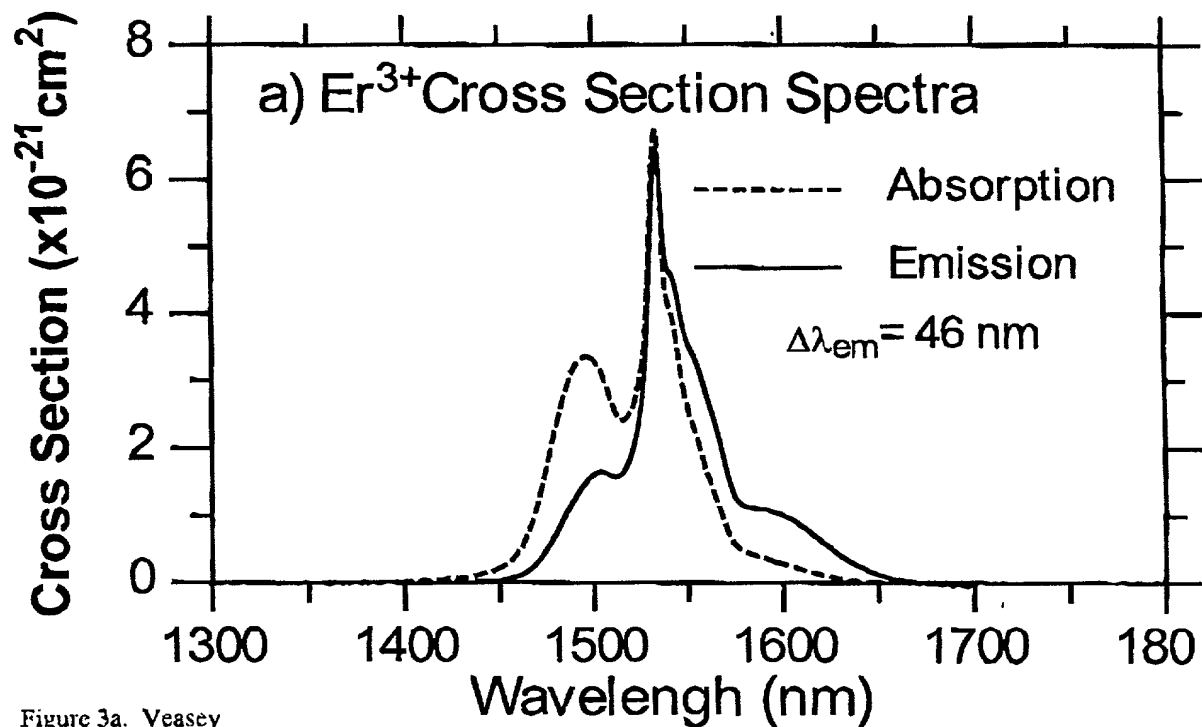


Figure 3a. Veasey

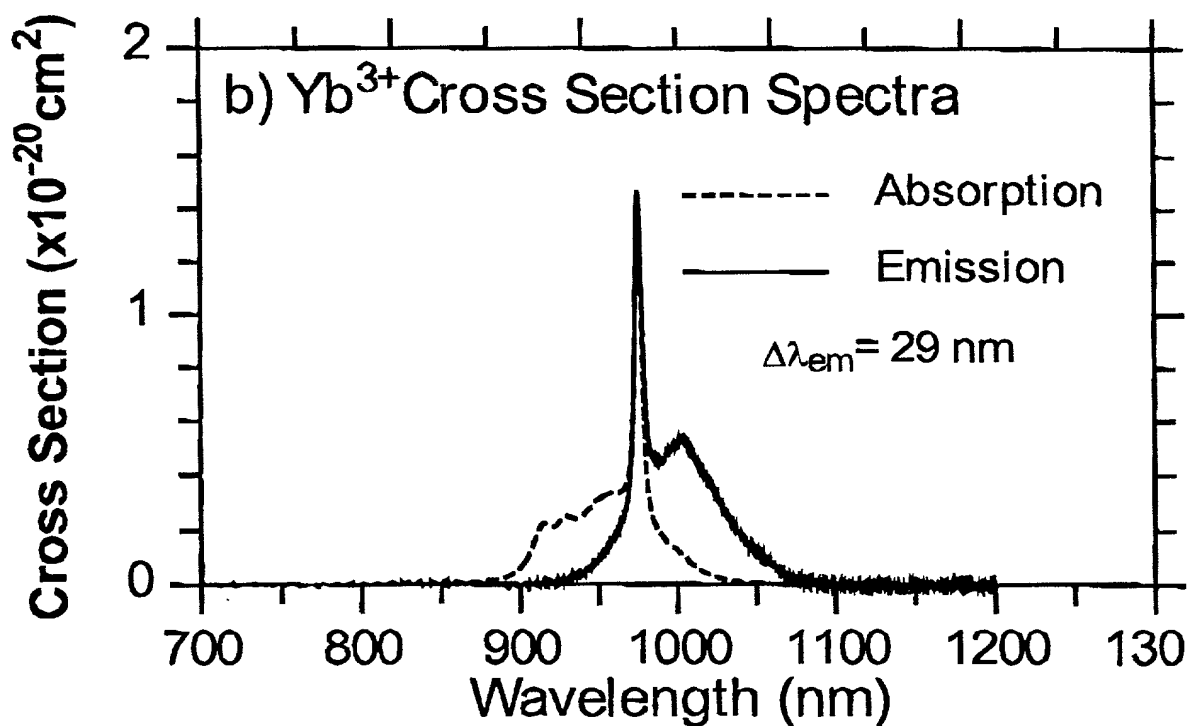


Figure 3b. Veasey

DRAFT DRAFT DRAFT

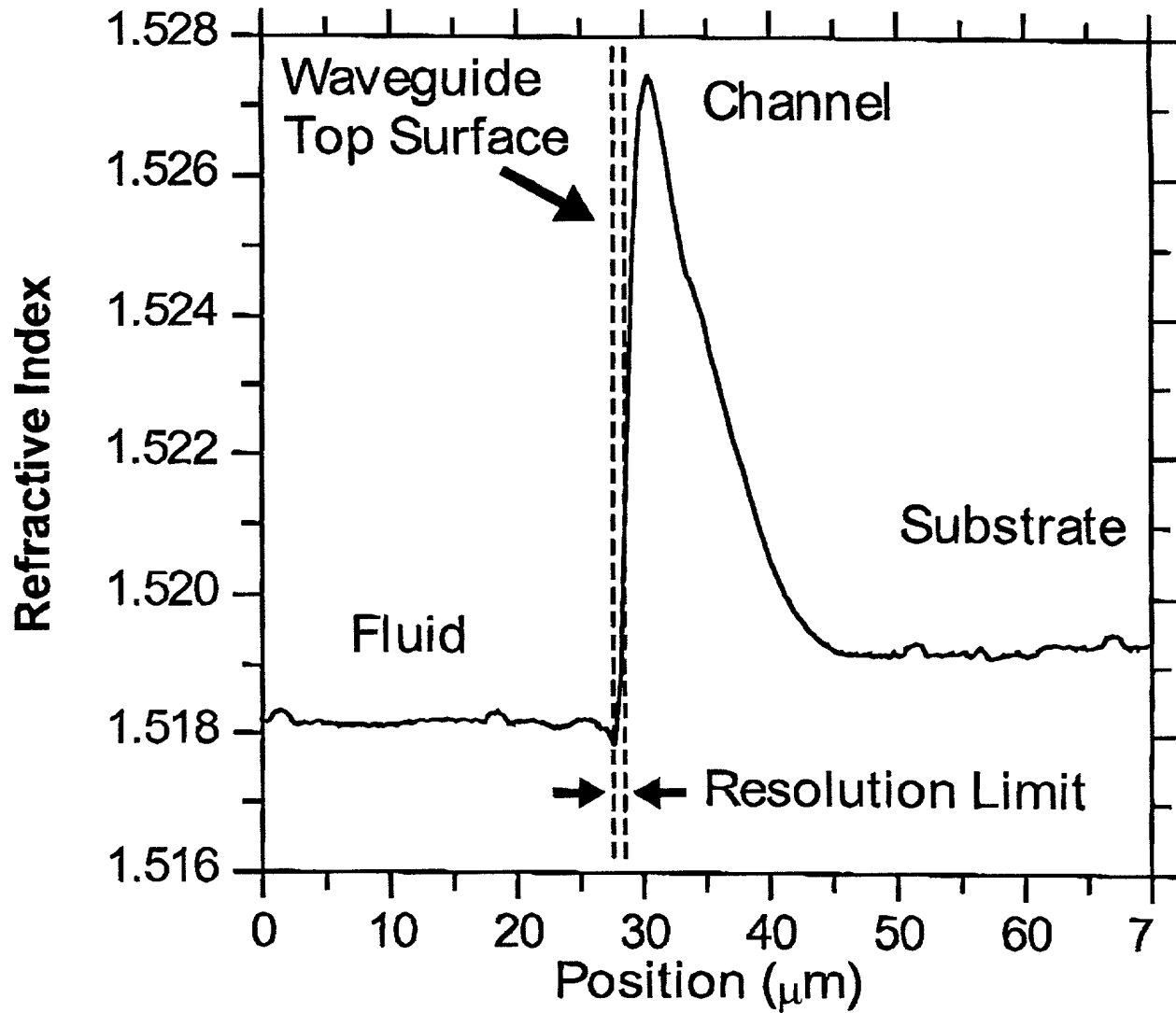


Figure 4. Veasey

DRAFT DRAFT DRAFT

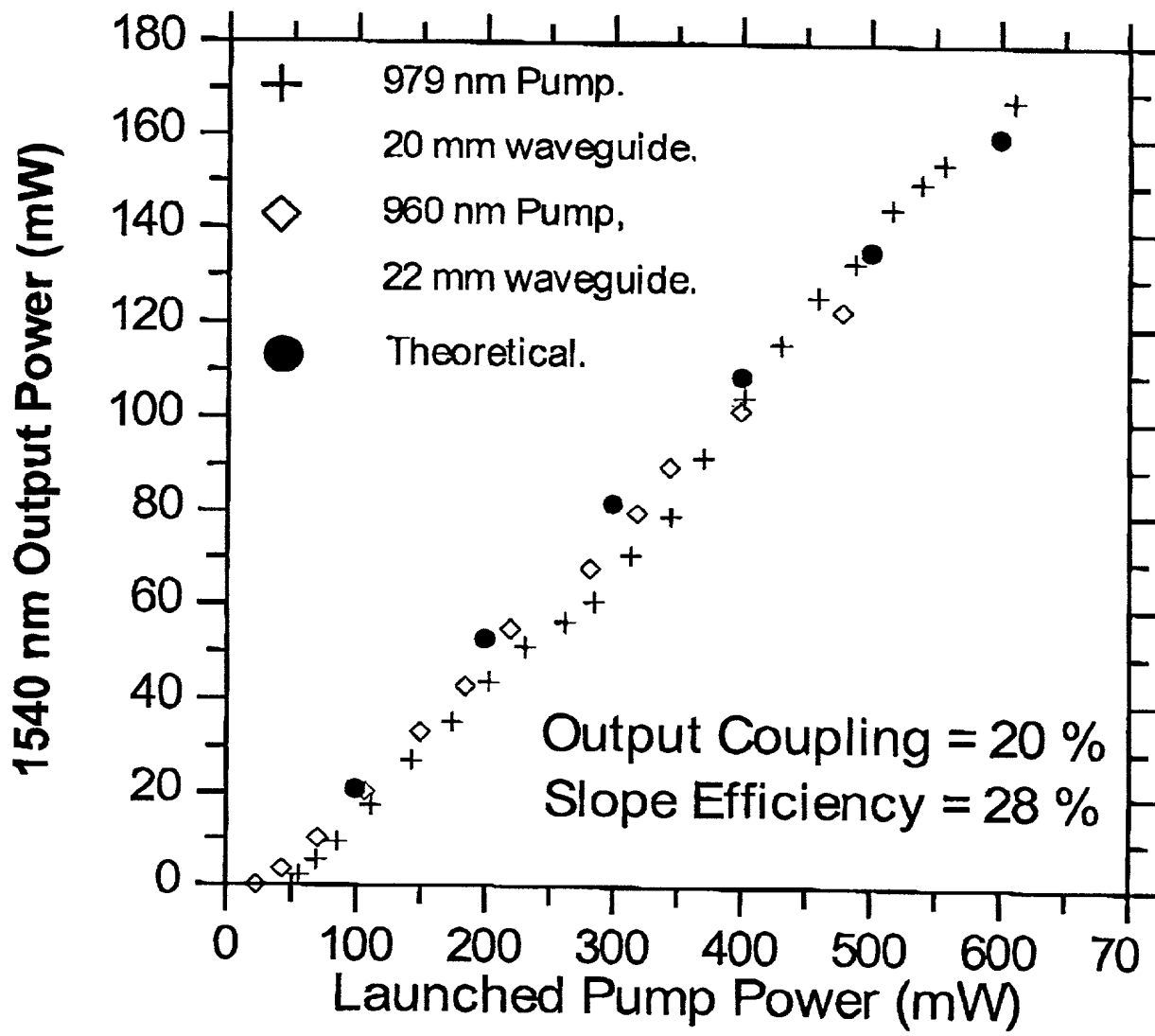


Figure 5. Veasby

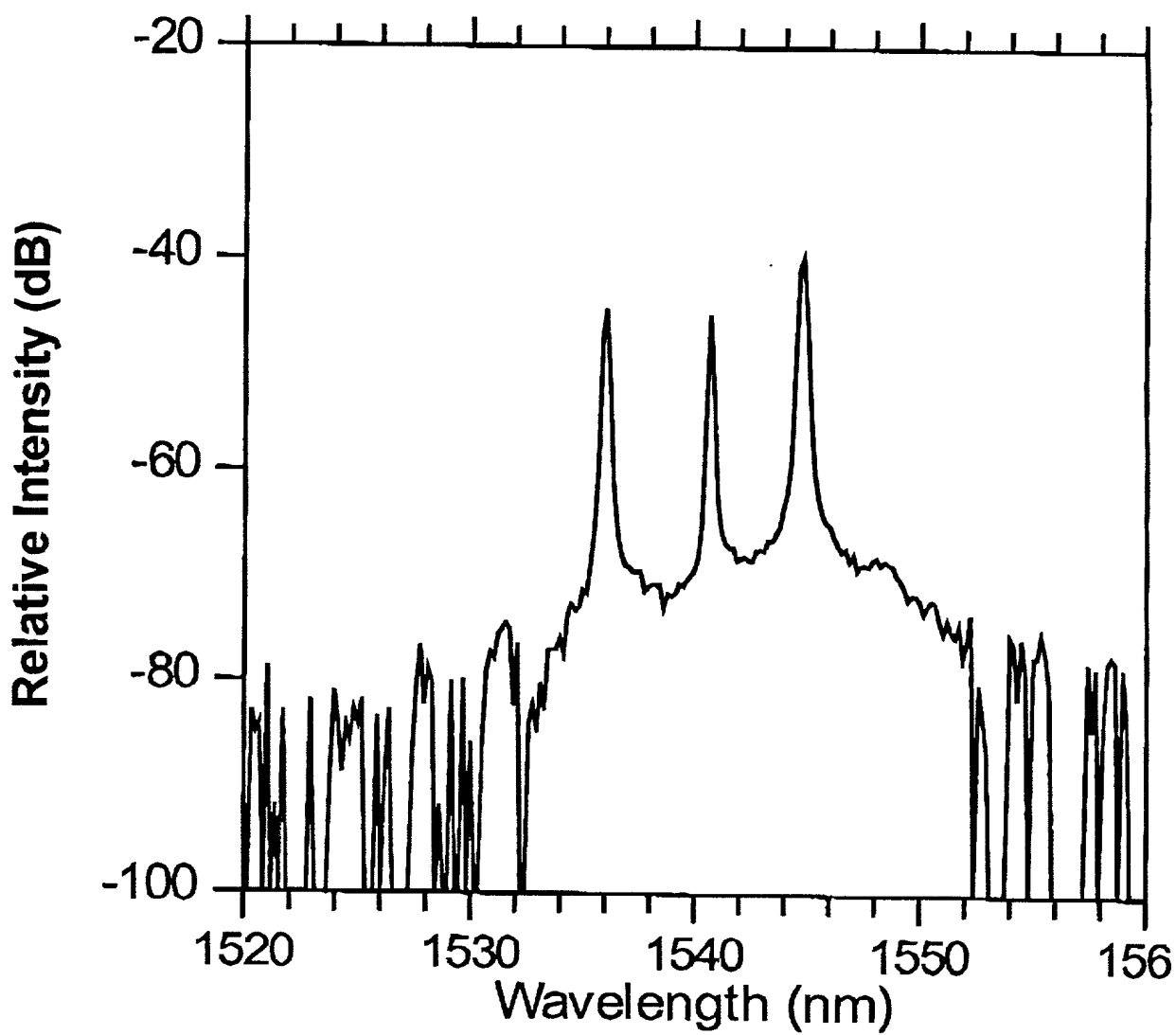


Figure 6. Veasey

DRAFT DRAFT DRAFT

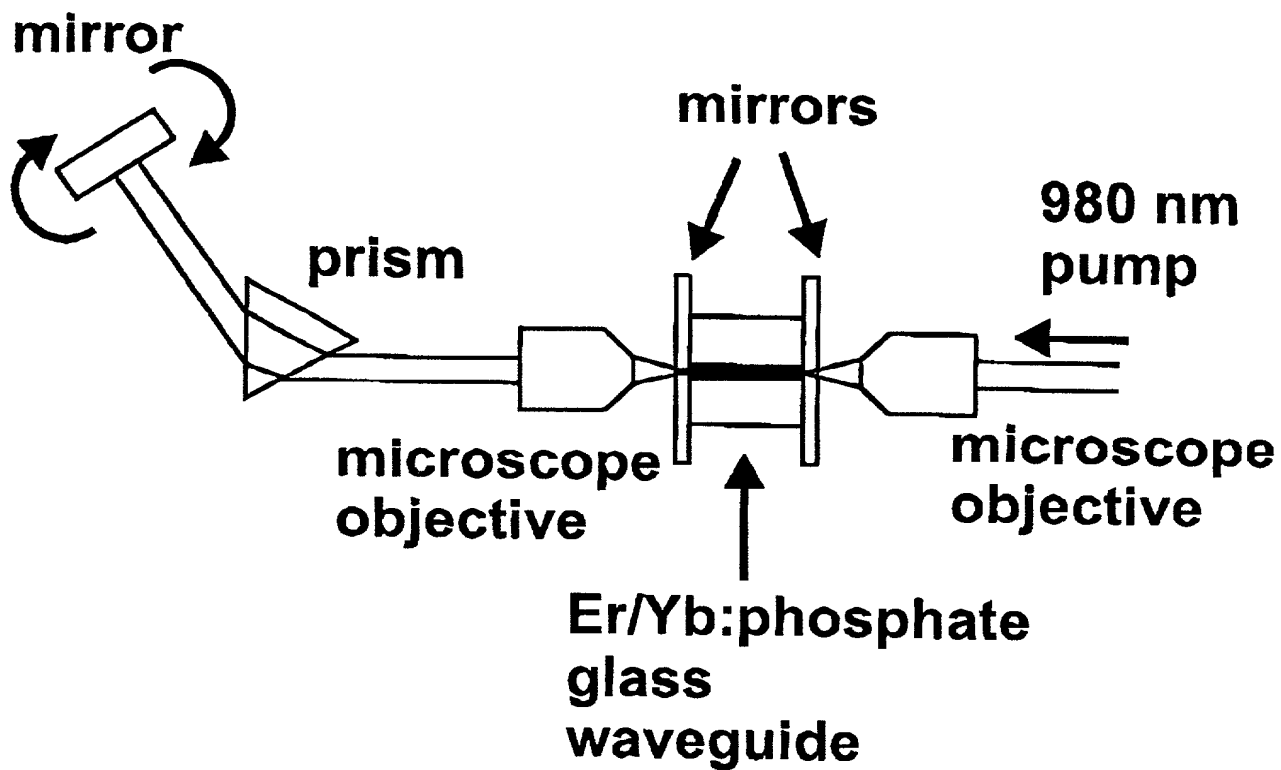


Figure 7a. Vcasey

DRAFT DRAFT DRAFT

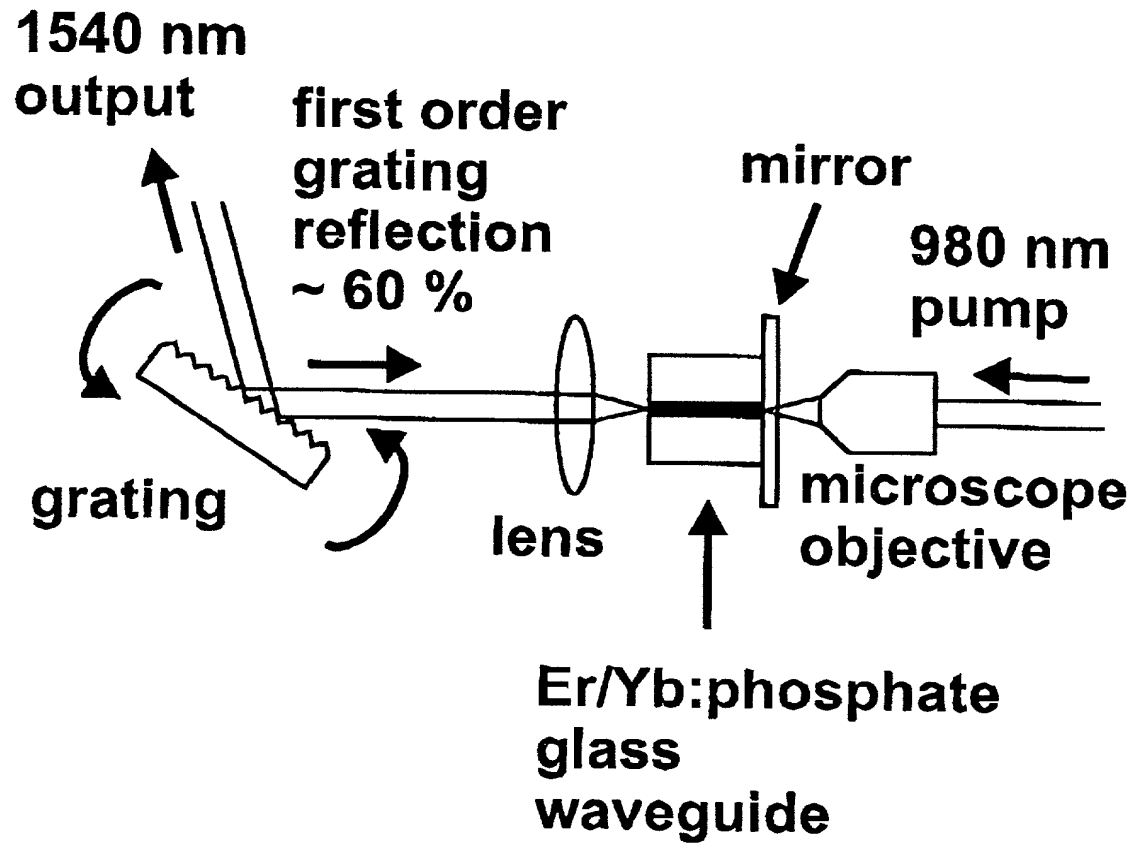


Figure 7b.

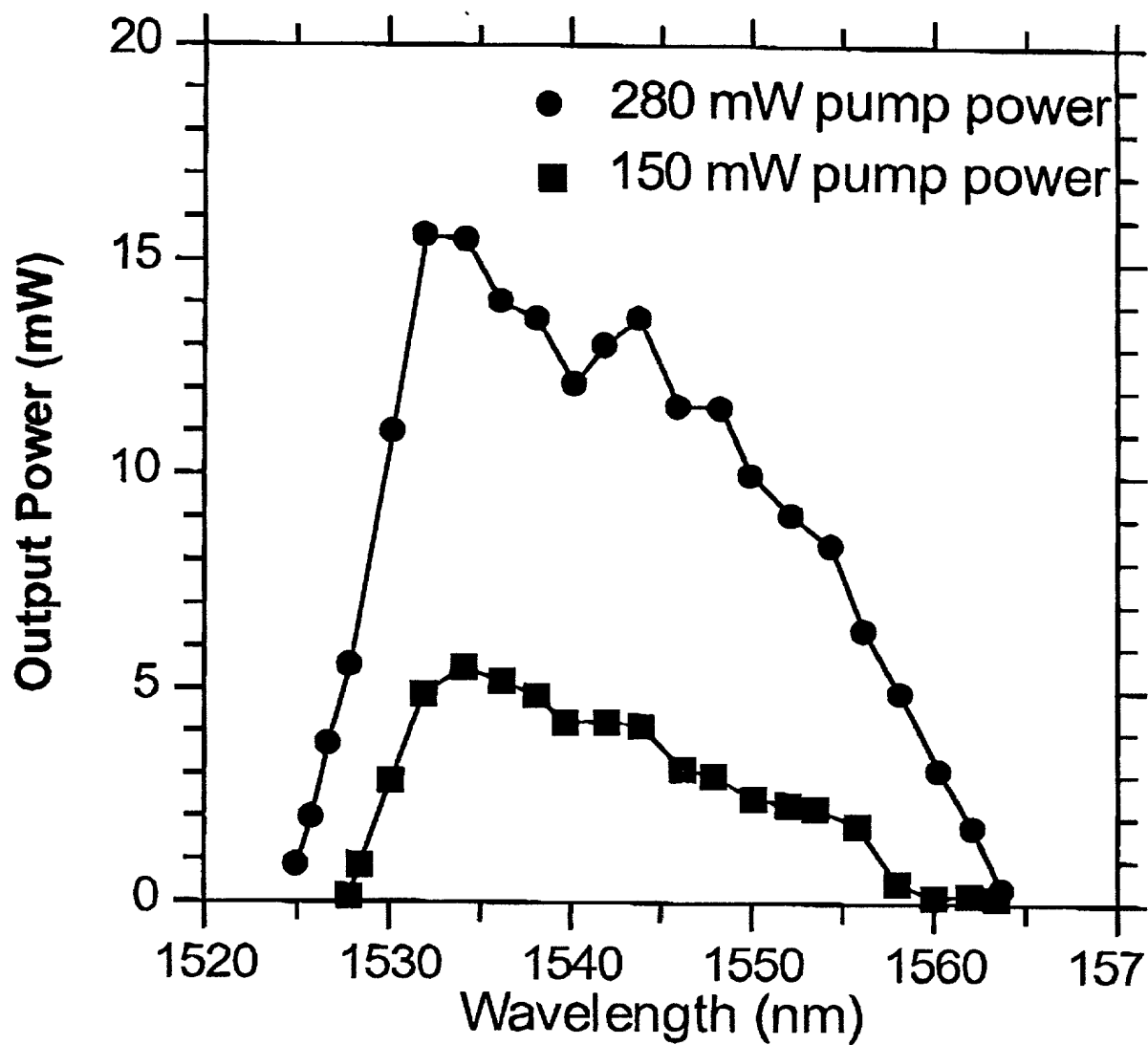


Figure 8a. Vcasey

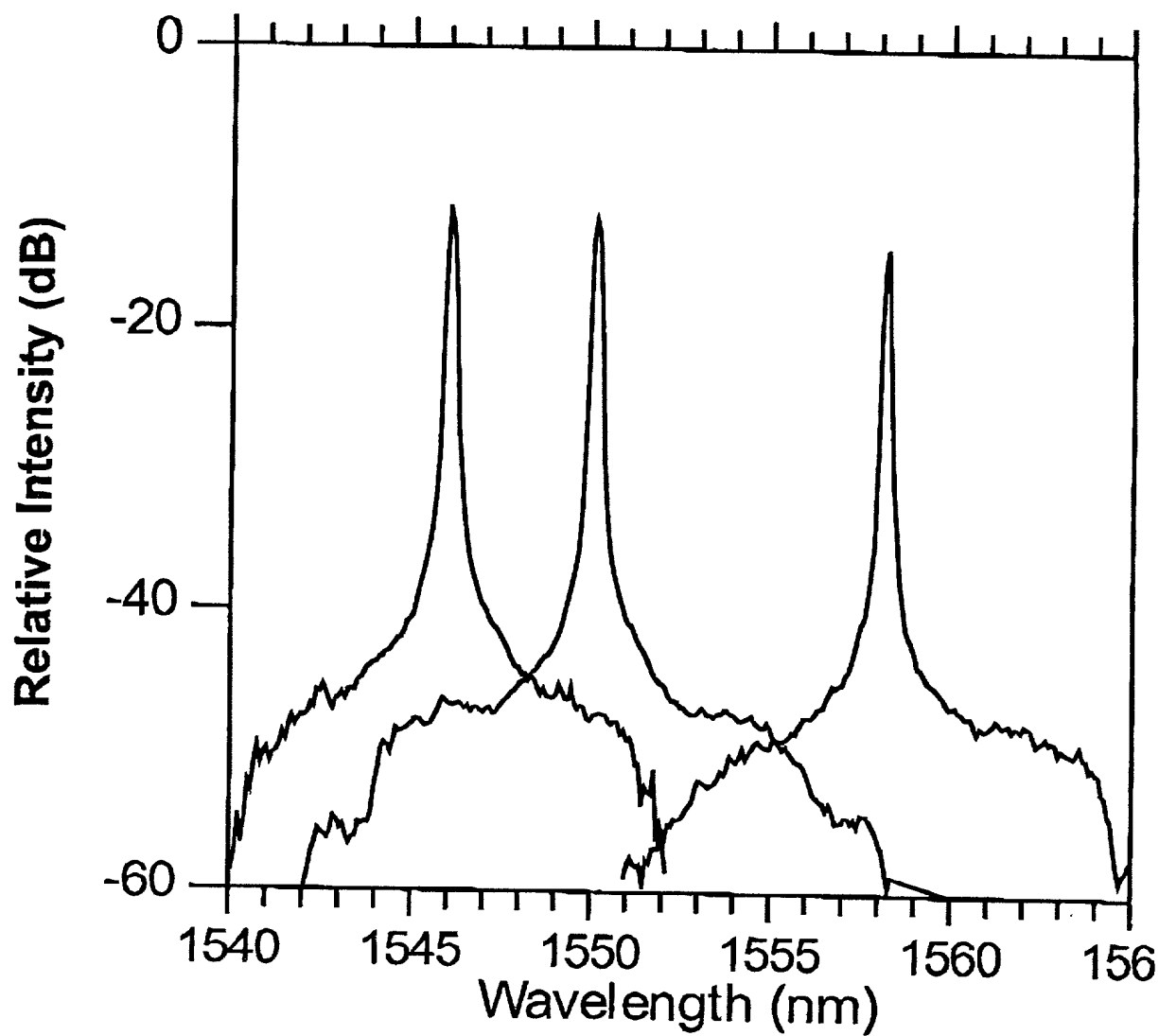


Figure 8b. Vercy

DRAFT DRAFT DRAFT

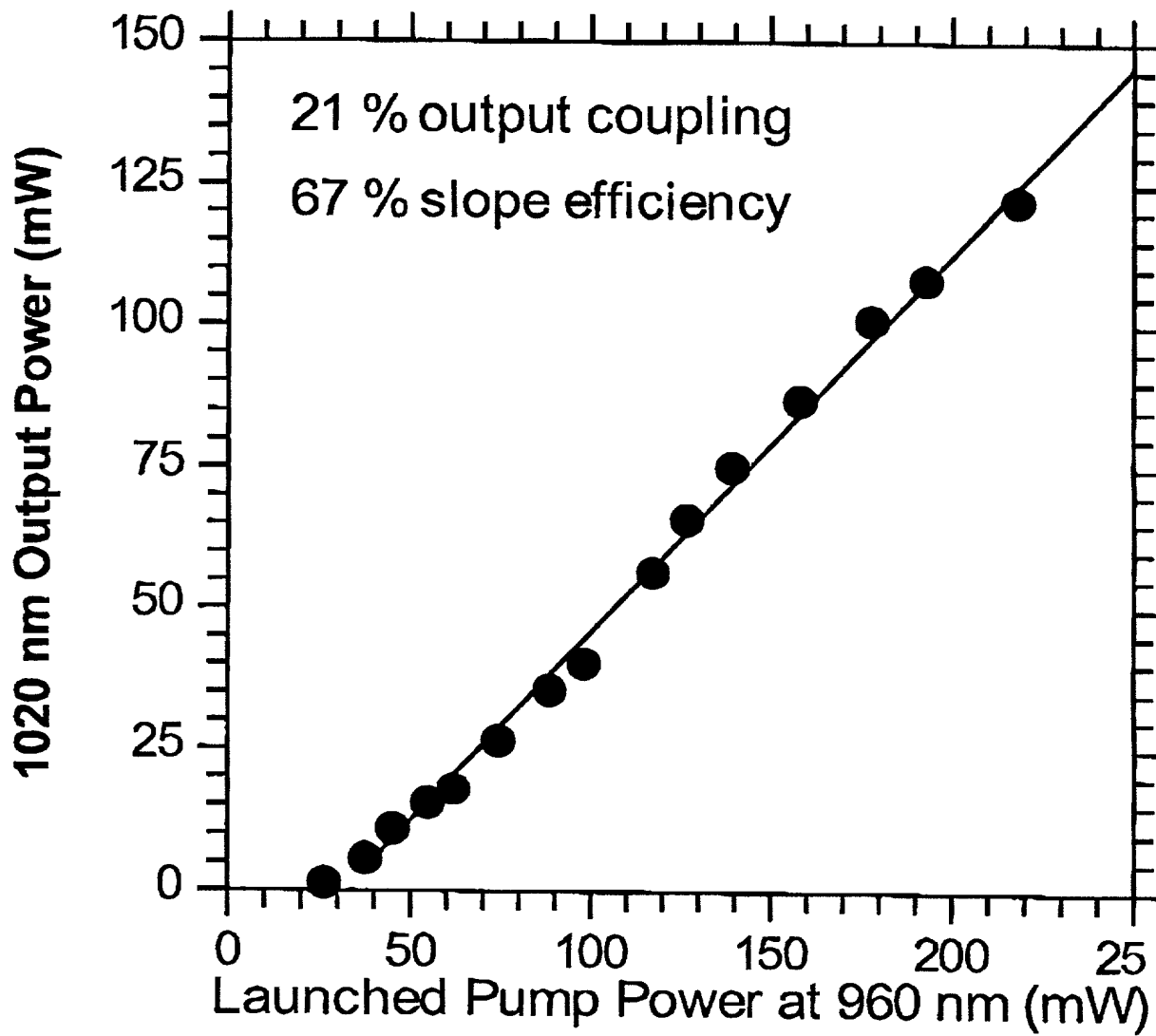


Figure 9. Veasey

DRAFT DRAFT DRAFT

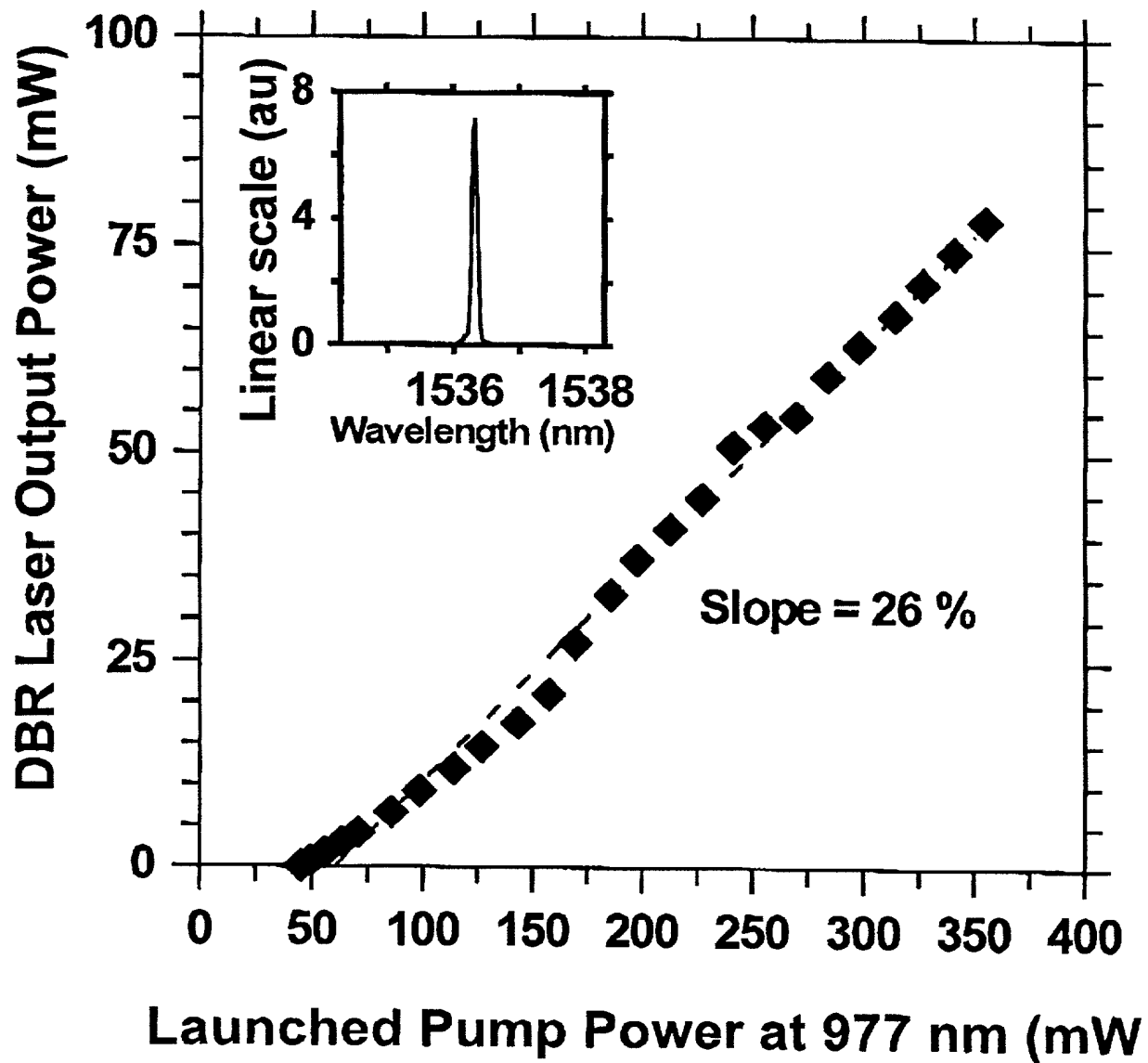


Figure 10. Veasny

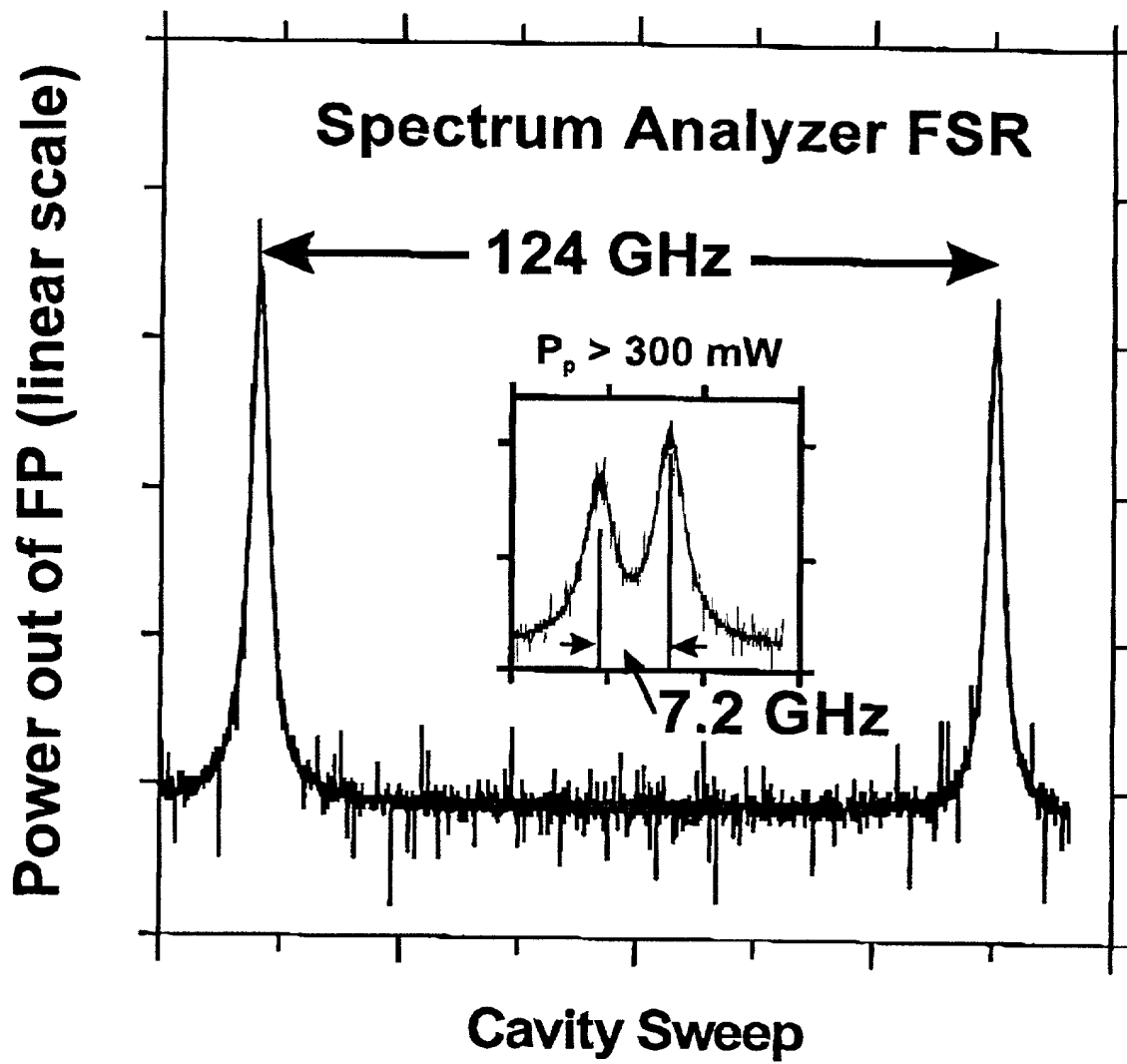
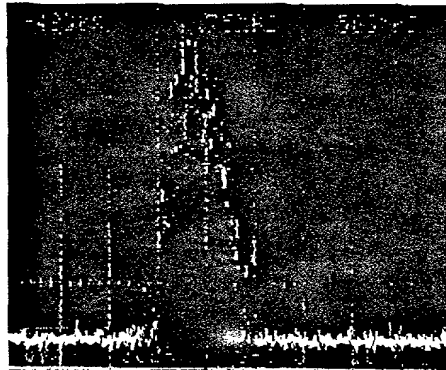


Figure 11. Veasey

DRAFT DRAFT DRAFT**Beat signal (linear scale)****75 MHz****Frequency (500 kHz/div.)****Figure 12. Veascy**

DRAFT DRAFT DRAFT

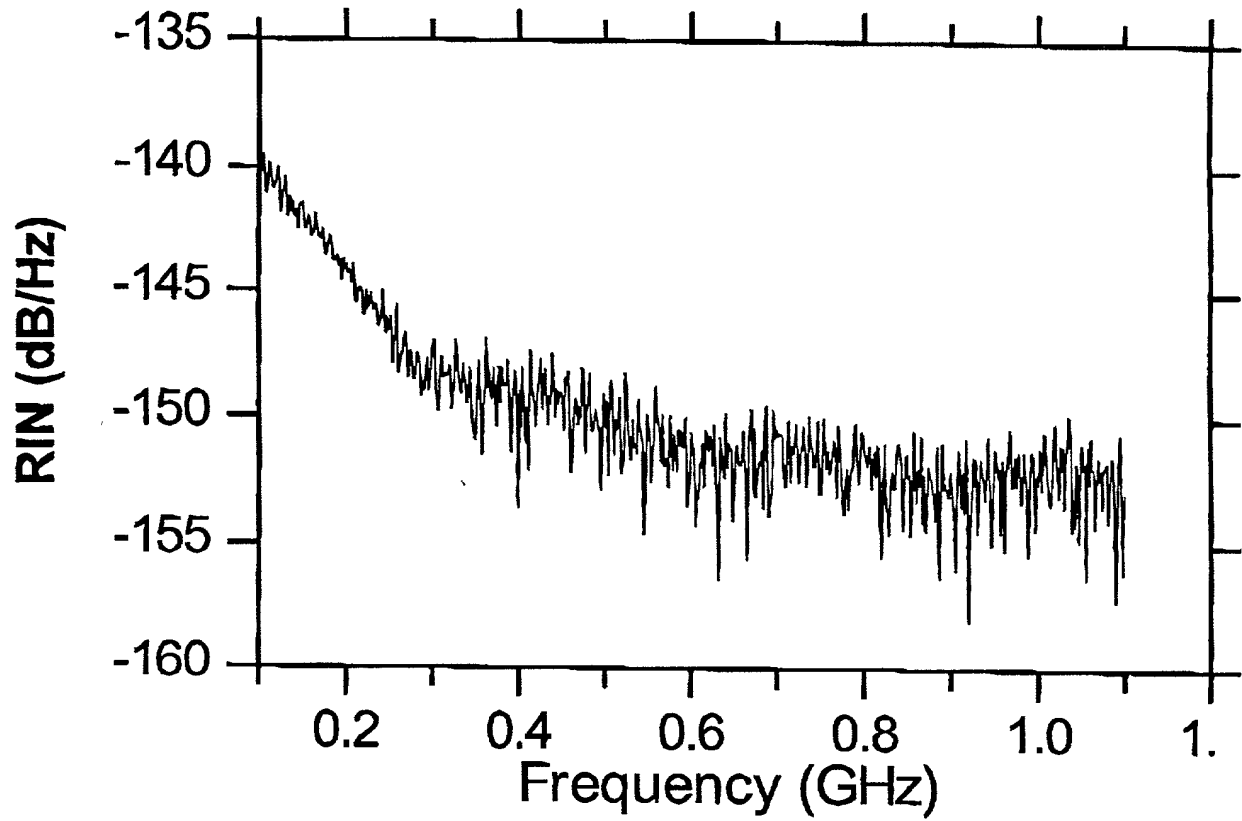


Figure 13a. Veasey

DRAFT DRAFT DRAFT

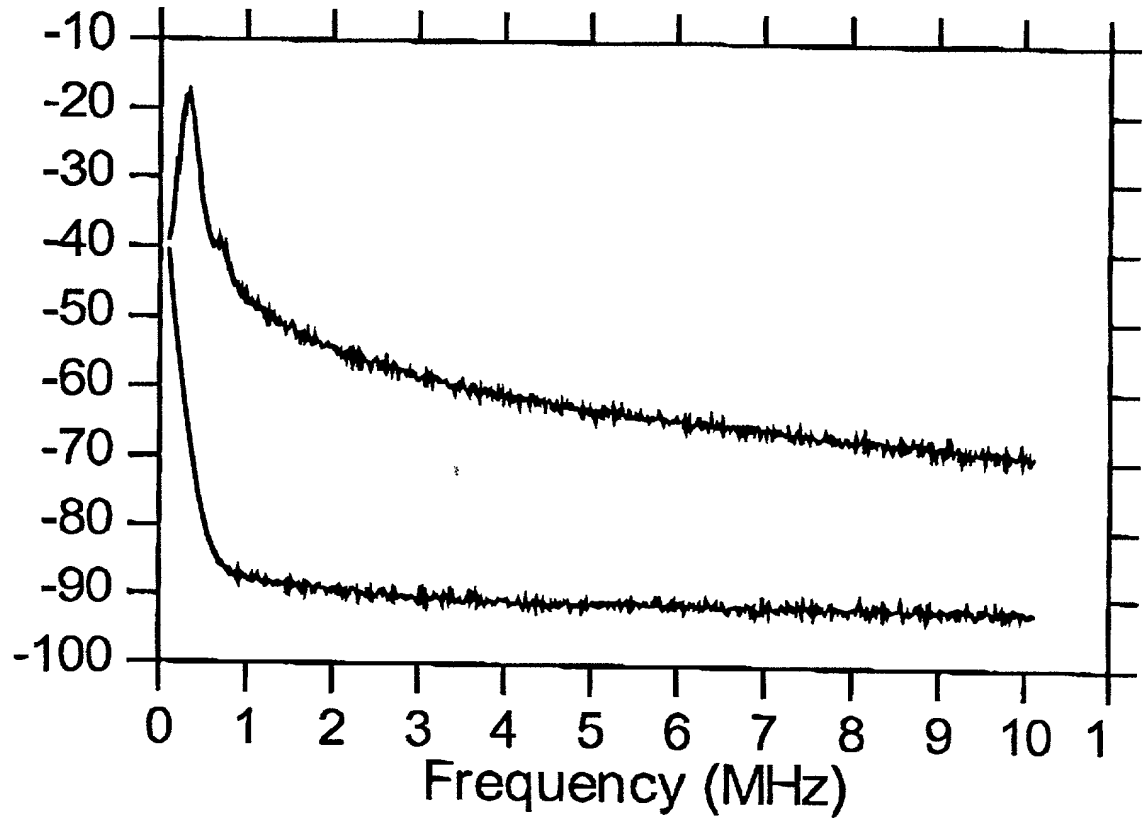
Uncalibrated Amplitude Noise (relative scale)

Figure 13b. Veasey

DRAFT DRAFT DRAFT

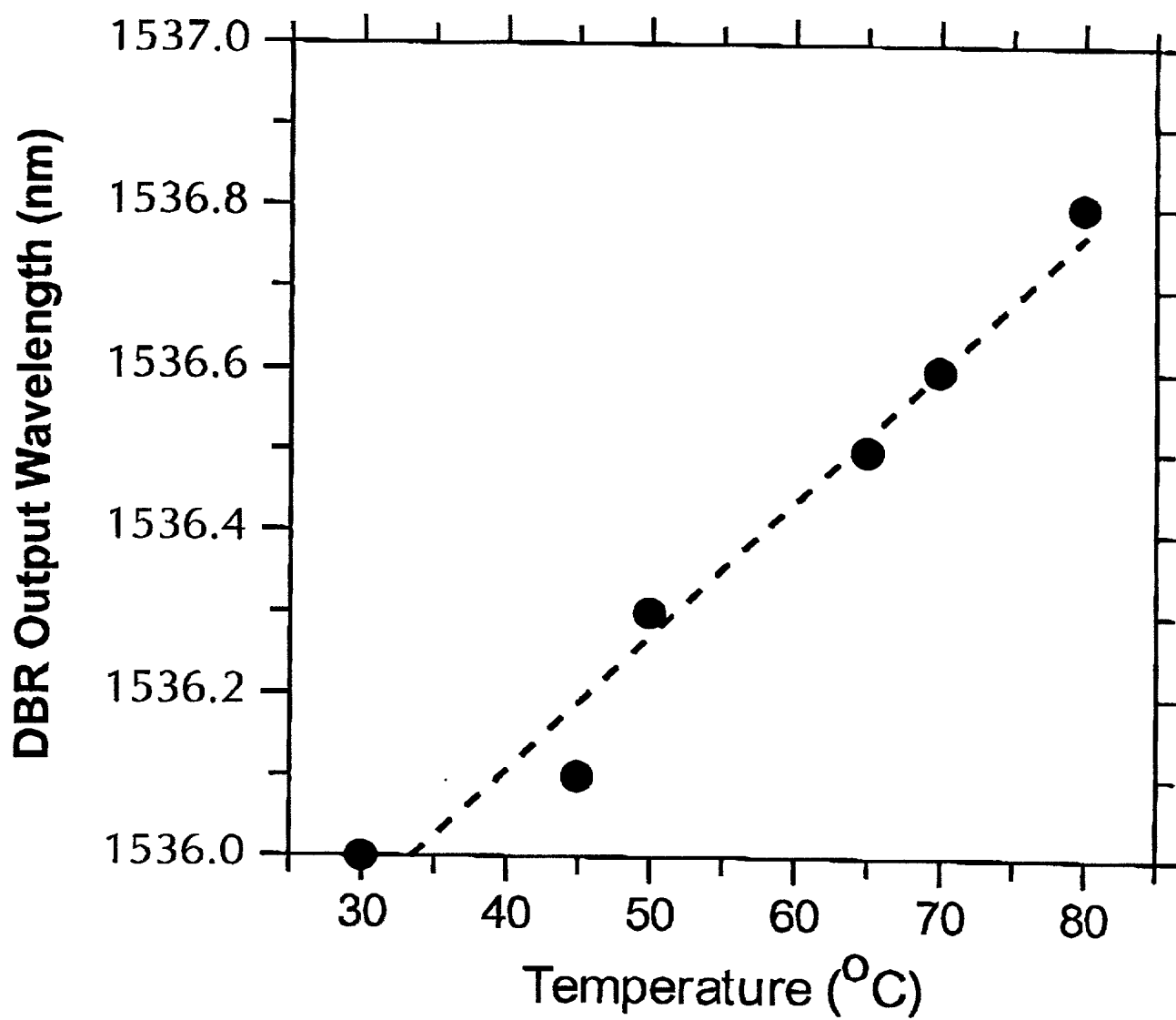
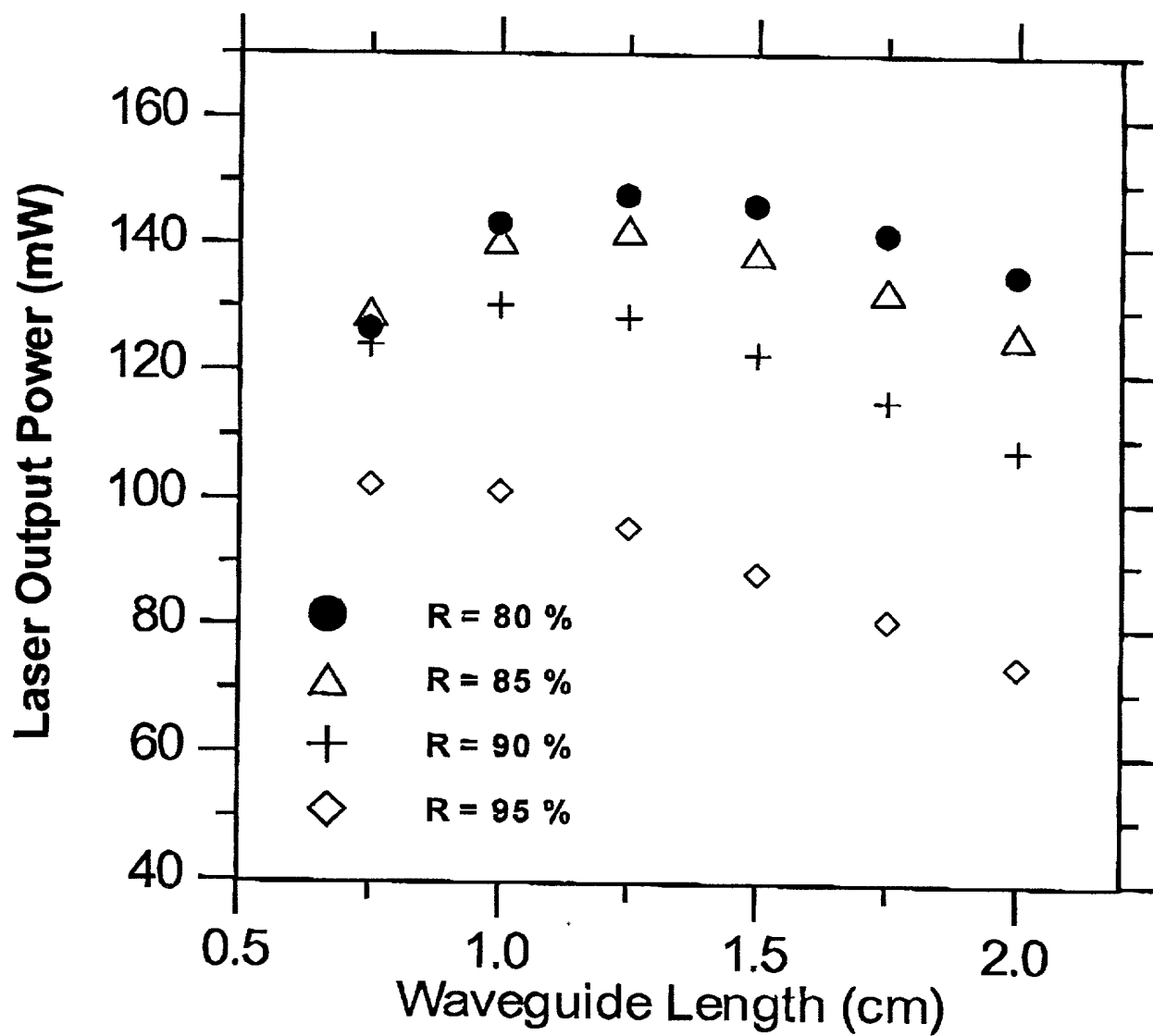


Figure 14. Veasycy

DRAFT DRAFT DRAFT



References

- [1] M. Saruwatari and T. Izawa, *Appl. Phys. Lett.* **24**, 603 (1974).
- [2] K.J. Malone, N.A. Sanford, and J.S. Hayden, *Electron. Lett.* **29**, 691 (1993).
- [3] T. Feuchter, E.K. Mwarania, J. Wang, L. Reckie, J.S. Wilkinson, *IEEE Photon. Technol. Lett.* **4**, 542, (1992).
- [4] D. Barbier, J. Hubner, J.M. Jouanno, A. Kevorkian, A. Lupascu, Post deadline Conf. Digest, European Conf. On Integrated Optics (1993).
- [5] G.L. Vossler, C.J. Brooks, and K.A. Winik, *Electron. Lett.* **31**, 1162 (1995).
- [6] J.E. Roman, M. Hempstead, W.S. Brocklesby, S. Nouh, and J.S. Wilkinson, P. Camy, C. Lermiaux, and A. Beguin, Post deadline Conf. Digest, European Conf. On Integrated Optics, (1995).
- [7] P. Fournier, P. Meshkinfam, M.A. Fardad, M.P. Andrews, and S.I. Najafi, *Electron. Lett.* **33**, 293 (1997).
- [8] F.D. Patcl, E.C. Honca, D. Krol, S.A. Payne, J.S. Hayden, Conf. Digest, OSA Advanced Solid State Laser Conference, p. 338, (1999).
- [9] J. Shmulovich, A. Wong, Y.H. Wong, P.C. Becker, A.J. Bruce, and R. Adar, *Electron. Lett.* **28**, 1181 (1992).
- [10] Y.C. Yan, A.J. Faber, H. de Waal, P.G. Kik, and A. Polman, *Appl. Phys. Lett.* **71**, 2922 (1997).
- [11] S. Guldberg-Kjaer, J. Hubner, M. Kristensen, C. Laurent-Lund, M. Rysholt Poulsen, and M.W. Sckerl, *Electron. Lett.* **35**, 302, (1999).
- [12] T. Kitagawa, K. Hattori, M. Shimizu, Y. Ohmori, M. Kobayashi, *Electron. Lett.* **27**, 334 (1991).
- [13] G.N. van den Hoven, R.J.I.M. Kopce, A. Polman, C. van Dam, J.W.M. van Uffelen, and M.K. Smit, *Appl. Phys. Lett.* **68**, 1886 (1996).
- [14] R. Serna, J.M. Ballesteros, M. Jimenez de Castro, J. Solis, and C.N. Afonso, *J. Appl. Phys.* **84**, 2352 (1998).
- [15] M. Benatou, B. Capoen, M. Bouazaoui, W. Tchana, and J.P. Vilcot, *Appl. Phys. Lett.* **71**, 428 (1997).
- [16] A.F. Obaton, J. Bernard, C. Parent, G. LeFlem, J.M. Fernandez-Navarro, J.L. Adam, M.J. Myers, G. Boulon, Conf. Digest, OSA Advanced Solid State Laser Conference, p. 335, (1999)
- [17] IOG-1 laser glass, Schott Glass Technologies, Inc., 400 York Avenue, Duryea, PA. The IOG-1 trade name is used to allow the reader to reproduce the experiment and does not imply endorsement by the National Institute of Standards and Technology.
- [18] Laser Glass: Nd-Doped Glass Spectroscopic and Physical Properties, Lawrence Livermore National Laboratory, M-095, Rev. 2, November 1981.
- [19] D.E. McCumber, *Phys. Rev.* **134**, A299, (1964).
- [20] W.J. Miniscalco and R.S. Quimby, *Optics. Lett.* **16**, 258 (1991).

DRAFT DRAFT DRAFT

- [21] D.L. Veasey, K.J. Malone, J.A. Aust, N.A. Sanford, and A. Roshko, Conf. Digest, Proc. 7th Eur. Conf. on Integrated. Optics. p. 579, Delft, (1995), J.E. Roman and K.A. Winick, Appl. Phys. Lett. **61**, 2744 (1992).
- [22] L. Li, M. Xu, G.I. Stegeman, C.T. Seaton, SPIE Proc. **835**, 72 (1987)
- [23] N. H. Fontaine and M. Young, "Refracted near-field scanning of fibers and waveguides," submitted to Appl. Optics.
- [24] D.H. McMahon, W.A. Dyes, J. Lightwave Technol. **6**, 1162 (1988).
- [25] J.W. Goodman, *Statistical Optics*, Wiley&Sons, 1985, p. 168.
- [26] W.H. Loh, B.N. Samson, L. Dong, G.J. Cowle, and K. Hsu, J. Lightwave Technol. **16**, 114 (1998).
- [27] W.W. Rigrod, J. Appl. Phys. **36**, 2487 (1965).
- [28] E. Miskovic, Photonics Spectra **33**, 105 February (1999).
- [29] D.L. Veasey, J.M. Gary, and J. Amin, SPIE Proc. **2996**, 109 (1997)
- [30] L. Ingber, "Adaptive Simulated Annealing (ASA)," Global optimization C-code, Lester Ingber Research, Chicago, IL (1993).
URL <http://www.ingber.com/#ASA-CODE>
- [31]: R.E. Smith, S.N. Houde-Walter and G.W. Forbes, J. Quan.Electron. **QE-28**, 1520 (1992).

Figure Captions

- Fig. 1. Distributed-Bragg-reflector waveguide laser array realized using a single pitch grating and diffused waveguides with varying effective index.
- Fig. 2. Schematic of Fabry-Perot waveguide laser test bed
- Fig. 3. a) Emission and absorption cross sections as a function of wavelength for Er^{3+} ions in IOG-1 phosphate glass. Spectral emission was calculated using the method of McCumber. b) Emission and absorption cross sections as a function of wavelength for Yb^{3+} ions in IOG-1. $\Delta\lambda_{\text{em}}$ indicates the spectrum width as defined by $\Delta\lambda_{\text{em}} = \int \sigma(\lambda)d\lambda / \sigma(\lambda_{\text{peak}})$.
- Fig. 4. Refractive index depth profile, measured at 635 nm, of an $\text{Er}^{3+}/\text{Yb}^{3+}$ phosphate glass waveguide obtained using a refracted near-field scanning method.
- Fig. 5. 1540 nm output power as a function of pump power for a 20 mm and a 22 mm long $\text{Er}^{3+}/\text{Yb}^{3+}$ waveguide lasers. 20 mm long device was pumped at 979 nm and the 22 mm device was pumped at 960 nm. Also shown is a theoretical fit to the data using a waveguide laser model.
- Fig. 6. Typical multi-wavelength output spectrum for Fabry-Perot waveguide lasers.
- Fig. 7. Extended cavity designs used for tuning of waveguide lasers. a) prism-tuned weakly coupled cavity, b) grating-tuned extended cavity.
- Fig. 8. a) tuning curve obtained for grating-tuned Fabry-Perot waveguide laser. Solid lines connect the points as a guide to the eye, b) typical multiwavelength output spectrum of F-P waveguide laser.
- Fig. 9. Output power as a function of coupled pump power for a Yb-doped waveguide laser operating at a wavelength of 1.02 μm . The solid line represents the best linear fit to the data from which the slope efficiency was derived.
- Fig. 10. Single frequency laser output power at 1536.3 nm as a function of launched 977 nm pump power. The dotted line represents the best linear fit to the data from which the slope efficiency was derived. The inset shows the spectrum of the DBR laser on a linear scale.
- Fig. 11. Fabry Perot (F-P) interferometer scan of the DBR laser output showing single frequency operation. Inset shows dual frequency operation for pump powers (P_p) exceeding 300 mW. Longitudinal mode spacing is 7.2 GHz, corresponding to an optical cavity length of 1.4 cm.
- Fig. 12. Self heterodyne beat spectrum at 75 MHz. The full-width, half-maximum linewidth is approximately 500 kHz.
- Fig. 13. a) Relative intensity noise (RIN) in the frequency band from 0.1 to 1.1 GHz using a shot noise calibrated RIN system, b) uncalibrated amplitude noise spectrum showing relaxation oscillation noise peak near 300 kHz. The lower curve represents the noise floor of the measurement system.
- Fig. 14. Wavelength of DBR waveguide laser as a function of temperature. Dotted line is for the aid of the eye in following the wavelength trend.
- Fig. 15. Simulated laser output power as a function of laser length for several values of output coupler reflectance, b) simulated laser output power as a function of mode-field diameter for a 1-cm long laser cavity.
- Fig. 16. Output power as a function of waveguide mode width and height at 1.54 μm and output mirror reflectance for optimized waveguide lasers. Range of output powers in mW is indicated by color bar.

Rigorous scalar modeling of Er and Er/Yb-doped waveguide lasers*

David L. Veasey[@], John M. Gary, and Jaymin Amin

National Institute of Standards and Technology, Boulder, CO 80303-3328

ABSTRACT

A rigorous scalar model for predicting the characteristics of rare-earth-doped waveguide lasers has been developed. The model consists of two nonhomogeneous wave equations: one for the forward-propagating laser signal power, the other for the backward-propagating laser signal. These equations are coupled with one forward-propagating, nonhomogeneous wave equation representing the pump signal. The three wave equations are coupled with the space dependent laser rate equations to form a system of time dependent differential equations. This large system of equations is solved, using appropriate initial and boundary conditions, by the method of lines using collocation for the spatial approximation. The solutions to this system yield data which predict the time and position-dependent laser signal power, pump power, and population densities in a waveguide laser cavity supporting an arbitrary guided mode. The assumptions made in this new model are that the transverse field maintains the same shape as a function of longitudinal position in the laser cavity and that the effects of spatial hole burning and standing waves are neglected. We have used this model to predict continuous wave and Q-switched laser performance for Er and Er/Yb-doped lasers. We have achieved favorable comparisons with actual laboratory operation of cw Yb/Er-co-doped waveguide lasers. Results from simulations of Er-doped and Yb/Er-doped Q-switched lasers are presented which show that high peak powers on the order of 500 W and 1 ns pulse widths can be achieved.

Keywords: waveguide, laser, Q-switch, erbium, ytterbium, modeling, ion-exchange, sources

2. INTRODUCTION

Over the past several years, there has been considerable interest in the development of solid state waveguide laser sources in dielectric materials such as bulk glasses,¹⁻⁶ dielectric films,⁷ and electro-optic hosts such as LiNbO₃ and LiTaO₃.⁸⁻¹⁰ The interest in such sources has been motivated primarily by the successful deployment of erbium-doped fiber amplifiers in optical communication systems operating in the 1.55 μ m band. Rare-earth-doped glass waveguide lasers offer several advantages over their semiconductor laser counterparts. These advantages include lower manufacturing costs due to relaxed fabrication tolerances over semiconductor lasers, broad wavelength tunability, inherently low relative intensity noise (RIN), and narrower laser linewidths. In addition, the beam profiles and numerical apertures can be nearly exactly matched to optical fibers. They also exhibit high energy storage capacity which is necessary for high-power pulsed operation. One of the primary limitations of planar waveguide devices is that they require short cavity lengths. This means that optically pumped thresholds are somewhat higher than for fiber lasers where the lengths can be arbitrarily extended. In order to overcome this problem, several different approaches can be pursued. One is to increase the doping concentration of the active ion. This increases the gain per unit length of material, thus lowering thresholds. However, when doping concentration is increased, there is a risk in most host materials of concentration quenching. This causes severe performance degradation because of increased cooperative up-conversion.¹¹ Other solutions for the optimization of waveguide laser sources include optimizing host materials, cavity design (by judiciously choosing cavity lengths and output coupler reflectivities), pump coupling, and the pumping rate (through the introduction of co-dopants such as ytterbium (Yb) with erbium (Er)). It is also very important to carefully design the waveguide index profiles so that they yield ideal mode fields and overlap for the signal and pump waves. In order to achieve ideal performance, one must be careful to do all of the above simultaneously. This exercise is clearly not trivial since one is dealing with a many-parameter, highly nonlinear

* Contribution of the U.S. Government, not subject to copyright.

[@] email: veasey@boulder.nist.gov

system. For these reasons, we have developed a laser model to accurately predict waveguide laser performance for continuous wave and pulsed operation modes. This predictive design tool allows us to determine optimum waveguide laser design which will lead to useful, and reliable manufacturable products.

3. THE MODEL FORMULATION

In our model, we have attempted to realistically model a waveguide laser by making as few assumptions as possible while maintaining practical computer run times for the simulation. A picture of a typical waveguide laser and cavity is shown in Figure 1.

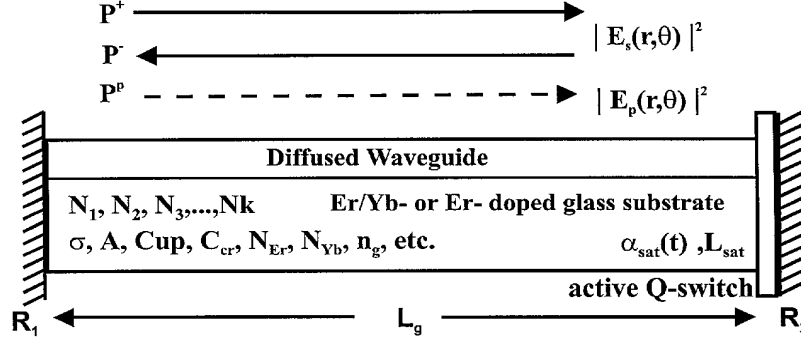


Figure 1. Schematic of laser cavity to be simulated

We have started from basic differential calculus using a semi-classical approach to derive the wave equations which accurately describe propagation in a waveguide laser cavity. A similar derivation of the wave equations was presented by Millonni and Eberly.¹² We also use the semi-classical laser rate equations which are coupled with propagating signals in a laser cavity. The model we have developed for multiple frequencies and a multi-energy level system is described in this section.

The model is grouped into two specific types of equations. These are time dependent scalar wave equations and time/space dependent laser rate equations. The wave equations describe mathematically the forward and backward propagation of the optical frequencies in the laser cavity. For simplicity, we have included only two optical frequencies in the model presented in this paper. These are the laser signal frequency at $\lambda=1542$ nm and the pump signal at $\lambda=980$ nm. This simplification produces three first order wave equations: one for the forward-propagating laser signal, one for the backward-traveling laser signal, and one for the forward-propagating pump signal. The computer code can accommodate other frequencies simply by adding additional wave equations for each wavelength and direction of propagation.

These wave equations,

$$\frac{\partial P^+(z, t)}{\partial t} = -\frac{c}{n_g} \frac{\partial P^+(z, t)}{\partial z} + \frac{c}{n_g} \alpha_s(z, t) P^+(z, t) + \frac{B_{sp} \int_{\perp} N_2 dA}{\tau_{21}} \quad (1)$$

$$\frac{\partial P^-(z, t)}{\partial t} = \frac{c}{n_g} \frac{\partial P^-(z, t)}{\partial z} + \frac{c}{n_g} \alpha_s(z, t) P^-(z, t) + \frac{B_{sp} \int_{\perp} N_2 dA}{\tau_{21}} \quad (2)$$

$$\frac{\partial P^p(z, t)}{\partial t} = -\frac{c}{n_p} \frac{\partial P^p(z, t)}{\partial z} + \frac{c}{n_p} \alpha_p(z, t) P^p(z, t) \quad (3)$$

are coupled with sets of time-dependent laser rate equations, in which the energy level population densities, $N_i = N_i(t, z, r, \theta)$ are functions of time and position. The rate equations are

$$\begin{aligned}
\frac{\partial N_1}{\partial t} &= -W_{12}N_1 - W_{13}N_1 + A_{21}N_2 + W_{21}N_2 \\
&\quad + C_{up}N_2^2 - C_{14}N_1N_4 + C_{up3}N_3^2 - C_{cr}N_1N_6, \\
\frac{\partial N_2}{\partial t} &= W_{12}N_1 - W_{21}N_2 - A_{21}N_2 + A_{32}N_3 - 2C_{up}N_2^2 + 2C_{14}N_1N_4, \\
\frac{\partial N_3}{\partial t} &= W_{13}N_1 - A_{32}N_3 + A_{43}N_4 - 2C_{up3}N_3^2 + C_{cr}N_1N_6, \\
N_{Er} &= N_1 + N_2 + N_3 + N_4, \\
\frac{\partial N_5}{\partial t} &= -W_{56}N_1 + A_{65}N_6 + W_{65}N_6 + C_{cr}N_1N_6, \\
N_{Yb} &= N_5 + N_6.
\end{aligned} \tag{4}$$

These equations describe the rates at which rare-earth ion energy levels in the material are populated and depleted by absorption, stimulated emission, and spontaneous emission as functions of longitudinal and transverse dimensions. This set of equations was presented by Pasquale.¹³ The number of rate equations in a set is determined by the number of energy levels one wishes to track in a simulation. For the Er/Yb-co-doped system in this paper there are six time-dependent equations in a set which means we are tracking six energy levels. There are two time-dependent conservation equations in this system. It is straightforward to alter the rate equation set to account for other interesting energy level transitions. This provides great flexibility for modeling many rare-earth-doped lasers and amplifiers. The transverse dependence of the propagating mode fields is accounted for by sampling a transverse field solution or measured transverse field for a waveguide as a function of two transverse dimensions. At each sample point a set of laser rate equations is introduced into the model to account for the interaction of the transverse field with the stationary ions in the host material.

P^+ and P^- are the forward and backward-propagating laser powers as a function of longitudinal position in the laser cavity. P_p is the forward-propagating pump power in the laser cavity. The pump power, in this case, is assumed to be launched from the end opposite the output coupler which has reflectance, R_2 . The optical intensity (in W/cm^2) of the laser signal is $P^\pm(z, t) |E_s(r, \theta)|^2$, where $|E_s|^2$ is the normalized intensity distribution and has units of cm^{-2} . The pump signal P^p is treated in a similar fashion. The N_i 's are the population densities of the various energy levels in the Er/Yb co-doped material. N_1 is the $^4I_{15/2}$ ground state of Er, N_2 is the $^4I_{13/2}$ laser level of Er, N_3 is the $^4I_{11/2}$ 980 nm pump level for Er, N_4 is the $^4I_{9/2}$ 800 nm pump level and upconversion level of Er, N_5 is the $^2F_{7/2}$ ground state of Yb, and N_6 is the $^2F_{5/2}$ pump level of Yb. Figure 2 shows an energy level diagram for the Er/Yb-co-doped system. The Yb pump level is shown as split to illustrate that it has very wide energy range.

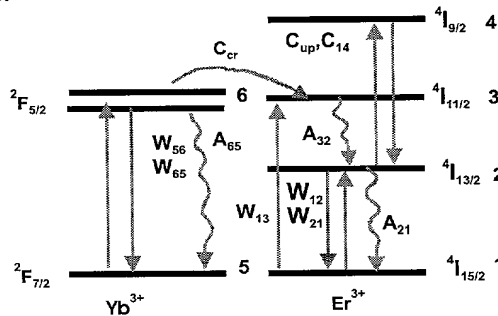


Figure 2. Energy level diagram for Er/Yb-co-doped laser host.

C_{up} is the cooperative upconversion coefficient from the Er $^4I_{13/2}$ laser level, C_{up3} is the cooperative upconversion coefficient from the Er $^4I_{11/2}$ 980 nm pump level, C_{cr} is the cross relaxation coefficient or net forward coupling from the Yb $^2F_{5/2}$ level to

the Er $^4I_{11/2}$ level, and C_{14} is the cooperative down-conversion coefficient or the opposite of cooperative upconversion. The A 's are the nonradiative spontaneous emission rates from the first subscript energy level to the second subscript energy level. c is the speed of light in vacuum, n_s is the effective index of the laser mode, n_p is the effective index of the pump mode, and α_s is the gain coefficient as a function of longitudinal position and time inside the laser cavity.

The second term on the right side of equations (1-3) represents the contribution or loss of power in the laser line width due to stimulated emission or absorption and excess waveguide loss at each point z and time t . $n_0 \times m_0$ represents the number of nodes in the transverse dimensions and the two-dimensional grid on which intensities are sampled and on which the N_i 's are calculated.

The gain or loss coefficient α_s is computed after Bjarklev¹⁴ by calculating the overlap integral of the normalized propagating power distribution and the population density and then multiplying by the emission or absorption cross sections:

$$\begin{aligned}\gamma_{21}(z, t) &= \sigma_{21} \iint_{\perp} N_2 |E_s|^2 dA, \\ \gamma_{12}(z, t) &= \sigma_{12} \iint_{\perp} N_1 |E_s|^2 dA.\end{aligned}\quad (5)$$

σ_{21} and σ_{12} are the emission and absorption cross sections of the host material at the laser wavelength. The normalized intensity propagating in the waveguide is assumed to be independent of z , and is normalized by requiring that:

$$\iint_{\perp} |E_s|^2 dA = 1. \quad (6)$$

The gain coefficient as a function of z and t is then given by

$$\alpha_s(z, t) = \gamma_{21}(z, t) - \gamma_{12}(z, t) - \alpha_{is}. \quad (7)$$

α_{is} is the waveguide loss coefficient, which is subtracted to account for excess waveguide losses from scattering and absorption not due to the rare earth ions. It is also possible to add other position dependent losses in this term which are functions of fabrication parameters or cavity configuration. For example, a position and time dependent term can be added to account for mirror losses or localized losses from waveguide loading or for an intracavity coupler.

The pump absorption coefficient α_p is calculated similarly by computing the overlap integral of the ground state populations for the Er ions and the Yb ions with the normalized pump intensity $|E_p|^2$ and multiplying by the pump absorption cross sections, giving:

$$\begin{aligned}\gamma_{13}(z, t) &= \sigma_{13} \iint_{\perp} N_1 |E_p|^2 dA, \\ \gamma_{56}(z, t) &= \sigma_{56} \iint_{\perp} N_5 |E_p|^2 dA, \\ \alpha_p(z, t) &= -\gamma_{13}(z, t) - \gamma_{56}(z, t) - \alpha_{ip}.\end{aligned}\quad (8)$$

α_{ip} is the excess absorption and scattering loss at the 980 nm pump wavelength. The pump intensity $|E_p|^2$ is normalized in the same way as the signal field, and is written as

$$\iint_{\perp} |E_p|^2 dA = 1. \quad (9)$$

The third term on the right side of equations (1) and (2) represents the contribution of spontaneous emission to the propagating optical power. τ_{21} is the spontaneous emission lifetime of the laser level. The coefficient B_{sp} is given by

$$B_{sp} = \eta c h \nu_s, \quad (10)$$

where η is the efficiency of spontaneous emission in the laser line width and is approximated by the ratio of the waveguide

numerical aperture solid angle to the solid angle of a sphere times the integral over frequency of the equivalent spontaneous emission spectrum. $h\nu_s$ is the energy of a single laser photon. This approximation of spontaneous emission is similar to the equivalent bandwidth approximation described by Bjarklev.¹⁴

W_{21} , W_{12} , W_{13} , W_{56} , and W_{65} are the stimulated emission and absorption rates as a function of longitudinal and transverse dimensions and are given by

$$\begin{aligned} W_{12} &= \frac{\sigma_{12}(P^+ + P^-)|E_s|^2}{h\nu_s}, & W_{21} &= \frac{\sigma_{21}(P^+ + P^-)|E_s|^2}{h\nu_s}, \\ W_{13} &= \frac{\sigma_{13}(P^p)|E_p|^2}{h\nu_p}, & W_{56} &= \frac{\sigma_{56}(P^p)|E_p|^2}{h\nu_p}, \\ W_{65} &= \frac{\sigma_{65}(P^p)|E_p|^2}{h\nu_p}. \end{aligned} \quad (11)$$

We have not included other energy levels in the model as of yet but have plans to add other levels as (outlined by Desurvire¹⁵) to the Er model. This will allow consideration of excited state absorption (ESA) and its effect on device performance. Each additional energy level adds an extra equation to the rate equation set for each transverse field sample point.

Equations (1)-(4) must be solved simultaneously with appropriate initial conditions and boundary conditions. These conditions determine the laser or amplifier state in which the system will operate. For the laser model, the initial conditions are assumed to be

$$\begin{aligned} P^+(z, 0) &= P^-(z, 0) = 0, \\ P^p(z, 0) &= P_{p0} e^{-(\sigma_{13}N_1(z, 0) + \sigma_{56}N_5(z, 0))z}, \\ N_1(t=0) &= N_{Er}, \quad N_{2,3,4}(t=0) = 0, \quad N_5(t=0) = N_{Yb}, \quad N_6(t=0) = 0. \end{aligned} \quad (12)$$

These conditions assume that the laser system is initially at rest and that the pump wave has propagated a single cavity length without significantly affecting the population densities in the sample. This is done to avoid sharp discontinuities in the initial condition for the pump.

Boundary conditions are imposed on the values of P^+ , P^- , and P^p as follows:

$$\begin{aligned} P^+(0, t) - R_1 P^-(0, t) &= 0, \\ P^-(L, t) - R_2 (e^{2\alpha_{sat} L_{sat}}) P^-(L, t) &= 0, \\ P^p(0, t) - P_{p0} &= 0. \end{aligned} \quad (13)$$

R_1 is the reflectance of a highly reflecting mirror at the pump input end of the laser, R_2 is the reflectance of the output coupler for the laser, and α_{sat} is the time-varying absorption coefficient for an arbitrarily thin absorbing switch placed in the laser cavity just inside of the output coupling mirror. L_{sat} is an effective length of the thin absorber providing the switch with an extinction of $\exp(-\alpha_{sat} L_{sat})$. P_{p0} is the pump power launched at the input end of the sample and held constant from time 0. L is the length of the cavity. For cw operation α_{sat} is set to 0, and for Q-switched operation α_{sat} is set to a function representing the dependence of the absorption coefficient on time. This is an approximate representation of active Q-switching. We could easily make the absorption coefficient of the switch a function of intensity, thus modeling passive Q-switching with a saturable absorber without introducing any more complexity into the model.

4. METHOD OF SOLUTION

At this point our model consists of a large set of coupled integral-differential equations in the form of an initial value problem. The first step in the solution procedure is to transform the integrals so that they can be computed by a generalized Gauss-Laguerre quadrature formula.¹⁶ Using cylindrical coordinates to represent elliptical electrical fields given by

$$|E_s|^2 = e^{-2\beta_s(\theta)r^2}, \quad |E_p|^2 = e^{-2\beta_p(\theta)r^2}, \quad (14)$$

the integrals in equation (5) and (8) have the form

$$\int_0^{2\pi} \int_0^\infty F(r, \theta) e^{-2\beta(\theta)r^2} r dr d\theta. \quad (15)$$

This integral under the transformation $s=2\beta\theta r^2$, and $\phi = \theta$, becomes

$$\int_0^{2\pi} \int_0^\infty \frac{F(s, \phi) e^{-s}}{4\beta(\phi)} ds d\phi. \quad (16)$$

This is the form required for the use of Gauss-Laguerre quadrature in integration variable s .

Once the number n_0 of points, s , used to approximate the integrals in s is selected, then the location of the points and the corresponding weights for the quadrature are determined by a library routine.¹⁶ Then the integral over s is approximated by

$$\frac{2\pi}{m_0} \sum_{k=1}^{m_0} \sum_{j=1}^{n_0} \frac{F(s_j, \phi_k)}{4\beta(\phi_k)} w_j. \quad (17)$$

The w_j 's are the weights generated by the quadrature routine. The trapezoidal rule is used to approximate the integrals over ϕ . Thus the problem is discretized over the transverse (s, ϕ) planes resulting in a hyperbolic initial value problem

$$\frac{\partial U}{\partial t} = f(U, U_z, t). \quad (18)$$

The vector $U(z, t)$ contains the values of the solution at the discrete points (z_i, s_j, ϕ_k) ; that is, $U(t) = (P_1^+, P_1^-, P_1^p, N_{1,j,k}, \dots, N_{4i,j,k})$ for $1 \leq i \leq I_0$, $1 \leq j \leq n_0$, $1 \leq k \leq m_0$.

Next, an approximation by cubic Hermite collocation¹⁷ is used to discretize these equations in the z -direction. First a set of nodal points z_i with $z_i < z_{i+1}$ covering the length of the device is selected. The solution is represented by the value of the solution vector U and its spatial derivatives U_z at each nodal point. These values determine a cubic polynomial in each subinterval (z_i, z_{i+1}) . These polynomials are used to approximate the solution. The spatial derivatives, within each interval, are determined by differentiating these polynomials. Instead of representing $U(z)$ by the values of U and its derivative at each node, it is convenient to determine the cubic polynomials by the values of $U(z)$ at two Gaussian quadrature points in each subinterval. In addition the values $U(0)$ and $U(L)$ at the endpoints are needed. The Gaussian quadrature points and the endpoints are the collocation points at which the right side of the partial differential equation is evaluated. This results in a system of ordinary differential equations (ODE); that is, a method-of-lines approximation.¹⁸ Finally, the vector of unknowns in the system of ODE's is $W(t) = ((P_v^+, P_v^-, P_v^p, N_{1v,j,k}, \dots, N_{4v,j,k})$ where the P 's approximate the value at the v th collocation point z_v . Here $1 \leq v \leq 2I_0$, therefore the total number of unknown functions is $(3+n_0m_0)2I_0$. Typical computations we use have $I_0=10$, $n_0=16$, and $m_0=1$, although we have used m_0 up to 12. This ODE system is solved using a public domain software package by Petzold.¹⁹

5. CONTINUOUS WAVE LASER RESULTS

We have used this time dependent model to predict the performance of an Er/Yb-co-doped waveguide laser operating in cw mode and Q-switched mode. In both cases the laser is initially assumed to be in a rest state where all of the ions are assumed to be in the ground state and the laser signal powers in the cavity are 0. The pump is turned on at $t=0$ and is assumed to instantaneously propagate to the other end of the laser cavity without affecting the population inversion. This process in a 2 cm waveguide laser takes approximately 0.1 ns. The solver is started at this point, and the laser cavity powers and energy level populations are tracked as functions of position and time.

For steady state solutions, the code is run until the output power from the laser cavity reaches a steady state. Clearly, this is not the most computationally efficient way to solve for steady state laser performance if that is all we want. Since our primary purpose is to predict time response, we have not yet implemented a more efficient steady state computer code. During the period of below-threshold and above-threshold operation we resolve the time dependent powers in the laser cavity and the variations in population inversions.

Figure 3 shows the predicted steady state output power for a waveguide laser as a function of coupled pump power and as the Yb concentration is increased from 3:1 to 10:1 while leaving the Er concentration constant. All of these simulations were done using 16 transverse nodes in s . Similar results are obtained by using only 7 nodes in the s dimension. Since the solutions for elliptical fields were typically within several percent of those using circular fields, we only used 1 node in ϕ in order

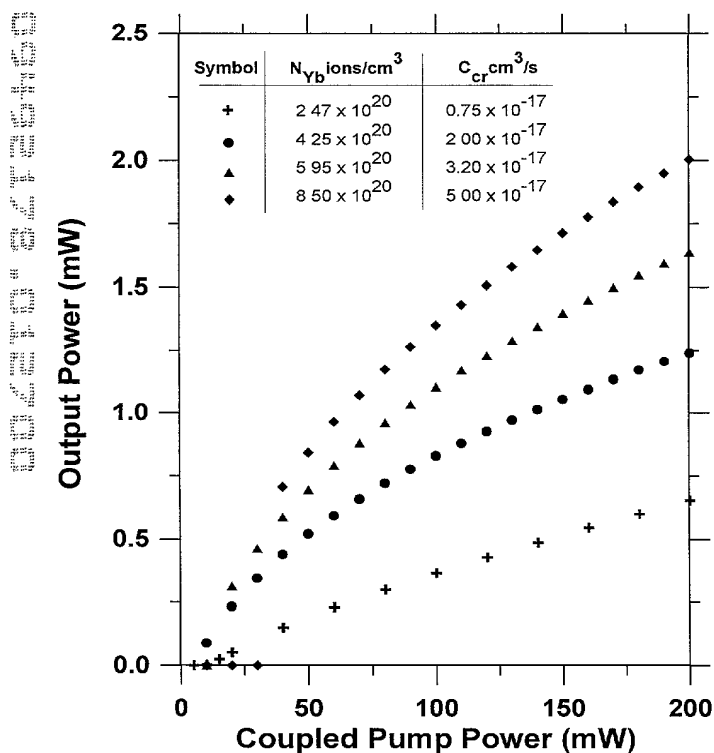


Figure 3. Plot of predicted output power as a function of coupled pump power as the Yb concentration is increased while the Er concentration is constant at 1×10^{20} ions/cm³.

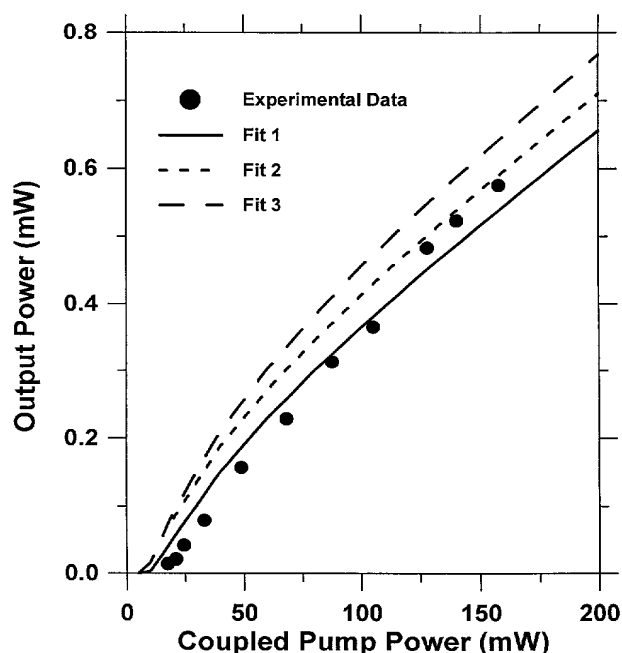


Figure 4. Comparison of theory and experimental data for the Yb/Er co-doped laser. Table 1 lists the bulk of the parameters used in the modeling of the laser device, with the upconversion rate (C_{up}) and the Yb-Er cross relaxation coefficient (C_{cr}) as the variable parameters. For fit 1, $C_{up} = 1 \times 10^{-18}$ cm³/s and $C_{cr} = 0.75 \times 10^{-17}$ cm³/s. For fit 2, $C_{up} = 1 \times 10^{-18}$ cm³/s and $C_{cr} = 1 \times 10^{-17}$ cm³/s. Fit 3 represents $C_{up} = 0$ and $C_{cr} = 0.75 \times 10^{-17}$ cm³/s.

to conserve computer time. Table 1 shows the values of the parameters used for these simulations. These parameters are close to those of a phosphorous free alkali-silicate glass which we refer to as NIST-10. Parameters we were not certain of, like the stimulated emission cross sections for the Er/Yb-co-doped material, we obtained by consulting the literature on Yb/Er and Er-doped glasses which are similar in composition to NIST-10.^{2,3,11,13,20} Other parameters such as waveguide near field profiles, absorption cross

sections, and lifetimes have been measured and inserted into the model.

It is not instructive to generate a curve like that of Figure 3 for variation in Yb concentration if the cross relaxation coefficient is left constant. This coefficient C_{cr} is a strong function of Yb concentration and increases as the Yb concentration is increased. The primary reason for this increase is that the Yb ions, on average, move closer to the Er ions and thus the transfer efficiency is increased. Discussions of the energy transfer in Er/Yb-co-doped glass are presented by Román et al.^{2,21} They present a formula which can be used to determine the cross relaxation coefficients. Upon using this somewhat approximate formula, one finds that for device in Román, the C_{cr} coefficient is approximately $0.5 \times 10^{-17} \text{ cm}^3/\text{s}$. This calculation assumes a lifetime of the $^2F_{7/2}$ Yb level to be 2.0 ms and the lifetime of the $^4I_{11/2}$ Er level to be 10 μs . Román also indicates that the efficiency increases as a function of Yb concentration. For the data generated in Figure 3, we have assumed that, as the Yb concentration varies from $2.47 \times 10^{20} \text{ ions/cm}^3$ up to $8.5 \times 10^{20} \text{ ions/cm}^3$, the cross relaxation coefficient increases linearly from $0.75 \times 10^{-17} \text{ cm}^3/\text{s}$ to $5 \times 10^{-17} \text{ cm}^3/\text{s}$. These numbers are close to those deduced from references 2 and 21 for a similar glass composition. We intend to measure these parameters for various concentrations of Yb in the NIST-10 glass in the very near future. If the transfer efficiency is left constant as the Yb concentration is increased, the performance of the lasers is actually degraded slightly due to decreased pumping efficiency for samples of equal length. The laser thresholds increase for higher Yb concentrations. This is due to the fact that, as the Yb concentration is increased, more of the pump is absorbed at the front end of the laser, thus the pumping of the output end of the device is reduced. This has the effect of increasing absorption losses in the laser cavity toward the output end, and thus the thresholds increase. It is clear from the simulation that doping concentration and sample length must be concurrently optimized. The curvature of the power curves is attributed to the gradual saturation of the upper Yb level as the pump power is increased, as reported by Fermann, et al.²²

We have demonstrated laser operation in several NIST-10 waveguide samples doped with Er and with Er/Yb. The waveguides were prepared by molten salt ion-exchange. Details of the process will follow in subsequent publications. Figure 4 shows a comparison of laboratory data with the predictions obtained from the simulation. To generate these theoretical curves, we used the Yb-Er cross relaxation coefficient C_{cr} and the uniform upconversion coefficient C_{up} as fitting parameters since these spectroscopic parameters have not yet been determined in a systematic way for our glass. The values we used for the fits are indicated on Figure 4 and typify values quoted in the literature for dopant concentrations used in the NIST-10 silicate glass.^{2,3,11,13,20} For all of the fits, the waveguide excess loss at the 1542 nm laser signal wavelength was set at 0.15 dB/cm, which was slightly lower than the measured value of 0.2 dB/cm at 1300 nm. The excess loss at the pump wavelength was set at 0.3 dB/cm. These values represent what we think are realistic loss values for the pump and signal fields, given the values measured by the cut-back method at 1300 nm. Fit 1, represented by the solid line, is the closest of the three fits to slope efficiency and threshold, and we think that it falls within our experimental error. However, the error in our power measurements has not yet been fully characterized. Fit 2 shows the effect of increasing the cross relaxation coefficient slightly from $0.75 \times 10^{-17} \text{ cm}^3/\text{s}$ to $1.0 \times 10^{-17} \text{ cm}^3/\text{s}$ while the upconversion rate is held constant. This small change has the effect of increasing the output power of the laser due to increased pumping efficiency, however, the threshold is not changed significantly. This is most likely due to the low propagation losses in the waveguides. Fit 3 shows the effect of eliminating uniform upconversion from the simulation while maintaining the cross relaxation coefficient at its original value of $0.75 \times 10^{-17} \text{ cm}^3/\text{s}$. The effect of this is to increase the laser output power by a small amount, thus showing that the low upconversion rate used in the model does not significantly deteriorate performance.

Figure 5 is a plot which shows how the slope efficiency and the threshold of this laser will vary as a function of the output coupler reflectivity. The experimental laser characteristics shown in Figure 4 are for an output coupler reflectivity of 98 percent. This operating point is marked on Figure 5 by the circled diamond. This operating point is good for low threshold operation, but is a poor for high output power. Note that this is a poor operation point if high output power is desired, but is a point of lower laser threshold. A good compromise between output power and threshold would be to adjust the output coupler from 98 percent reflectance to 75 percent. This would increase the slope efficiency nearly four times while only doubling the threshold. This is an excellent illustration of the necessity for an accurate laser model, in that it allows for rapid design convergence for optimized rare-earth-doped waveguide lasers.

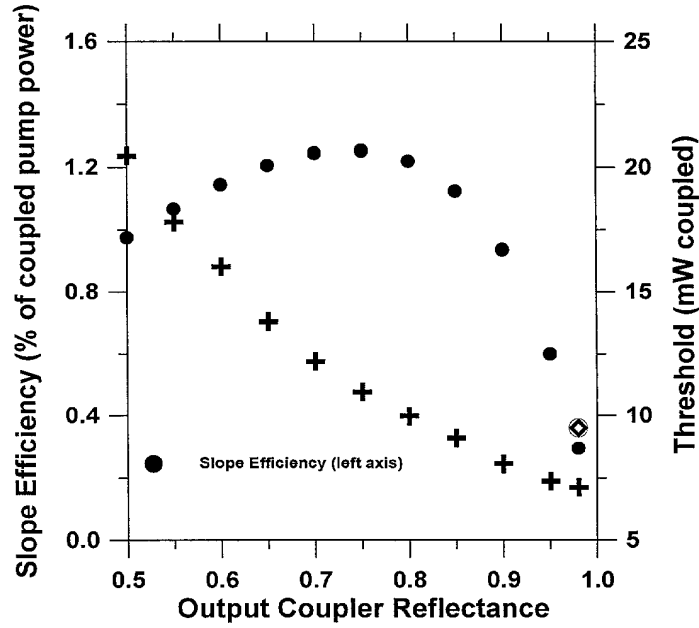


Figure 5. Plot showing the dependence of the laser slope efficiency (left axis) and the laser threshold (right axis) as a function of the cavity output reflectance R_2 . The slope efficiency of the laboratory demonstration of the device is marked by the circled diamond.

6. Q-SWITCHED LASER SIMULATIONS

Finally, we have used the time-dependent laser simulation to model a Q-switched waveguide laser. We have used the cavity configuration of Figure 1, in which the Q-switch is an active switch which is mounted onto the end of a waveguide facet. An integrated mirror is deposited on the back side of the switch material. Such a switch is possible using a semiconductor multi-quantum-well structure. Again, the simulation is run with the laser system starting at rest but with the Q-switch closed or in the high absorption state. This allows the pump to rapidly create a population inversion which is well above threshold for the laser when the Q-switch is opened. We have programmed the active Q-switch to open in 5 ns using a cosine s-bend function. The initial extinction was set at $\alpha_s = -50$, which holds the laser well below threshold with $L_{\text{sat}} = 0.5$ mm. The coupled pump power was set to 200 mW and the system was pumped for 2 ms before the switch was opened. What makes our model unique from other Q-switch models is that we have not assumed that we have a high-Q cavity or a uniform intensity in the cavity. We have not assumed a plane wave electric field, we include several levels and transitions instead of the typical two or three, and we track the saturation of the pumping intensity. In addition, we do not assume that the distribution of energy level population densities assumes the same shape as the pump or the signal field. The populations are allowed to vary freely as functions of position and intensities.

Figure 6 is a family of Q-switch pulse simulations using the same parameters that were used in Fit 1 of Figure 4. These simulations varied only the output coupler reflectance. As the reflectance is decreased, a more nearly optimal point for the extraction of power is reached and the pulses narrow slightly and have higher peak powers. The optimum for this cavity length is approximately 80 percent reflectance, resulting in a peak power prediction of 346 W. If the reflectivity is decreased beyond this point, the round trip gain of the cavity coupled with the average lifetime of a photon in the laser cavity causes the pulses to widen and have less peak power. We have not yet determined the primary factor that determines pulse width. We have found that many parameters are involved in pulse width determination. We have shown that the peak pulse power can be optimized further by decreasing the cavity length from 2 cm to 1.4 cm. At this point, the optimum pulse is slightly narrower in width and the simulated peak power is over 400 W. Other important parameters which affect the pulses, such as near field size, signal-pump overlap, Yb-doping concentration, and Er-doping concentration, are being investigated.

7. SUMMARY

In summary, we have presented a detailed time dependent model for use in the simulation of integrated photonic waveguide lasers. The model treats the waveguide laser with very few approximations. Approximations which we do make are those concerned with the tracking of signal and pump phase. We do not track the phases of waves propagating in the laser cavity. This prohibits us from predicting effects such as cavity standing waves and spatial hole burning, and the dependence of the population densities and

intensities related to these effects.

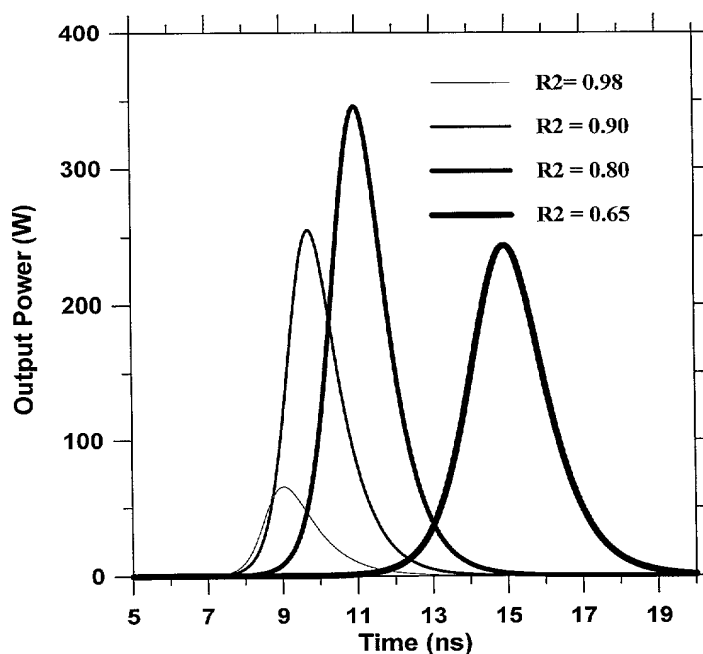


Figure 6. Prediction of Q-switch pulses from the demonstrated Er/Yb-co-doped waveguide laser. The reflectance of the output coupler is varied from 98 percent to 65 percent. The graph shows that the optimum pulse (highest peak power and small width) is extracted when the reflectance is optimized to 80%. The FWHM pulse width for the $R_2 = 98\%$ pulse is 1.58 ns, the $R_2 = 90\%$ pulse width is 1.5 ns, the $R_2 = 80\%$ pulse width is 1.68 ns, and the $R_2 = 65\%$ pulse width is 2.32 ns.

Other approximations we make are that the intensity distributions in the waveguide do not vary as functions of z or time and spontaneous emission is not discretized into many frequencies. The model in its present form, gives us the capability to accurately model waveguide lasers and amplifiers. We have successfully used the model in a predictive fashion to simulate laboratory results for continuous wave Yb/Er co-doped waveguide lasers. The fits from the simulation to the slope efficiency data are excellent using realistic values for all of the pertinent input parameters.

In addition, we have reported the predicted Q-switched performance of Er/Yb-co-doped glass waveguide lasers and have shown that values of peak power can reach hundreds of watts for sample lengths of the order of 1-2 cm. These simulations have used parameters for fabricated waveguide lasers. We have not sufficiently investigated the design space and we strongly believe that more optimum designs can be achieved. An exhaustive investigation of the design space and the interplay among laser parameters is currently underway. Simulations not discussed here suggest that powers on the order of 1 kW can be achieved through the optimization of cavity design and the careful engineering of waveguide index profiles to maximize overlap of the pump and signal guided waves.

We anticipate that this model will be used extensively to model several different rare earth systems for laser and amplifier performance. This work will be done in order to optimize the designs of waveguide and fiber lasers and also to determine the most critical host parameters. In this way, the model acts as a metrology tool by indicating which parameters have the greatest effect on laser performance. These parameters can then be measured more accurately to facilitate the development of more suitable host materials. These simulations have proven to be an invaluable tool for our current work in rare-earth-doped materials and devices.

ACKNOWLEDGEMENTS

The authors thank Bradley Alpert of NIST for helpful discussions and for the provision of several computer codes which greatly benefited the development of the equation solver.

REFERENCES

1. T. Feuchter, E.K. Mwarania, J. Wang, L. Reekie, and J.S. Wilkinson, "Erbium-doped ion-exchanged waveguide lasers in BK-7 glass," *IEEE Photonics Technology Letters*, **4**, pp. 542-544 (1992).
2. J.E. Román, M. Hempstead, W.S. Brockleby, S. Nouh, J.S. Wilkinson, P. Camy, C. Lermينياux, and A. Béguin, "Ion-exchanged Er/Yb waveguide laser at 1.5 μm pumped by a laser diode," *Electronics Letters*, **31**, pp. 1345-1346 (1995).
3. G.L. Vossler, C.J. Brooks, and K.A. Winick, "Planar Er:Yb glass ion exchanged waveguide laser," *Electronics Letters*, **31**, pp. 1162-1163 (1995).
4. D. Barbier, J.M. Delavaux, R.L. Hyde, J.M. Jouanno, A. Kervorkian, and P. Gastaldo, "Tunability of Yb/Er integrated optical lasers in phosphate glass," *Proceeding of Optical Amplifiers and their Applications*, postdeadline paper PD3 (Davos, 1995).
5. D.L. Veasey, K.J. Malone, J.A. Aust, N.A. Sanford, and A. Roshko, "Distributed feedback lasers in rare-earth-doped phosphate glass," *Proceedings of the 7th European Conference on Integrated Optics* (Delft, 1995).
6. J.A. Aust, K.J. Malone, D.L. Veasey, and N.A. Sanford, "Passively Q-switched Nd-doped waveguide laser," *Optics Letters*, **19**, pp. 1849-1851 (1994).
7. T. Kitagawa, K. Hattori, M. Shimizu, Y. Ohmori, and M. Kobayashi, "Guide-wave laser based on erbium-doped silica planar lightwave circuit," *Electronics Letters*, **27**, pp. 334-335 (1991).
8. J. Amin, J.A. Aust, and N.A. Sanford, "Z-propagating waveguide lasers in rare-earth-doped Ti:LiNbO_3 ," *Applied Physics Letters*, **69**, pp. 3785-3787 (1996).
9. I. Baumann, R. Brinkmann, M. Dinand, W. Sohler, and S. Westhöfer, "Ti:Er:LiNbO₃ waveguide laser of optimized efficiency," *IEEE Journal of Quantum Electronics*, **32**, pp. 1695-1706 (1996).
10. N.A. Sanford, J.A. Aust, K.J. Malone, and D.R. Larson, "Nd:LiTaO₃ waveguide laser," *Optics Letters*, **17**, pp. 1578-1580 (1992).
11. M. Federighi and F. Di Pasquale, "The effect of pair-induced energy transfer on the performance of silica waveguide amplifiers with high $\text{Er}^{3+}/\text{Yb}^{3+}$ concentrations," *IEEE Photonics Technology Letters*, **7**, pp. 303-305 (1995).
12. P.W. Milonni and J.H. Eberly, *Laser*, New York, Wiley, 1988, ch. 10.
13. F. Di Pasquale and M. Federighi, "Improved Gain Characteristics in High-Concentration $\text{Er}^{3+}/\text{Yb}^{3+}$ Co-doped Glass Waveguide Amplifiers," *IEEE Journal of Quantum Electronics*, **30**, pp. 2127-2131 (1994).
14. A. Bjarklev, *Optical Fiber Amplifiers: Design and System Applications*, Artech House, Boston-London, ch 5, (1993).
15. E. Desurvire, *Erbium-doped Fiber Amplifiers*, Wiley, New York, p. 278 (1994).
16. G. Golub and J. Welsch, "Calculation of Gauss Quadrature Rules," *Math Comp*, **23**, pp. 221-230 (1969).
17. M. Schultz, *Spline Analysis*, Prentice Hall, Englewood Cliffs, N.J. (1973).
18. M. Davis, *Numerical Methods and Modeling for Chemical Engineers*, Wiley, New York (1984).
19. Petzold, "A description of DASSL: A Differential/Algebraic System Solver," *Proc. IMACS World Congress*, Montreal, Canada (1982).
20. J.E. Roman, M. Hempstead, C. Ye, S. Nouh, P. Camy, P. Laborde, and C. Lermينياux, "1.7 μm excited state absorption measurement in erbium-doped glasses," *Applied Physics Letters*, **64**, pp. 470-472 (1995).
21. J.E. Román, M. Hempstead, W.S. Brocklesby, S. Nouh, J.S. Wilkinson, P. Camy, C. Lermينياux, and A. Béguin, "Diode pumped, ion-exchanged Er/Yb waveguide laser at 1.5 μm in phosphorous-free silicate glass," *Proc. 7th European Conf. on Integrated Optics*, postdeadline paper, pp. 13-16 (Delft 1995).
22. M.E. Fermann, D.C. Hanna, D.P. Shepherd, P.J. Suni, and J.E. Townsend, "Efficient operation of an Yb-sensitized Er fibre laser at 1.56 μm ," *Electronics Letters*, **24**, pp. 1135-1136 (1988).

Table 1. Parameters used to model the Er/Yb co-doped waveguide laser

Length of Waveguide Laser Cavity	$L = 2 \text{ cm}$
Signal Field Width (circular gaussian, $1/e$ FW)	$W_s = 3.75 \times 10^{-4} \text{ cm}$
Pump Field Width (circular gaussian, $1/e$ FW)	$W_p = 2.40 \times 10^{-4} \text{ cm}$
Signal Effective Index	$n_s = 1.53$
Pump Effective Index	$n_p = 1.53$
Spontaneous Emission Lifetime of $^4I_{13/2}$	$\tau_{21} = 11 \text{ ms} = 1/A_{21}$
Stimulated Emission Cross Section 1542 nm ($^4I_{13/2} - ^4I_{15/2}$)	$\sigma_{21} = 6.3 \times 10^{-21} \text{ cm}^2$
Peak Absorption Cross Section 1542 nm ($^4I_{15/2} - ^4I_{13/2}$)	$\sigma_{12} = 5.7 \times 10^{-21} \text{ cm}^2$
Er Pump Absorption Cross Section 980 nm ($^4I_{15/2} - ^4I_{11/2}$)	$\sigma_{13} = 1.1 \times 10^{-21} \text{ cm}^2$
Yb Absorption Cross Section 980 nm ($^2F_{7/2} - ^2F_{5/2}$)	$\sigma_{56} = 8.2 \times 10^{-21} \text{ cm}^2$
Yb Emission Cross Section 980 nm ($^2F_{5/2} - ^2F_{7/2}$)	$\sigma_{65} = 11.9 \times 10^{-21} \text{ cm}^2$
Yb-Er Cross Coupling Coefficient C_{cr}	Fitting parameter, see text
Upconversion Coefficient C_{up}	Fitting parameter, see text
Signal Wavelength	$\lambda_s = 1542 \text{ nm}$
Pump Wavelength	$\lambda_p = 974 \text{ nm}$
Er Ion Density	$N_{er} = 0.85 \times 10^{20} \text{ cm}^{-3}$
Yb Ion Density	$N_{yb} = 2.47 \times 10^{20} \text{ cm}^{-3}$
High Reflector Reflectance	$R_1 = 0.995$
Output Coupler Reflectance	$R_2 = 0.98$
Nonradiative Lifetime of Level $^4I_{11/2}$	$\tau_{32} = 10 \text{ ms} = 1/A_{32}$
Excess Waveguide Scattering Loss	$\alpha_{is} = 0.15 \text{ dB/cm}$ $\alpha_{ip} = 0.3 \text{ dB/cm}$